

AD-A149 743

EROSION CONTROL OF SCOUR DURING CONSTRUCTION REPORT 5

1/2

EXPERIMENTAL MEASUR. (U) ARMY ENGINEER WATERWAYS

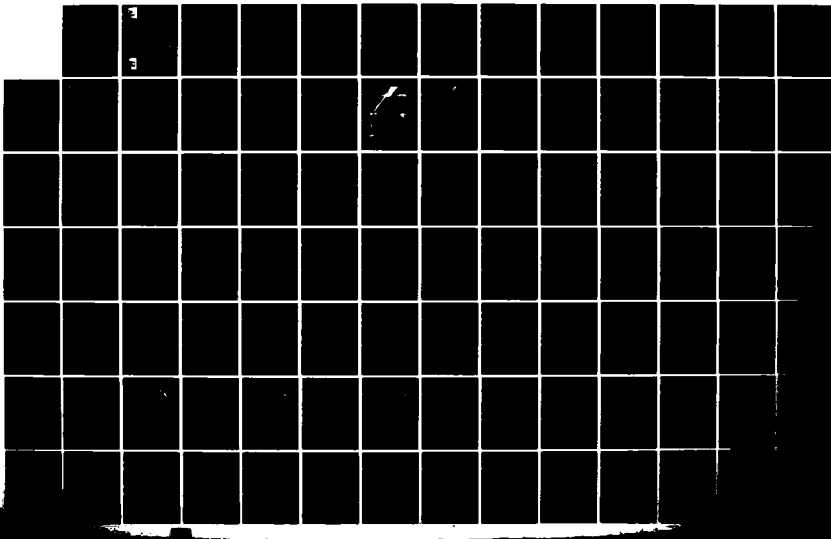
EXPERIMENT STATION VICKSBURG MS HYDRA. L Z HALE

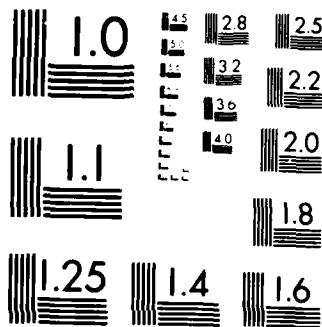
UNCLASSIFIED

SEP 84 WES/TR/HL-80-3-5

F/G 13/2

NL





MICROCOPY RESOLUTION TEST CHART
NATIONAL BUREAU OF STANDARDS 1964



US Army Corps
of Engineers

AD-A149 743

TECHNICAL REPORT HL-80-3

EROSION CONTROL OF SCOUR DURING CONSTRUCTION

Report 5

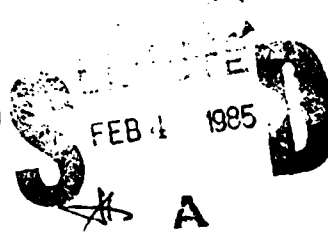
EXPERIMENTAL MEASUREMENTS
OF REFRACTION AND DIFFRACTION
DOWNCOAST OF AN OBLIQUE BREAKWATER

by

Lyndell Z. Hales

Hydraulics Laboratory

DEPARTMENT OF THE ARMY
Waterways Experiment Station, Corps of Engineers
PO Box 631
Vicksburg, Mississippi 39180-0631

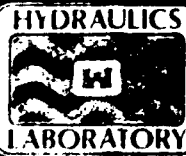


September 1984

Report 5 of a Series

Approved For Public Release Distribution Unlimited

DMC FILE COPY



Prepared for

DEPARTMENT OF THE ARMY
US Army Corps of Engineers
Washington, DC 20314-1000

85 01 24 126

Destroy this report when no longer needed. Do not return it to the originator.

The findings in this report are not to be construed as an official Department of the Army position unless so designated by other authorized documents.

The contents of this report are not to be used for advertising, publication, or promotional purposes. Citation of trade names does not constitute an official endorsement or approval of the use of such commercial products

Unclassified

SECURITY CLASSIFICATION OF THIS PAGE (When Data Entered)

REPORT DOCUMENTATION PAGE		READ INSTRUCTIONS BEFORE COMPLETING FORM
1. REPORT NUMBER Technical Report HL-80-3	2. GOVT ACCESSION NO. 11D P147743	3. RECIPIENT'S CATALOG NUMBER
4. TITLE (and Subtitle) EROSION CONTROL OF SCOUR DURING CONSTRUCTION; Report 5, EXPERIMENTAL MEASUREMENTS OF REFRACTION AND DIFFRACTION DOWNCOAST OF AN OBLIQUE BREAKWATER		5. TYPE OF REPORT & PERIOD COVERED Report 5 of a series
7. AUTHOR(s) Lyndell Z. Hales		6. PERFORMING ORG. REPORT NUMBER
9. PERFORMING ORGANIZATION NAME AND ADDRESS US Army Engineer Waterways Experiment Station Hydraulics Laboratory PO Box 631, Vicksburg, Mississippi 39180-0631		10. PROGRAM ELEMENT, PROJECT, TASK AREA & WORK UNIT NUMBERS
11. CONTROLLING OFFICE NAME AND ADDRESS DEPARTMENT OF THE ARMY US Army Corps of Engineers Washington, DC 20314-1000		12. REPORT DATE September 1984
		13. NUMBER OF PAGES 140
14. MONITORING AGENCY NAME & ADDRESS (if different from Controlling Office)		15. SECURITY CLASS. (of this report) Unclassified
		15a. DECLASSIFICATION/DOWNGRADING SCHEDULE
16. DISTRIBUTION STATEMENT (of this Report) Approved for public release; distribution unlimited.		
17. DISTRIBUTION STATEMENT (of the abstract entered in Block 20, if different from Report)		
18. SUPPLEMENTARY NOTES Available from National Technical Information Service, 5285 Port Royal Road, Springfield, Virginia 22161.		
19. KEY WORDS (Continue on reverse side if necessary and identify by block number) Scour (Hydraulic engineering) (LC) Breakwaters (LC) Water waves--Diffraction (LC) Refraction (LC) Shore protection (LC)		
20. ABSTRACT (Continue on reverse side if necessary and identify by block number) When major stone structures are erected in the coastal zone, they alter currents that are in dynamic equilibrium with the existing conditions. Waves breaking on the structures may cause bottom material to be suspended and transported from the region. The result is scour, or erosion, that usually develops along the toe of the structure. To minimize potential cost increases due to scour during construction, it is necessary to quantify the probability and ultimate extent of potential scour during the scheduled		
(Continued)		

Unclassified

SECURITY CLASSIFICATION OF THIS PAGE(When Data Entered)

20. ABSTRACT (Continued).

construction period. Objectives of this research program are to develop techniques to minimize and control scour during nearshore construction, and to predict the probable magnitude of scour that may result as a function of currents and wave climate. One phase of the research program is development of numerical techniques (incorporating both refraction and diffraction effects near the structure) for computing wave-induced velocities, tidal currents, and wave heights in the vicinity of structures, and applying these results to determine sediment transport of the bottom material at the particular site.

The present state of nearshore current and wave theories has reached the point where detailed experimental investigations are required for the verification of analytical developments and numerical models. To provide a foundation for further advancements, a simple beach profile consisting of straight, uniform contours parallel with the shoreline was experimentally studied by Hales (1980). A shore-connected, vertical, thin, impermeable barrier (breakwater) was installed perpendicular to the shoreline to simulate prototype jetties and breakwaters commonly occurring along many coasts. The purpose of the present study is to extend the previous work of Hales (1980) by installing a shore-connected, vertical, thin, impermeable breakwater at a 60-deg angle to the shoreline to simulate a larger range of prototype jetties and breakwaters in existence at the present time. Experimental measurements of refraction and diffraction downcoast of this oblique structure were made to obtain quantitative knowledge of this phenomenon in the lee of the jetty or shore-connected breakwater. These data were then compared with the uniformly valid asymptotic theory of Liu, Lozano, and Pantazaras (1979) for the same arrangement.

The numerical model for determining wave heights downcoast of a straight breakwater at an angle to the shoreline under combined refraction and diffraction, based on the uniformly valid asymptotic theory, was obtained by contract with Dr. Philip Liu, Cornell University. Because the uniformly valid asymptotic theory is developed from the small amplitude wave assumptions, the effect of varying the incident wave height on the wave-height amplification factor, H/H_0 , was investigated. The theory and experimental data were found to compare favorably for all wave heights tested in the shadow zone, but diverged with increase in incident wave height farther downcoast out of the shadow zone. While the uniformly valid asymptotic theory is far superior to diffraction theory alone under these conditions, additional numerical work should incorporate nonlinear wave theories for completeness.

Unclassified

SECURITY CLASSIFICATION OF THIS PAGE(When Data Entered)

PRIVACY

The study reported herein was authorized as a part of the Research and Development Program by the Office, Chief of Engineers, US Army. This particular work unit, Erosion Control of Seabed Sedimentation, is part of the Improvement of Operations and Maintenance Techniques (IOMT) Program. Mr. James L. Gottesman was the OCE Technical Monitor for the IOMT Program during preparation and publication of this report.

This study was conducted during the period 1 May 1980 through 30 September 1981 by personnel of the Hydraulics Laboratory of the US Army Engineer Waterways Experiment Station (WES) under the general supervision of Messrs. H. B. Simmons, Chief of the Hydraulics Laboratory; F. A. Hermann, Jr., Assistant Chief of the Hydraulics Laboratory; R. A. Sager, Chief of the Estuaries Division and IOMT Program Manager; Dr. R. W. Whalin, former Chief of the Wave Dynamics Division; Mr. D. D. Davidson, Chief of the Wave Research Branch; and Dr. J. R. Houston, Research Engineer and Principal Investigator for the Erosion Control of Scour During Construction work unit. The Wave Dynamics Division was transferred to the Coastal Engineering Research Center (CERC) of WES on 1 July 1983 under the direction of Dr. R. W. Whalin, Chief, and Dr. L. E. Link, Jr., Assistant Chief. Dr. L. Z. Hales, Research Hydraulic Engineer, Mr. K. A. Turner, Computer Specialist, Ms. M. L. Hampton, Computer Technician, Mr. R. E. Ankeny, Computer technician, and Mr. K. M. Strausbaugh, Civil Engineering Technician, performed the experimental portion of the study described herein. The numerical model for determining wave heights downcoast of a straight breakwater at an angle to the shoreline under combined refraction and diffraction, based on the uniformly valid asymptotic theory, was obtained by contract with Dr. Philip Liu, Cornell University. Dr. Hales prepared this report.

Commanders and Directors of WES during the conduct of this investigation and the preparation and publication of this report were COL Nelson P. Conover, CE, and COL Telford C. Creel, CE. Technical Director was Mr. F. R. Brown.

CONTENTS

	<u>Page</u>
PREFACE	1
CONVERSION FACTORS, US CUSTOMARY TO METRIC (SI) UNITS OF MEASUREMENT	3
PART I: INTRODUCTION	4
Statement of the Problem	4
Objective and Scope of the Study	5
PART II: EXPERIMENTAL INVESTIGATION	7
Experimental Layout	7
Instrumentation for Wave-Height Determination	8
Wave Gage Locations	12
PART III: LITERATURE REVIEW OF COMBINED REFRACTION AND DIFFRACTION	17
Water Wave Refraction	17
Water Wave Diffraction	22
Combined Water Wave Refraction and Diffraction	26
PART IV: UNIFORMLY VALID ASYMPTOTIC THEORY	31
Background	31
Development of Asymptotic Theory	31
PART V: DISCUSSION AND RESULTS	36
Background of the Study	36
Experimental Requirements	36
Degree of Linearity	37
Wave-Height Data	40
Study Results	40
PART VI: CONCLUSIONS	43
REFERENCES	44
TABLES 1-19	
PHOTOS 1-9	
PLATES 1-50	
APPENDIX A: NOTATION	A1
APPENDIX B: UNIFORM ASYMPTOTIC THEORY, LIU, LOZANO, AND PANTAZARAS (1979) FOR COMBINED REFRACTION AND DIFFRACTION DOWNCOAST OF AN OBLIQUE BREAKWATER	B1

CONVERSION FACTORS, US CUSTOMARY TO METRIC (SI)
UNITS OF MEASUREMENT

US customary units of measurement used in this report can be converted to metric (SI) units as follows:

Multiply	By	To Obtain
feet	0.3048	metres
feet per second	0.3048	metres per second
feet-feet per second	0.0929	metres-metres per second
feet per second per second	0.3048	metres per second per second
pounds-second-second per foot per foot per foot per foot	52.5540137	kilograms-second-second per metre per metre per metre per metre
square feet	0.09290304	square metres

EROSION CONTROL OF SCOUR DURING CONSTRUCTION

EXPERIMENTAL MEASUREMENTS OF REFRACTION AND DIFFRACTION DOWNCOAST OF AN OBLIQUE BREAKWATER

PART I: INTRODUCTION

Statement of the Problem

1. When major structures are erected in the coastal zone, they alter currents that are in dynamic equilibrium with the existing bathymetry. These altered currents may change the existing bathymetry. In addition, waves breaking on the new structure will cause bottom material to be suspended and transported from the region by longshore or other currents. This removal of material from around structures is often not compensated by an influx of additional material; the result is scour, or erosion, that usually develops along the toe of the structure. In order to ensure structural stability, the scour area must be filled with nonerodible material (sufficiently stable to withstand the environmental forces to which it will be subjected). This may result in additional quantities of material being required during construction that can potentially be very costly. To minimize potential cost increase due to scour during construction, it is necessary to quantify the probability and ultimate extent of potential scour during the scheduled construction period.

2. Effective, comprehensive, and low cost procedures do not exist for eliminating scour during construction in the nearshore environment. Determination of potential alternative procedures is seriously hampered by the inability to predict the extent of potential scour. Objectives of the Erosion Control of Scour During Construction research program are to develop techniques to minimize and control scour during nearshore construction, and to predict the probable magnitude of scour that may result as a function of currents and wave climate. One phase of the research program is development of numerical techniques (incorporating both refraction and diffraction effects) for computing the wave field in the vicinity of structures.

3. The present state of nearshore current and wave theories has reached the point where detailed experimental investigations are required for the verification of analytical developments and numerical models. To provide a

firm foundation for further advancements, a simple beach profile consisting of straight, uniform contours parallel to the shoreline was experimentally studied by Hales (1980). A shore-connected, vertical, thin, impermeable barrier (breakwater) was installed perpendicular to the shoreline to simulate prototype jetties and breakwaters commonly occurring along many coasts. This single jetty (shore-connected breakwater) simplified the experiment, facilitated direct comparisons with numerical model results, and provided greater understanding and insight into the phenomenon of wave-height variations down-wave of a breakwater than would a more complex geometry.

4. Analytical models of wave fields surrounding shore-normal breakwaters have been developed based on asymptotic theory and the parabolic approximation (for example, Liu and Mei 1975, 1976; Liu, Lozano, and Pantazaras 1979; and Lozano and Liu 1980). These analytical models have been compared with the experimental data of Hales (1980) by Liu (1982) and Tsay and Liu (1982), and the overall agreement between theory and experiment was considered to be good. Knowledge of these important phenomena can be used as the basis for advanced studies of sediment movement around major structures under combined effects of refraction and diffraction, when the structure is oriented perpendicular to the shoreline.

Objective and Scope of the Study

5. The objective of the present study was to extend the previous experimental work of Hales (1980) by installing a shore-connected, vertical, thin, impermeable barrier (breakwater) at a 60-deg angle to the shoreline to simulate a larger range of prototype jetties and breakwaters in existence and to test a new theory of waves in the lee of a structure. The experimental measurements were made to obtain quantitative knowledge of combined refraction and diffraction in the lee of a jetty or shore-connected breakwater. These data were then compared with the uniformly valid asymptotic theory of Liu, Lozano, and Pantazaras (1979) for the same arrangement, thus providing verification data for this numerical approximation which has not been previously available. This report presents details of the experimental investigation to measure combined refraction and diffraction in the lee of a jetty or breakwater. A literature review of the theory of refraction and diffraction is presented. In addition, a new uniformly valid asymptotic theory of combined

subtraction and multiplication, and division, and division
comparisons made with other effective procedures.

PART II: EXPERIMENTAL INVESTIGATION

Experimental Layout

6. This study to investigate wave heights downcoast of an obliquely oriented shore-connected breakwater or jetty under the combined effects of refraction and diffraction was conducted in the experimental facilities of the US Army Engineer Waterways Experiment Station (WES). The experimental arrangement, which was molded in cement mortar, consisted of a 50- by 60-ft* area, with a water depth of 1 ft in the open-ocean region (Figure 1). The

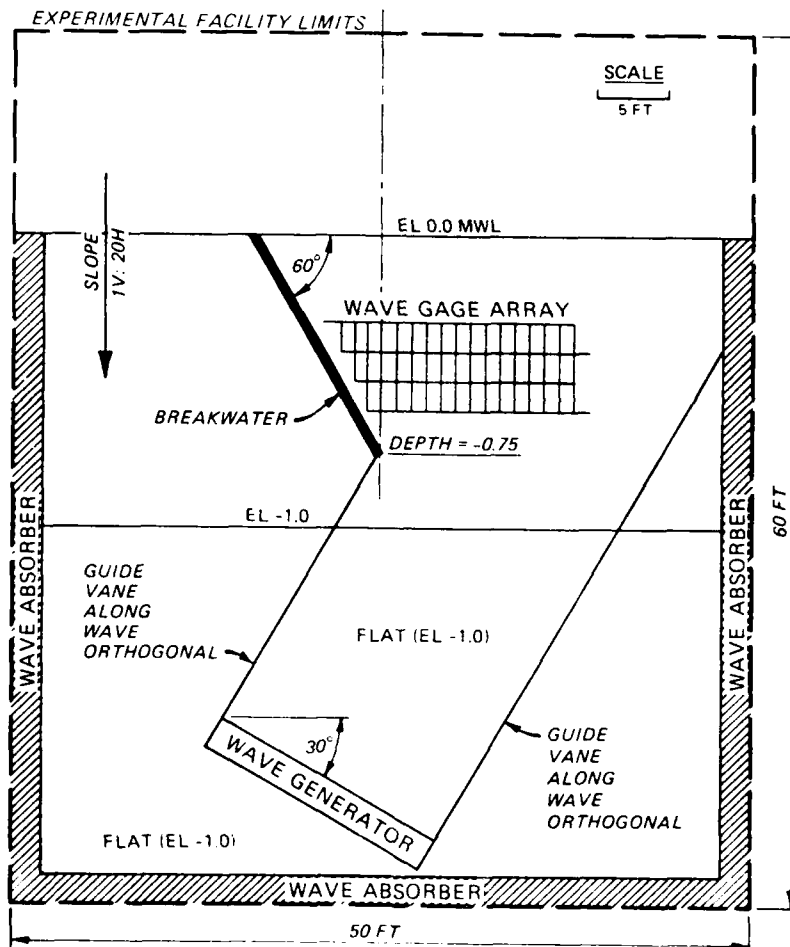
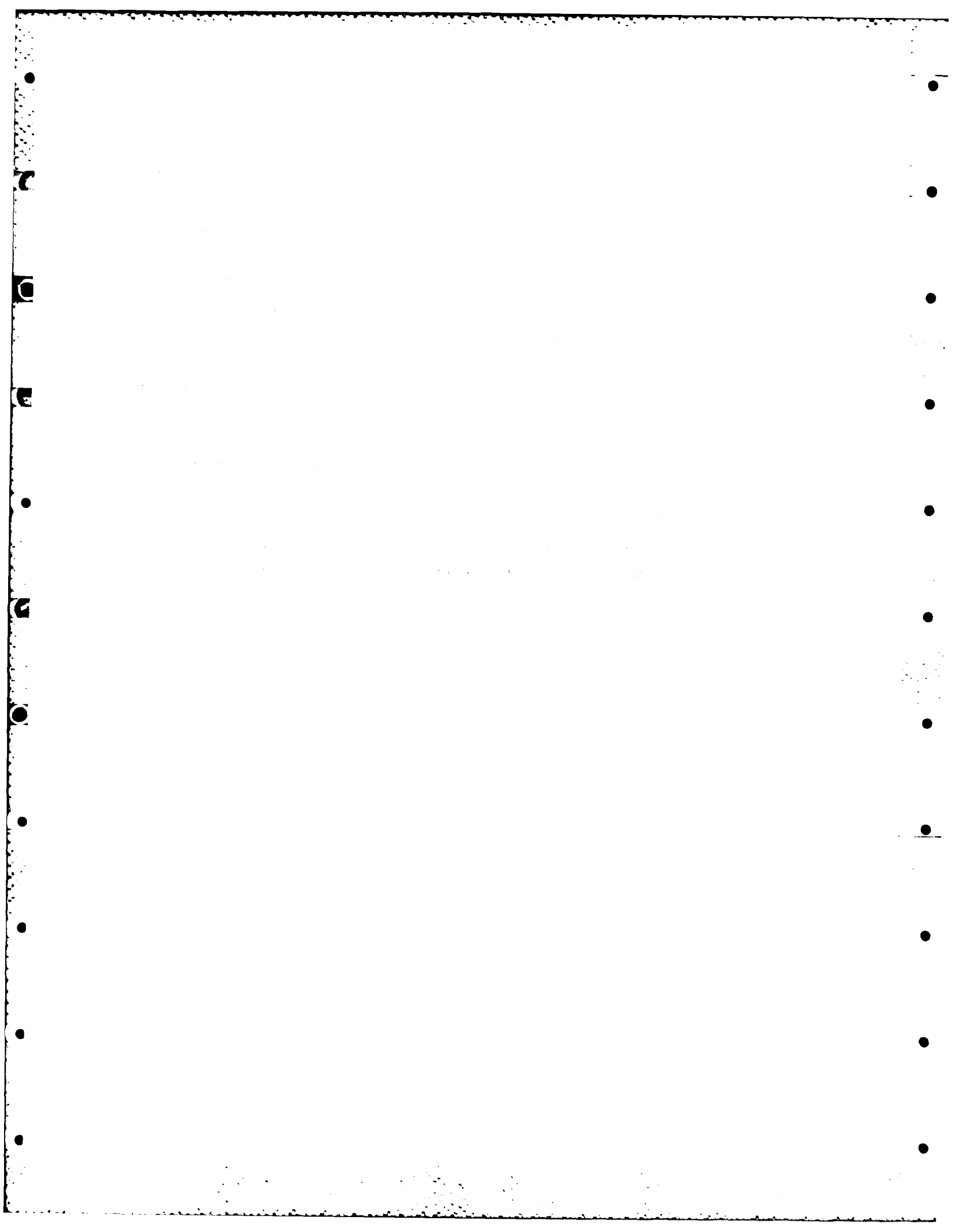


Figure 1. Experimental layout

* A table of factors for converting US customary units of measurements to metric (SI) units is presented on page 3.



9. The ADACS are capable of automatically calibrating the wave sensors, controlling wave generators, acquiring data from the sensors at a high sampling rate, and analyzing test data. Data are taken and recorded on disc or magnetic tape for direct analyses by the minicomputer system or on magnetic tape in a format compatible with a Honeywell DPS1 for backup analyses. Automatic calibration of wave sensors has reduced the time required to calibrate the sensors by a factor of four. In addition, several times the number of tests can be run during a day with test results analyzed at completion of model tests by minicomputer. The system configuration (Figure 2) of ADACS consists of the following subsystems: (a) digital data recording and controls; (b) analog recorders and channel selection circuits; (c) wave sensors and interfacing equipment; and (d) wave generators and control equipment.

Wave sensors

10. The data acquired from wave experiments are the water-surface

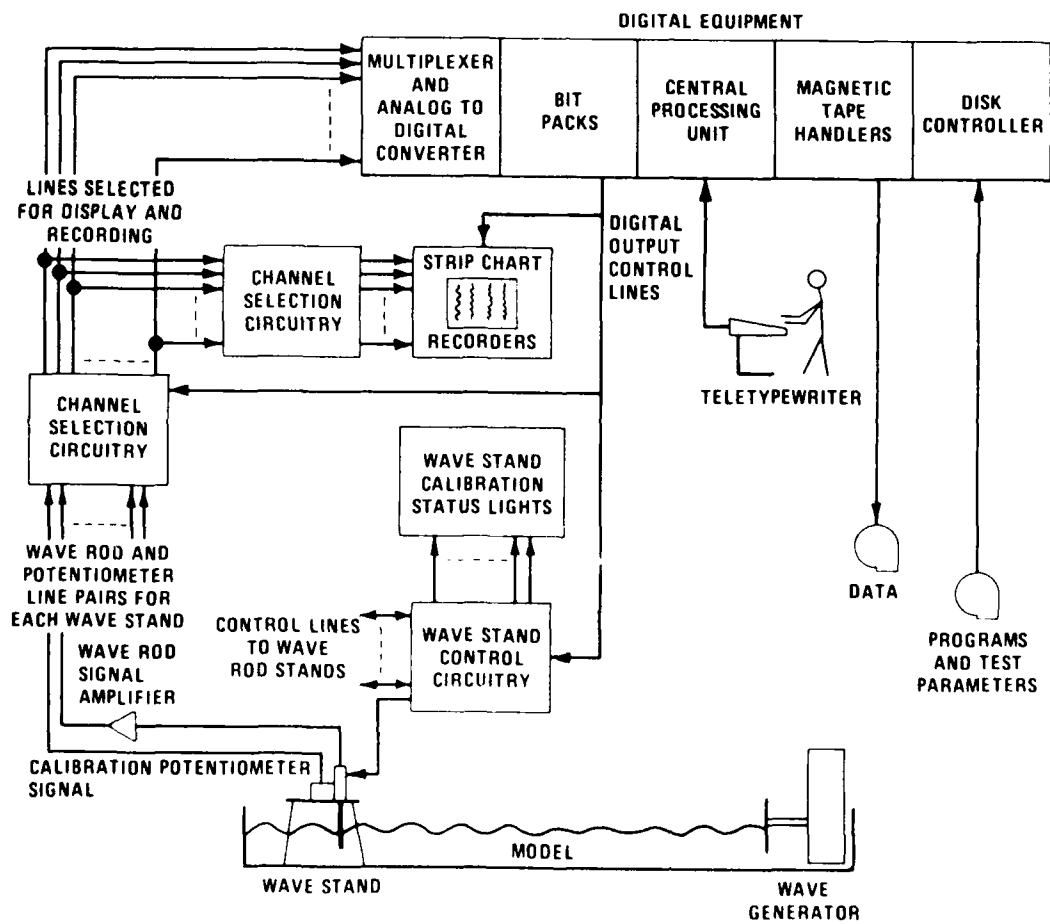


Figure 2. Schematic of components of ADACS

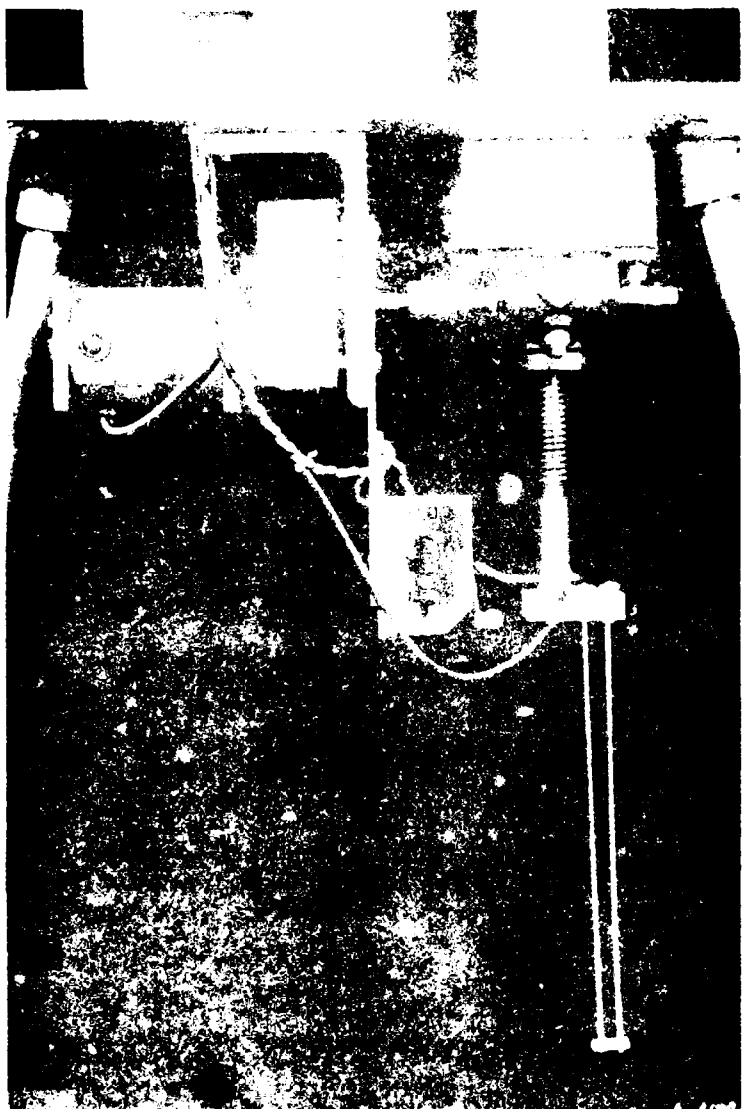


Figure 3. Prototype

variations about a reference water level. This information is collected at selected geographic locations within the experimental facility for specified wave conditions at the generator. Wave sensors are used to obtain this information at selected locations in the facility. Each of the water-surface-piercing, parallel rod wave sensors is connected to a Wheatstone bridge, and a transducer measures the conductance of the water between the two parallel rods that are mounted vertically (Figure 3). The conductance is directly proportional to the depth of submergence of the two rods in the water. The output of each wave sensor is routed through shielded cables to its signal conditioning equipment where it is processed for recording. The

ADCS

can make surface elevations to an accuracy of 0.001 ft.

ADCS

can supply power supplies and good signal-to-noise

ADCS

and the wave sensor bridge maintains

ADCS

the wave sensor bridge provides elevation data in millivolts to the computer. Before the wave sensor must be calibrated. The calibration is done by wave sensors (maximum of 25 rods per wave) provided by ADACS. To calibrate

each set of parallel rods, the voltage from the signal conditioning equipment is monitored and recorded as the parallel rods are moved vertically a known distance into or out of the water. A precision, linear-position potentiometer is located on the wave sensor stand and is coupled directly to the parallel rods by a gear train driven by an electric motor. By moving vertically the coupled wave sensor and potentiometer with the electric motor and by monitoring the output voltage from the potentiometer, the wave sensor can be moved vertically a precise distance. The electric motor for each wave sensor is controlled by a control/sense line and a relay contact. The minicomputer controls the vertical movement of each wave sensor by actuating the control/sense line. The central processing unit acts as a voltage comparator by monitoring the potentiometer voltage and comparing it with a reference voltage which is determined from desired displacement and potentiometer calibration. When the voltage comparison is satisfied, the control/sense line is reactivated, the electric motor stops, and voltage samples from the rods and potentiometers are acquired. By systematically moving each wave sensor through 11 quasi-equally spaced locations over the range of rod length used, voltage versus known displacements are obtained from which a calibration curve for each sensor can be calculated and recorded on magnetic tape or disc. After collecting the calibration data, the minicomputer analyzes these data by least-squares fitting a set of curves (linear, quadratic, or spline) to the data, determining the best order of fit, and comparing the maximum deviation of the best fit with a previously acceptable value for this maximum deviation.

Data acquisition and analysis

12. During the acquisition mode, wave data for a specified wave condition at the wave generator are collected from a maximum of 50 wave sensors, recorded on analog strip charts, digitized, and recorded on magnetic tape or disc for further analyses. The sampling scheme is flexible and can be tailored for different applications with maximum throughput rates theoretically limited by the multiplexer rate and allocatable buffer size. The sampling scheme used in this investigation was 60 discrete voltage samples equally spaced over each wave period for a predetermined number of 90 wave periods for each of the sensor locations. The minicomputer calculated from input parameters the lag at the beginning of data acquisition by 10 wave periods after starting the generator, provided timing pulses for synchronizing and controlling the recorders, and determined completion of the test. The determination of the height of

each wave of the monochromatic wave train was performed (at each sensor location), the average of these 90 individual heights was calculated, and the standard deviation of these individual observations about the mean was computed. The value ultimately determined as the wave height at each sensor location was this mean value plus or minus one standard deviation.

Wave Gage Locations

13. The wave-height data downcoast of the experimental breakwater that was positioned at a 60-deg angle with the shoreline were obtained by operating 36 wave-height sensors simultaneously for each test condition. Two of these wave-height sensors were located in the deeper water (1 ft deep) near the wave generator to ascertain the initial generated wave height. The remaining 34 sensors were positioned along four lines parallel with the shoreline at distances of 6, 8, 10, and 12 ft from the shoreline (Figure 4); the still-water depths at these four sections were 0.3, 0.4, 0.5, and 0.6 ft, respectively. The wave gages were placed on a supporting platform such that only the wave sensor probe penetrated the water surface, thereby eliminating any local disturbance caused by instrument stands touching the water surface. A dry bed photograph of the experimental facility with the experimental breakwater in place is shown in Figure 5.

14. In order to compare experimental results with numerical or analytical investigations, it is necessary to have good definition of the experimental data. The 34 wave-height sensors were initially placed at 2-ft intervals along the four sections parallel with the shoreline, and the complete set of experimental data was obtained (gage arrangement No. 1, Figure 6). To provide a more dense data display, the entire physical arrangement of the wave sensors was displaced laterally along the four section lines for a distance of 1 ft, and the same set of wave data (period and height) was repeated. This second testing arrangement is shown as gage arrangement No. 2, Figure 7. All data from these two gage arrangements resulted in a data set that presented the wave heights at 1-ft increments along the four sections which run parallel with the shoreline, with the data extending from very near the breakwater deep in the shadow zone and extending across the region where the waves experience both refraction and diffraction. These precise experiments provide data that define the wave height downcoast of the structure and can be used for comparison with numerical or analytical studies of the same concept.

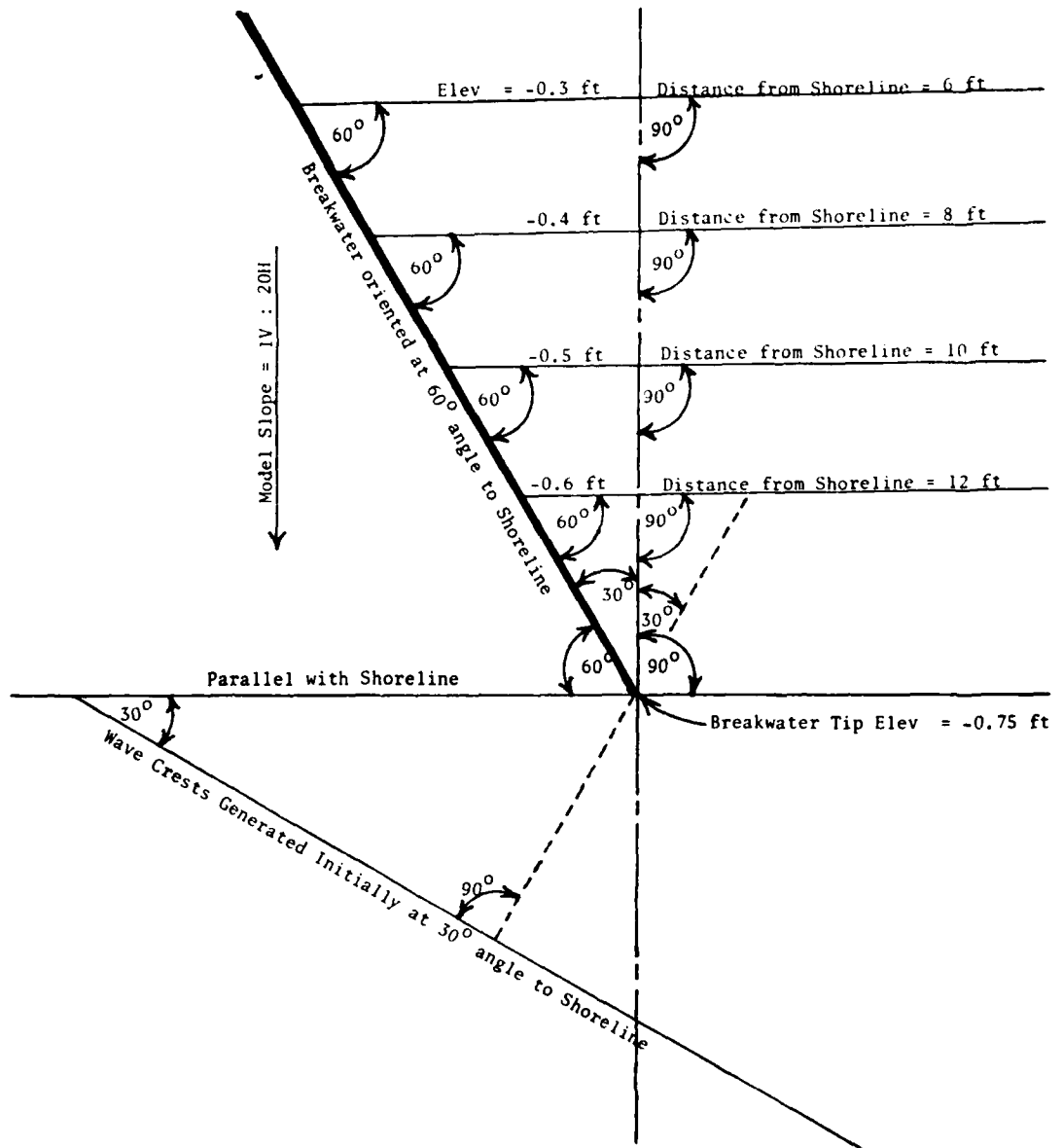


Figure 4. Experimental layout showing location of four sections parallel with shoreline along which wave-height sensors were positioned

Fig. 1. Graph of experiment facility with breakwater in place, showing four test sites which have eight transects, one point-one-m elevation of each section.



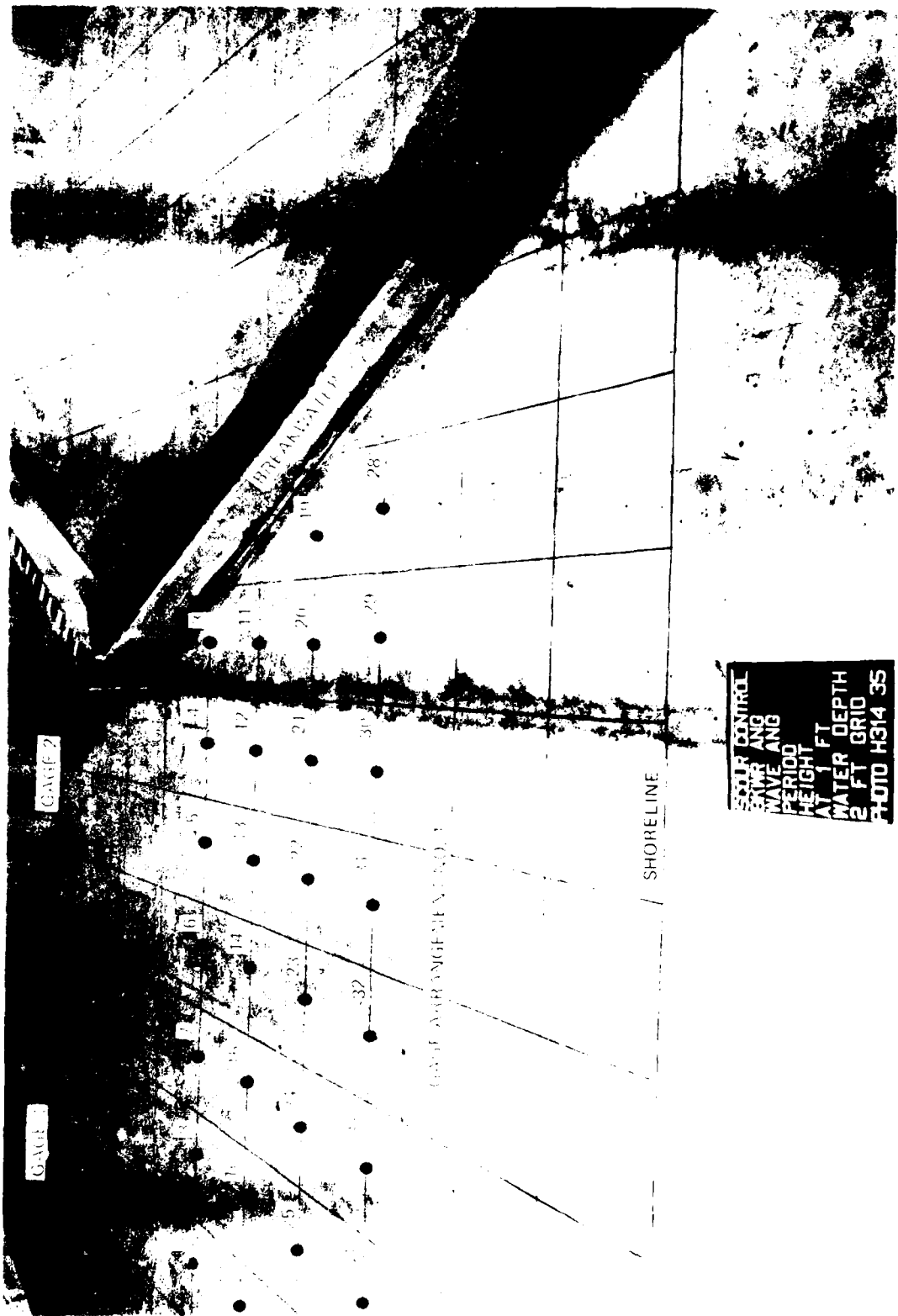


Figure 6. Wave gage arrangement No. 1, showing location of wave-height sensors

FIGURE 2. Wave gauge arrangement No. 2, showing location of wave-height sensors.



PART III: LITERATURE REVIEW OF COMBINED REFRACTION AND DIFFRACTION

15. The approximate solution of water wave refraction caused by a variable bathymetry is well known and can be derived by assuming that bottom reflections are negligible or by the more rigorous Wentzel-Kramers-Brillouin (WKB) approximation. The exact solution for the diffraction of surface waves by vertical barriers of simple cross section in water of constant depth also is well known (being analogous to classical problems of physics). However, an analytical theory for the practical case of combined refraction and diffraction has not been completely developed. The present engineering practice for determining wave heights under this condition is a stepwise procedure (Dunham 1951, Liu and Mei 1976, US Army Coastal Engineering Research Center 1977). The procedure involves the following steps: (a) calculate refraction effects up to the barrier (jetty or shore-connected breakwater); (b) calculate for a "few" wavelengths the effects of diffraction, assuming a constant water depth; and (c) beyond this region calculate the refraction effects only. This procedure is obviously imprecise, and Mobarek (1962) indicates that the method is suitable only for intermediate water depths. In addition, Whalin (1972) states that this procedure is only valid for small refraction effects.

Water Wave Refraction

16. In intermediate and shallow water, the phase speed of a surface gravity wave depends on water depth. Since wave celerity decreases as depth decreases, phase velocity varies along the crest of a wave propagating at an angle to underwater contours because that part of the wave in deeper water moves faster than that part in shallower water. This variation causes the wave crest to bend toward alignment with the contours. This bending effect due to changes in bottom topography, called refraction, depends on the relation of water depth to wavelength, d/L , and is analogous to refraction of other types of waves such as light. A basic assumption in wave refraction theory is the conservation of energy between wave orthogonals (i.e., no diffraction of energy along wave crests). The change in wave direction of different parts of the wave results in convergence or divergence of wave energy and materially affects the forces exerted by waves on structures and of the

capacity of waves to transport sand either alongshore or onshore/offshore.

17. Procedures for the computation of refraction of surface gravity waves on water of nonuniform depth involve the assumption that a wave with a curved crest pattern and variable amplitude along the crest behaves locally as a straight-crested wave of constant amplitude. Rayleigh (1877) appears to have been the first to use the approximations of geometrical optics in this analysis, and theoretical results have been developed with respect to energy flux and phase speed. As expressed by Keller (1958), the geometrical optics theory defines a propagation velocity at each point on the water surface, with this velocity being exactly that which waves of given period would have in water of uniform depth at all points. By employing Fermat's principle of optics, wave rays are defined and surface waves are assumed to propagate along these rays. The variation of the amplitude along the rays is determined by the use of the principle of conservation of energy. This principle (in its optical form) states that the flux of energy is the same at all cross sections between two adjacent wave rays. The energy flux is proportional to the square of the amplitude of the waves and to the distance between the rays, and hence the wave-height variation along the rays is available.

18. Keller's (1958) derivation is based upon an "asymptotic" solution of the equations of the exact linear theory for periodic waves in water of arbitrary nonuniform depth. The solution is asymptotic in the sense that the depth and wavelength are small compared with the horizontal scale of the bottom contours. The first term of the solution agrees exactly with the asymptotic form of the solution for waves in water with a uniformly sloping bottom as the bottom slope tends to zero. This solution conforms with all the principles of the geometrical optics theory of Rayleigh (1877) and thus provides a derivation of that theory. The results are not valid, however, at caustics or ray crossings.

19. In problems of linear wave propagation over mild slopes, the principle of geometrical optics has been applied by Carrier (1966) as the first approximation in a systematic perturbation scheme while the bottom is considered to be locally horizontal. The depth variation was dealt with afterward by requiring the appropriate energy conservation. This was also the basic idea for the work of Koh and LeMaître (1966) in which the transformation of progressive waves was investigated as they travel from deep water to shore. The Stokes' theory at a fifth order of approximation was applied along

with the method of conservation of energy flux. It is assumed that the wave is simply harmonic in time. The first, third, and fifth orders of approximation were compared with each other and with experiments. The differences between the predictions of wave-height changes based on the three orders of approximation were found to be small, on the order of 5 percent. For practical purposes, the third-order theory was found to give reliable results. The third and fifth order Stokes' theories are based on a series expansion in terms of H/L where terms of the order of $(H/L)^3$ and $(H/L)^5$, respectively, are retained and higher order terms are neglected. It should be noted that this theory is based on an expansion in term of the wave steepness, H/L , and consequently can be expected to better approximate limiting steepness waves in deep water. However, it cannot be expected to adequately predict wave characteristics in shallow water, since water depth is not a parameter in the series expansion. Thus the theory is a finite amplitude deepwater wave theory.

20. In cases of limiting shallow water, the wave conditions are nearly independent of wavelength, and the important parameters are water depth and the ratio of wave height to water depth. Keulegan (1950) showed that Stokes waves are most nearly valid in water deeper than about $d/L > 1/8$ to $1/10$. In shallower water, cnoidal wave theory appears to be more satisfactory, and Masch (1964) investigated the problem of wave shoaling using cnoidal wave theory with the formulas developed by Keulegan and Patterson (1940). Masch (1964) assumed hydrostatic pressure distribution and neglected the convective inertia term in his expression for the energy flux. The third and fifth order cnoidal theories are based on a series expansion in terms of H/d , where terms of the order of $(H/d)^3$ and $(H/d)^5$, respectively, are retained and higher order terms neglected. It should be noted that this theory is based on an expansion of the relative wave height (H/d) and can be expected to better approximate the wave form in shallow water. However, it cannot be expected to do a very good job of approximating the wave form for limiting steepness waves in deep water. In that case, water depth is unimportant and wavelength is crucial. This theory could be considered a finite amplitude intermediate and shallow-water theory.

21. A technique of "asymptotic expansion" was applied by Mei, Tlapa, and Eagleson (1968) to water wave propagation over an uneven bottom that has straight and parallel contours. Attention was focused on the establishment of a rigorous scheme of successive approximation for higher order corrections.

The bottom depth was assumed to vary with time as a smooth function of the horizontal coordinate, or in the direction normal to the coastline, and by assuming an expansion of the WKB type, the weakness of the depth variation in the normal direction was incorporated in the mathematical formulation. The conventional linearized theory of wave refraction was obtained in the first-order solution without the explicit assumption of smallness. In the second-order, a steady-state depression of the mean water surface was found for the geometric case where the incident wave approaches the coast obliquely. In the first order, this development was the same as the classical theory of hydrodynamics (1877). At higher order, some differences existed from the usual adaptation of the Stokes' theory for a horizontal bottom. The cause of the difference is the explicit appearance of the variation of the bottom boundary conditions for the first harmonic at second and higher orders. The theory is expected to hold up to the neighborhood where the wave breaks, except at the shoreline where a singularity exists for all orders.

22. The refraction of surface gravity waves, neglecting nonlinearity, third was investigated by Battjes (1968) with amplitudes small so that linear theory was applicable and harmonic in time. It was known a priori that the velocity of propagation of a wave crest to the first order and greater is a function of the wave height. The zone of convergence or divergence of wave energy, gradients in wave height and bending of the crests of the wave crests in the regions of greater wave height is appropriate to the theory of longer wave height and this will, in turn, create bending of the wave crests. In addition to that bending caused by the bottom topography, called *refraction*, this supplemental bending is not usually accounted for by refraction theory. Battjes (1968) developed an expression for the normal derivative to the wave crest because of wave-height variations along the crest from a direct derivation of the wave number, k_n . It was determined that the derivative of the exact wave number profile, $\partial k_n / \partial x$, plus corrections which depend on the wave height, is equal to the derivative of the phase speed, c_n , which is defined as

$$c_n = \left(\frac{k_n^2 + k_{\perp}^2}{k_n} \right)^{1/2} \left(1 + \frac{1}{2} \frac{\partial k_n^2}{\partial x} \right)^{-1/2}$$

where

g = gravitational constant, 32.174 ft/sec^2

k = wave number, $2\pi/L$, $1/\text{ft}$

d = local water depth, ft

a = local wave amplitude, ft

The second derivative of the wave amplitude in the horizontal plane is given by a_{xx} or a_{yy} . The rate of power transmission P , or energy flux, was determined to be:

$$P\Delta b = \left(\frac{1}{2} \rho g a^2 n \frac{\omega}{k} \Delta b \right) \left(1 + \frac{a_{xx} + a_{yy}}{k^2 a} \right)^{1/2} \quad (2)$$

where

Δb = wave ray spacing, ft

ρ = fluid density, $\text{lb-sec}^2/\text{ft}^4$

n = ratio of group velocity c_g , to phase velocity c , dimensionless

ω = angular frequency, $2\pi/T$, $1/\text{sec}$

Define:

$$\delta = \left(\frac{a_{xx} + a_{yy}}{k^2 a} \right)^{1/2} \quad (3)$$

The commonly used existing procedures (Dunham 1951, Liu and Mei 1976, CERC 1977) for construction or computation of refraction diagrams utilize phase speeds that are obtained by neglecting δ .

23. Battjes (1968) examined the omission of δ from a qualitative standpoint. In an area of strong local convergence, omission of δ from Equation 1 results in underestimating the local phase speed. The result is that in Equation 2 the ray separation Δb will be underestimated. Thus there are generally two contributions to the error that results in the computed wave amplitude a . However, these two contributions are of a different nature because the effect on the wave pattern of using an incorrect value for the phase speed is cumulative, whereas the effect on energy flux is local. In any case, the omission of δ will generate wave heights at variance with the height inferred from refraction diagrams based on linear small amplitude wave theory which neglects the effects of wave-height gradients along the wave crest, so that it would appear that energy had been transferred across orthogonals. An estimate of the magnitude of δ has been approximated by Battjes (1968) for four

distinctly different cases. For simple shoaling, the amplitude varies only in the direction of wave propagation, and for shallow water the variation was:

$$\delta = 8 \times 10^{-3} \left(\frac{L}{d} \right)^2 s^2 \quad (4)$$

where

L = local wavelengths

s = bottom slope

For short-crested waves where the distance along the wave crest is two or three times the wavelength, $\delta = -20$ percent or -10 percent, respectively. For the case of diffraction around a semi-infinite breakwater, δ was found to reach values between +10 percent and -10 percent at points a distance of one wavelength from the breakwater tip, decreasing inversely proportional to the distance from the tip. For the case of diffraction through a gap of width two times the wavelength, δ was evaluated in a few points on the center line of the gap where it was found to reach values of 25, 7, and 3 percent at distances of 1, 2, and 4 wavelengths, respectively, from the gap.

Water Wave Diffraction

24. Diffraction of water waves is the phenomenon by which wave energy propagates into the sheltered lee of structures even in the absence of bathymetric refraction. In these situations, wave crests bend (even in constant depth water) and gradients of wave height exist along the wave crest. This phenomenon is most visible when a train of regular waves is interrupted by an obstruction such as a jetty or shore-connected breakwater. The theory of water wave diffraction can be explained by Huygens' principle. Each point of an advancing wave front (wave crest) may be considered as the center of a secondary circular wave which advances in all directions. The resultant shape of the crest is the envelope of all these secondary waves. In a straight-crested wave train, the envelope of the secondary waves is a straight line also. When the wave passes an obstruction, the energy intensity at a certain point is a vector combination of all the circular waves emitted by every point of the passing wave train.

25. Sommerfeld (1896) presented a solution for the diffraction of light waves past the edge of a semi-infinite screen. Penny and Price (1944) showed that this is also the solution of the water wave diffraction problem at the

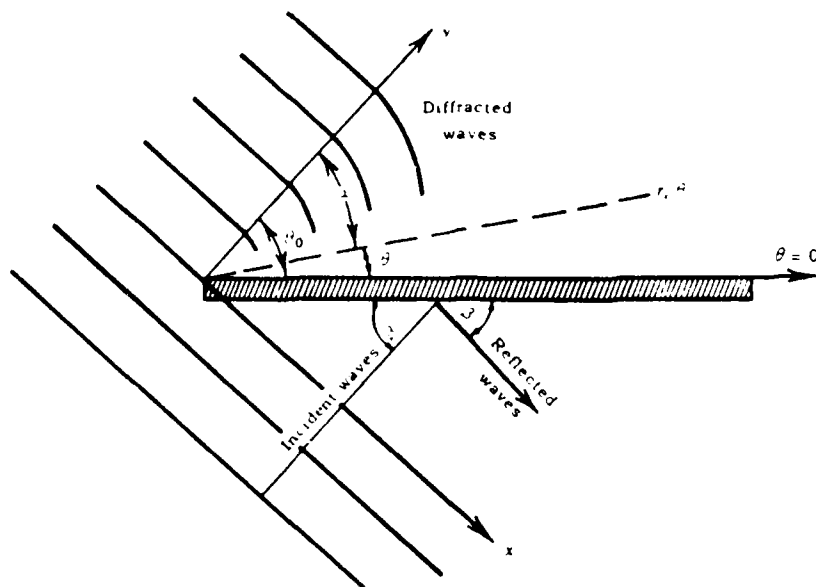


Figure 8. Definitive sketch, wave diffraction around a breakwater

end of a semi-infinite obstacle such as a jetty or shore-connected breakwater. This exact solution of the surface elevations behind the breakwater is applicable only to water of constant depth and waves of small amplitude. Putnam and Arthur (1948) summarized the solution of Penny and Price (1944) for the definitive sketch of Figure 8. In cylindrical coordinates, the water-surface elevation is:

$$\eta = \left(\frac{aikc}{g} \right) e^{ikct} \cosh kd F(r, \theta) \quad (5)$$

where

η = water-surface elevation, ft

i = square root of -1

and the other symbols have been previously defined. $F(r, \theta)$ is a function which satisfies the wave equation in cylindrical coordinates:

$$\frac{\partial^2 F}{\partial r^2} + \frac{1}{r} \frac{\partial F}{\partial r} + \frac{1}{r^2} \frac{\partial^2 F}{\partial \theta^2} + k^2 F = 0 \quad (6)$$

In the presence of a jetty or breakwater, the boundary condition is imposed so that the normal component of the fluid velocity is zero along the breakwater, leading to the solution:

$$F(r, \theta) = \frac{1}{\sqrt{2}} e^{i[(\pi/4) - kr \cos(\theta_o - \theta)]} \int_{-\infty}^{u_1} e^{-(i\pi u^2/2)} du + \frac{1}{\sqrt{2}} e^{i[(\pi/4) - kr \cos(\theta_o - \theta)]} \int_{-\infty}^{u_2} e^{-(i\pi u^2/2)} du \quad (7)$$

$$u_1 = 4 \sqrt{\frac{kr}{\pi}} \sin \left[\frac{1}{2} (\theta_o - \theta) \right] \quad (8)$$

$$u_2 = 4 \sqrt{\frac{kr}{\pi}} \sin \left[\frac{1}{2} (\theta_o + \theta) \right] \quad (8)$$

Bretschneider (1966) has presented computational procedures for evaluating the diffraction coefficients at arbitrary points behind jetties or breakwaters.

26. Wiegel (1962) developed a graphical procedure for determining diffraction coefficients of waves passing the tip of single breakwaters. The family of diagrams shows, for uniform water depth, lines of equal wave-height reduction displayed in terms of the diffraction coefficients. The diffraction diagrams (typical example, Figure 9) are constructed in polar coordinate form centered at the structure tip. The arcs behind the breakwater are spaced one radius-wavelength unit apart so in application, a specific diagram must be scaled up or down so that the particular wavelength corresponds to the scale of the hydrographic area under investigation. The set of diffraction diagrams of waves passing the tip of a single breakwater was presented by CERC (1977). Figure 9 is the configuration of the wave approach direction analogous to the physical hydraulic model layout used in this experimental investigation.

27. Laboratory tests were performed by Harms (1979) to investigate the distribution of wave heights in the lee of a breakwater (shore-connected) for waves normally incident upon the structure and with a horizontal bottom both in front of and in the lee of the structure. In general, satisfactory agreement was obtained between measurement and theory, but diffraction theory was not found to be conservative. At large distances in the shadow zone, measured wave heights consistently exceeded theoretical values. Close to the breakwater outside the shadow zone, the measured maximum wave height was also found to be larger than that predicted by theory. The diffraction behavior appeared

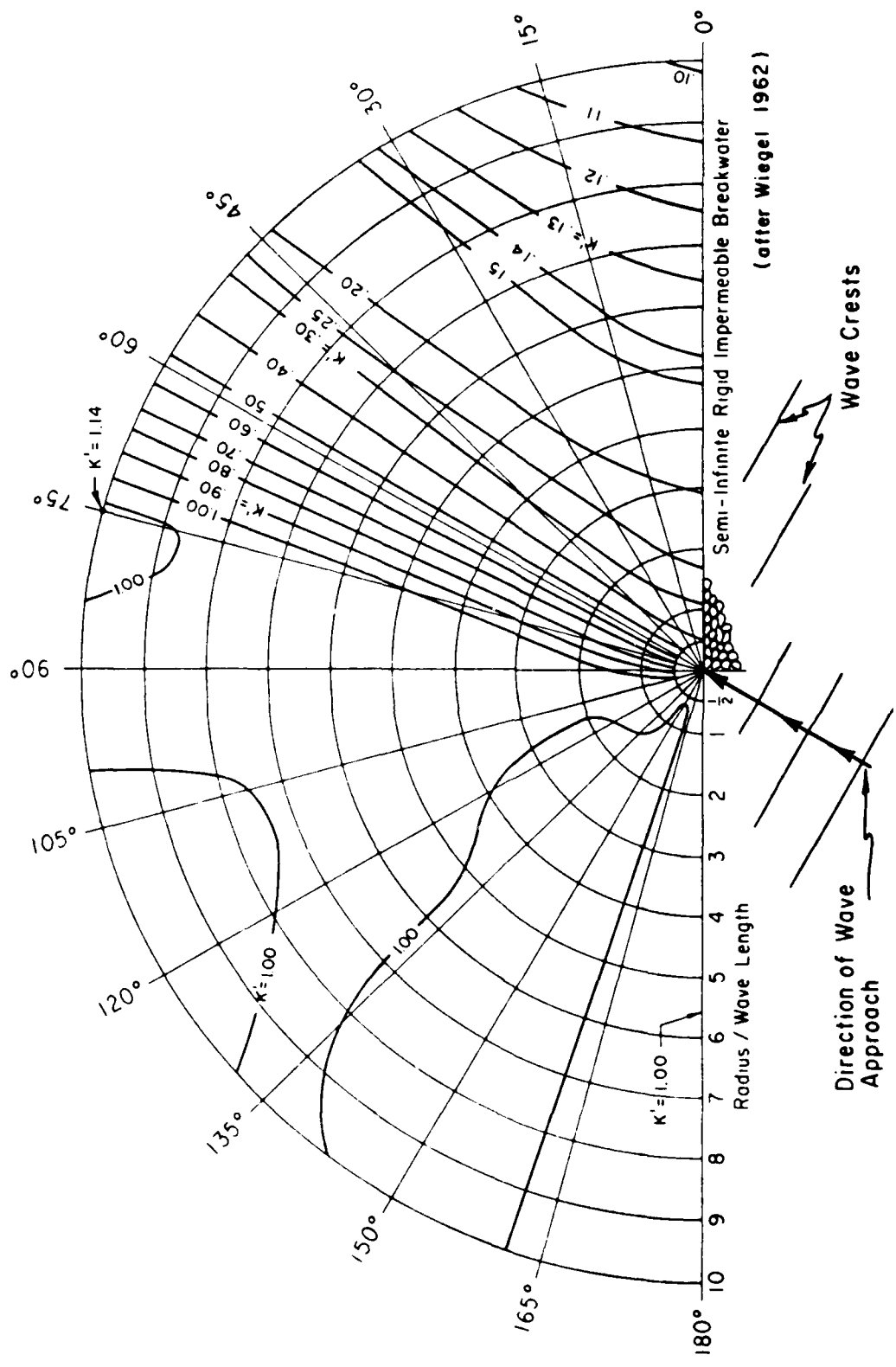


Figure 9. Typical example, wave diffraction past a semi-infinite breakwater, angle of incidence = 60 deg. This configuration is analogous to the physical hydraulic model layout of this experimental investigation

to be insensitive to the intensity of wave reflections from the seaward side of the breakwater.

Combined Water Wave Refraction and Diffraction

28. The bathymetry shoreward of a jetty or breakwater usually is not flat or even uniform; hence, refraction generally occurs in addition to the diffraction effects. While a general unified analytical approach to the simultaneous solution of these two distinctly different phenomena has not been entirely developed, considerable insight has been gained through the theoretical work of Liu and Mei (1975, 1976), Lick (1978), Liu and Lozano (1979), and through the earlier experimental work of Mobarek (1962). The procedure usually followed by coastal engineers concerned with wave-height variation behind jetties or breakwaters is to construct refraction diagrams shoreward to the structure, then construct diffraction diagrams for three or four wavelengths shoreward of the jetty, and finally refract the last wave crest on toward the shoreline. This procedure is schematized in Figure 10 where the overall refraction-diffraction coefficient, K_{r-d} , in the region behind the structure is:

$$K_{r-d} = K_r K_d \sqrt{b_1 b_2}$$

where

K_r = refraction coefficient at the structure, dimensionless

K_d = diffraction coefficient on last wave crest behind the structure from which additional refraction computations are performed, dimensionless

b_1 = orthogonal spacing at the last diffracted wave crest, ft

b_2 = orthogonal spacing near the shore, ft

29. Mobarek (1962) experimentally investigated the effect of bottom slope on wave diffraction through a gap in a breakwater normal to the incident wave direction. Also investigated was the effect of an abrupt increase or decrease in the water depth behind the breakwater. The theoretical analysis for the comparison of experimental results followed the treatment of Penny and Price (1944) restricted to the case of normal incidence for which the Sommerfeld (1896) solution is simplified and in the presence of a horizontal bottom. Two fundamentally different basin configurations were used in the study. The

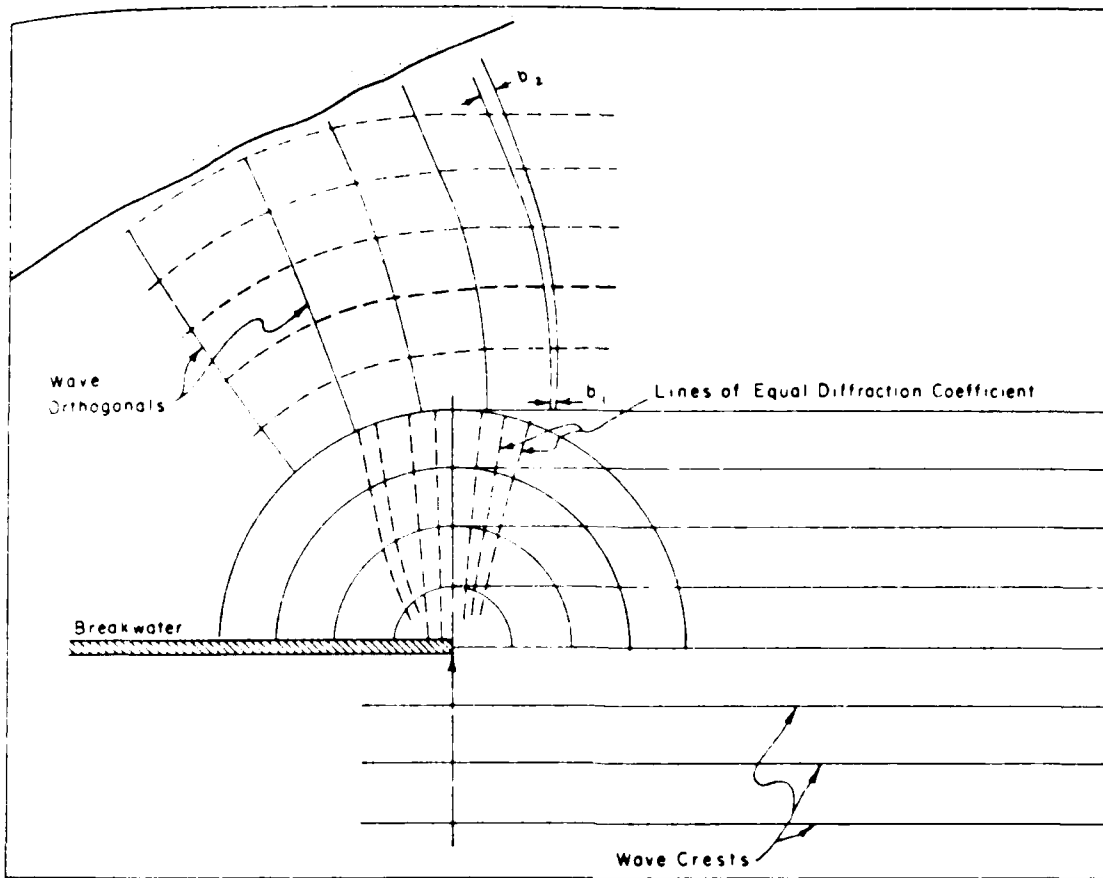


Figure 10. Graphical procedure for determining overall refraction and diffraction effects past a breakwater (after CERC 1977)

first consisted of a longitudinally sloping bottom with the slope commencing at the breakwater and extending to the shoreline. The second was constructed with a flat bottom extending beyond the breakwater gap but sloping laterally to the shoreline. Taking into consideration the serious limitations of the experimental equipment (very small model, 72 sq ft), the investigation led to the conclusion that the procedure usually followed for estimating wave heights behind jetties or shore-connected breakwaters (Figure 10) was sufficiently good for medium period waves; but in the case of long waves, the effect of the shoaling bottom on waves should be taken into consideration. Experiments on a larger scale were highly recommended.

30. For a long shore-connected breakwater on a slowly varying bottom, an asymptotic theory has been developed by Liu and Mei (1976) that accounts for the combined effects of refraction and Fresnel diffraction of water waves. However, for short jetties or groins, the reflection and diffraction effects

and the effect of wave reflection at the beach.

Figure 10 shows the results.

The effect of the reflection at the beach is to reduce the effect of the approximation of the combination of Korteweg-de Vries and geometric optics. This permits the transmission field near the beach to be calculated analytically and this can in turn be used for breaking-line estimates.

The Veldkamp's exact adaptive solution for water waves near a breakwater developed by van der Pol and Veldkamp (1970) that accounts for the combined effect of refraction due to shallow water, long water depth and diffraction by a long-shore-parallel breakwater. This solution is more general than the approximate solution developed by the present theory because this theory is valid near the edge and the tip of the breakwater. The wave behavior in the near-field is of particular interest to a study of the scour and erosion that may occur near the tip of a breakwater. In this analysis, recent developments in the field of Fourier analysis of optics have been included to extend the effect of diffraction.

As shown by the work of Dally and Smith and Sprinks (1976), the dependence of wave reflection on the wave parameter that governs short-wave propagation is given by the Rayleigh-Sommerfeld-Berschke expression. This can be written as

$$R = \frac{1}{\pi} \int_{-\infty}^{\infty} \frac{e^{ikx}}{k^2 - k_0^2} \frac{d\phi}{dk} dk \quad (10)$$

where

ϕ is the phase function defined by the equation

$$\partial_x \phi = \frac{1}{k} \partial_k \phi \quad (11)$$

and

$$\partial_k \phi = \frac{1}{k} \partial_x \phi \quad (12)$$

and k_0 is the parameter that governs short-wave propagation.

The reflection coefficient is given by

$$R = \frac{1}{\pi} \int_{-\infty}^{\infty} \frac{e^{ikx}}{k^2 - k_0^2} \frac{d\phi}{dk} dk \quad (13)$$

where

ϕ is a wavelet equivalent as defined by

$$\hat{n} = \text{a two-dimensional vector}$$

Equation 11 reduces to the diffraction Helmholtz equation in deep or constant-depth water. In shallow water, the equation reduces to the linear longwave equation.

33. Houston (1980) solved Equation 11 by the use of a hybrid finite element numerical model originally developed by Chen and Mei (1974) to solve the diffraction Helmholtz equation in a constant-depth region. The appropriate modifications, including variable depth and frequency dispersion, were incorporated by Houston (1980) and the solution of Equation 11 was applied to the geometry of the experimental study of Hales (1980) (i.e., a uniform slope with a shore-connected breakwater perpendicular to the shoreline). A problem in simulating those experimental hydraulic tests numerically was that the waves broke in the experimental facility near the shoreline and thus dissipated their energy. No mechanism existed to dissipate energy in the numerical model. However, dissipation was simulated by allowing waves to continue to propagate out of the problem area. The breakwater and uniform slope were simulated only to the point where breaking occurred. The depth was then increased to the depth of a semi-infinite ocean region surrounding the region of computation, and the waves were allowed to radiate away from the area of interest.

34. Figure 11 shows a typical comparison between the experimental

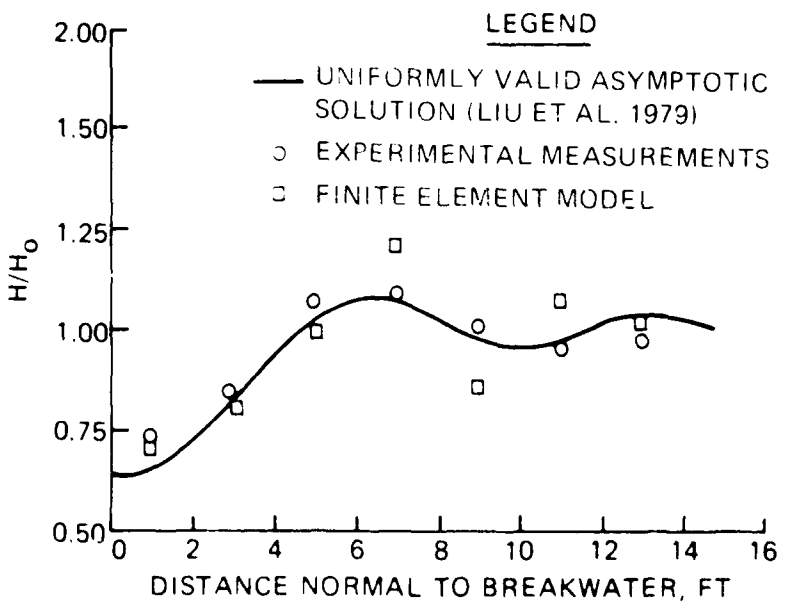


Figure 11. Comparison of asymptotic and finite element solutions with experimental measurements (breakwater normal to shoreline) (after Houston 1980).

measurement) and the finite element calculations off-axis ($\theta = 45^\circ$) were in the uniformly valid asymptotic solution derived by Liu and Lozano (1979). The solution derived by Liu and Lozano (1979) appears to be in good agreement with the experimental tests. The finite element calculation and the experiment agree quite well in the shadow zone with the experimental tests. The agreement is not as good outside the shadow zone. The difference is partially attributed due to the artificial increase in depth to allow the waves to refract from the inner region. This depth transition would cause some energy to reflect back into the region of interest.

PART IV: UNIFORMLY VALID ASYMPTOTIC THEORY

Background

35. In recent years, the parabolic approximation has been developed extensively for studying wave scattering problems in different branches of the physical sciences. Ridder (1979) and Lozano and Liu (1980) derived independently the parabolic approximation for water-wave problems. Analytical solutions were obtained for the combined refraction and diffraction wave field near a thin breakwater perpendicular to the shoreline on a plane beach. The background wave field was assumed to have straight-line wave rays.

36. Also based on the parabolic approximation, a numerical study of water-wave refraction and diffraction problems has been conducted by Tsay and Liu (1982), where the refraction index is not constant. Two problems were considered: (a) the wave field near a submerged shoal on a sloping bottom and (b) the wave field in the neighborhood of a breakwater on a sloping beach. In the latter problem, the orientation of the breakwater is no longer limited to be perpendicular to the shoreline. For the perpendicular case, the accuracy of the parabolic approximation numerical results was verified by comparing with the precise experimental data of Pantazaras (1979) and Hales (1980) (both sets of data having been obtained at WES). For this case, the uniformly valid asymptotic theory of Liu, Lozano, and Pantazaras (1979) was also used to verify the parabolic approximation.

Development of Asymptotic Theory

37. For the case of a shore-connected breakwater on a linear plane beach, Liu and Mei (1976) and Lozano and Liu (1980) have previously shown that an approximate closed form solution can be obtained by the parabolic approximation. However, Liu (1982) showed that this solution becomes invalid near the tip of the breakwater because of the inherent nature of the parabolic approximation. To remove this weakness, Liu, Lozano, and Pantazaras (1979) and Liu (1982) developed a a uniformly valid asymptotic solution for the same problem. This theory is verified by the experimental data of the present study. The beach topography, which is required to be uniform in the along-shore direction, can be arbitrary in the onshore-offshore direction.

38. Following the development of Liu, Lozano, and Pantazaras (1979), and in the notation of Liu (1982), the geometry of the breakwater is generalized to be one of radiated wave rays emitted from the tip of the breakwater (Figure 12). The relation between the incident wave angle and the reflected wave angle along the breakwater is shown in Figure 13. Small-amplitude incident

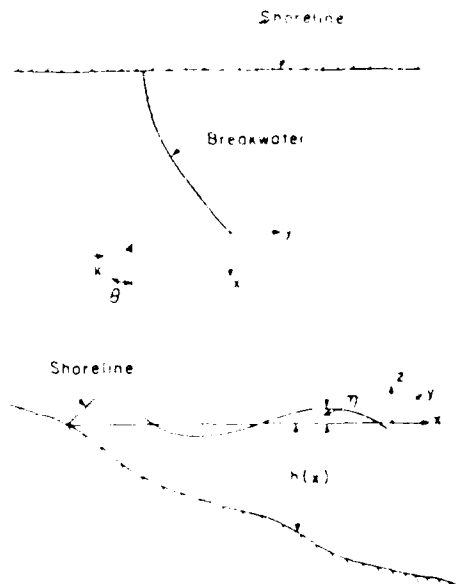


Figure 12. Definitive sketch, uniformly valid asymptotic theory (Liu, Lozano, and Pantazaras 1979)

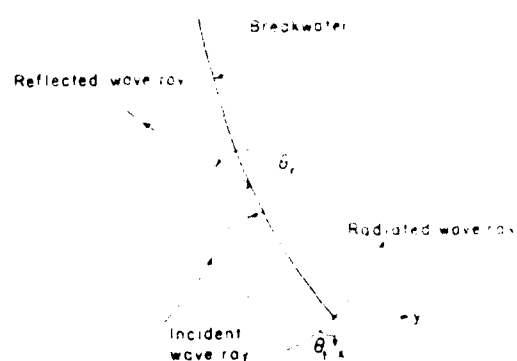


Figure 13. Definitive sketch, uniformly valid asymptotic theory, relation between incident wave angle and the reflected wave angle along the breakwater (Liu, Lozano, and Pantazaras 1979).

waves with the incident wave amplitude, a_0 , and radian frequency, ω , are assumed in the development. The angle of incidence is defined as θ_i . Liu, Lozano, and Pantazaras (1979) have shown that the leading order asymptotic solution for the free-surface displacement, η , is

$$\eta(x, y, t) = \gamma \Lambda(x) \left[G(0)e^{iS} + G(\infty)e^{-iS} \right] e^{-i\omega t} \quad (13)$$

and the velocity potential can be expressed as:

$$\phi(x, y, z, t) = -\frac{i\eta(x, y, t)}{\omega} \frac{\cosh kz + \sinh kz}{\cosh kh} \quad (14)$$

where

$$\gamma = \pi^{-1/2} \exp \left(-\frac{\pi}{4} \right) \quad (14)$$

and

$$G(\rho_1) = \int_{-\infty}^{\rho_1} e^{i\sigma^2} d\sigma \quad (15)$$

$A(x)$ represents the combined refraction and shoaling factor:

$$A(x) = a_o \left[\left(\frac{\cos \theta_o}{\cos \theta} \right) \left(\frac{2k_o h_o}{2kh} + \frac{\sinh 2k_o H_o}{\sinh 2kh} \right) \right]^{1/2} \frac{\cosh kh_o}{\cosh k_o h_o} \quad (16)$$

The subscript o in Equation 16 denotes the quantities associated with incident waves in the far field. The function $G(\rho_1)$ defined in Equation 15 can be given in terms of the Fresnel integrals, whence:

$$G(\rho_1) = \frac{\pi^{1/2}}{8^{1/2}} (1 + i) + \frac{\pi^{1/2}}{2^{1/2}} \left[C_2(\rho_1^2) + iS_2(\rho_1^2) \right] \quad (17)$$

where

$$C_2(\rho_1^2) = \frac{1}{2\pi} \int_0^{\rho_1^2} \frac{\cos \tau}{\tau^{1/2}} d\tau \quad (18)$$

and

$$S_2(\rho_1^2) = \frac{1}{2\pi} \int_0^{\rho_1^2} \frac{\sin \tau}{\tau^{1/2}} d\tau \quad (19)$$

are the Fresnel cosine and sine integrals, respectively. The arguments of the function $G(\rho_1)$ in Equation 15 were defined by Liu (1982) as:

$$\mathbf{Q}^2 = \mathbf{k}^2 + \mathbf{s}^2 \quad (20)$$

and

$$\tilde{\mathbf{Q}}^2 = \mathbf{k}^2 + \tilde{\mathbf{s}}^2 \quad (21)$$

where

S = phase function of the incident wave, deg

\tilde{S} = phase function of the reflected wave from the breakwater, deg

R = phase function of the radiated waves generated by an oscillatory point source at the tip of the breakwater, deg

These phase functions can be calculated according to the ray theory; i.e., S , \tilde{S} , and R can be evaluated by the integral:

$$I = \int_0^{\tilde{r}} \tilde{k} \cdot d\tilde{r} \quad (22)$$

where \tilde{k} is the wave number vector representing each wave field, respectively.

39. The zero-phase lines for S , \tilde{S} , and R intercept at the tip of the breakwater ($x = 0$, $y = 0$). From Equation 22, the value of the phase function (S , \tilde{S} , or R) at any arbitrary point can be considered as the sum of the wave number component in the radial direction between the arbitrary point and the tip of the breakwater. The value of the phase function for radiated waves at any arbitrary point is always greater than or equal to S and \tilde{S} . The branches of the multivalued functions Θ and $\tilde{\Theta}$ are defined by Liu (1982) as follows: The value of Θ is negative inside the shadow region defined according to the geometrical optics theory and is positive elsewhere. $\tilde{\Theta}$ is positive in the reflection region and is negative elsewhere. In the case where the breakwater has a curved shape and coincides with one of the radiated wave rays from the tip, the phase function for the reflected wave is:

$$\tilde{S} = - \int_{r_0}^x k_r \cos \theta_r dx + \tilde{k}_r y \quad (23)$$

where

$$\frac{\tilde{k}_r}{r} = k_r \sin \theta_r \quad (24)$$

k_r and θ_r represent the wave number and reflected wave angle along the breakwater, respectively.

40. The analytical development of the free-surface displacement down-coast of a shore-connected breakwater, based on the uniformly valid asymptotic theory (Equation 12), was based on the fundamental assumption that the breakwater geometry in planform followed a radiated wave ray emitted from the tip of the breakwater. The detailed derivation of this and other expressions

required in the development are presented in Liu, Lozano, and Pantazaras (1979). However, in actuality, the planform layout of most shore-connected breakwaters at an angle to the shoreline is that of a straight line. Hence, while the assumption of a planform layout following a wave ray radiated from the tip of the structure expedited the analytical development, the numerical model based on this development does not precisely conform with most prototype conditions. It was therefore desirable to adapt the numerical scheme to fit the case of a straight breakwater at an angle to the shoreline. For the case of a straight breakwater, the phase function S_s for the incident wave, the phase function \bar{S}_s for the reflected waves from the breakwater, and the phase function R_s for the radiated waves generated by the oscillatory point source at the tip of the breakwater can be expressed respectively as:

$$S_s = - \int_0^x k \cos \theta dx + \bar{K}_o y \quad (25)$$

$$\bar{S}_s = - \int_0^x k \cos \theta dx - \bar{K}_o y \quad (26)$$

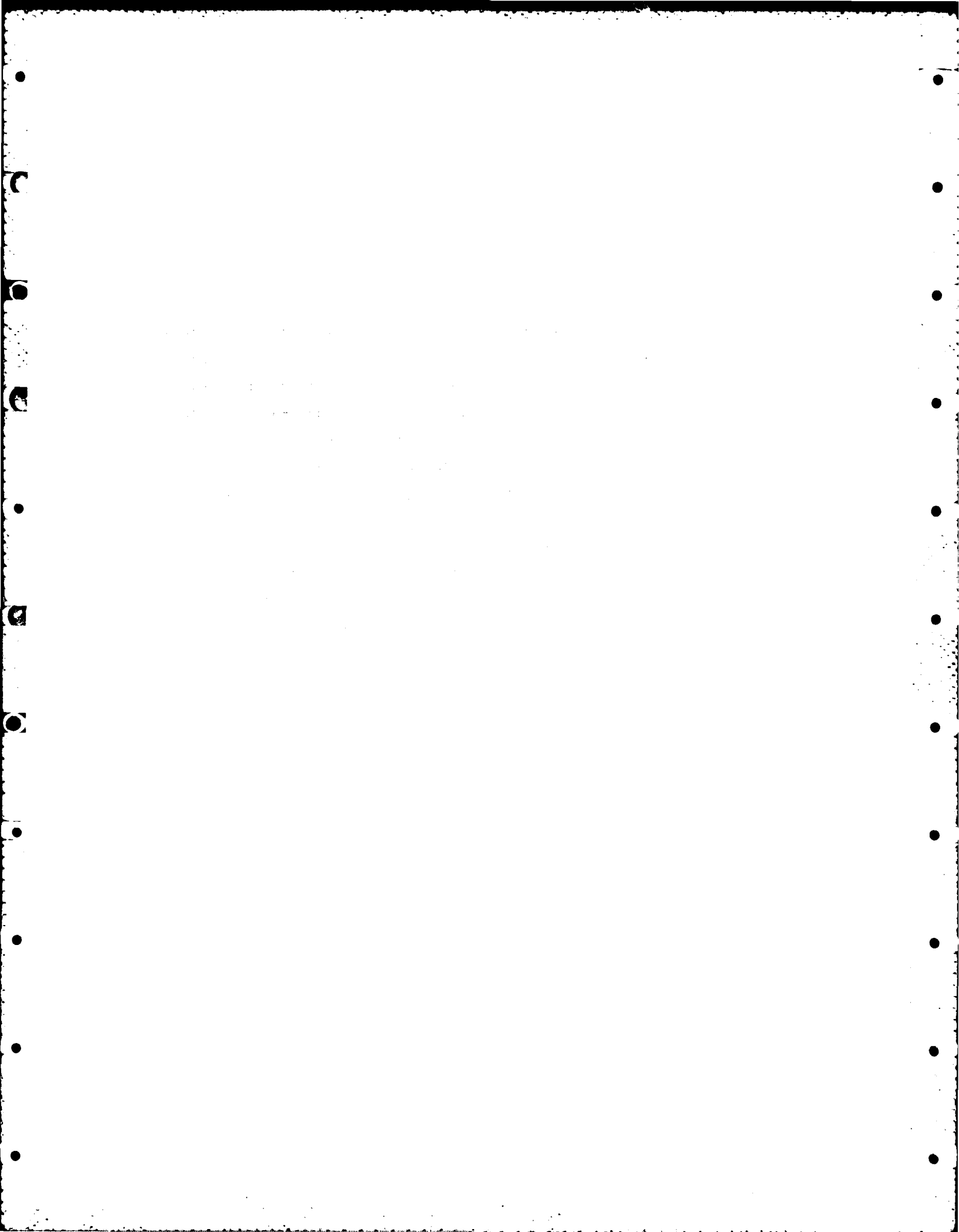
$$R_s = - \int_0^x k \cos \theta dx + \bar{K}_t y \quad (27)$$

where

$$\bar{K}_o = k \sin \theta = k_o \sin \theta_o \quad (28)$$

$$\bar{K}_t = k \sin \theta = k_t \sin \theta_t \quad (29)$$

k_t and θ_t represent the wave number and the initial angle of incidence of a radiated wave ray, respectively. The numerical model developed under contract by Liu based on the uniformly valid asymptotic theory of Liu, Lozano, and Pantazaras (1979) was modified to conform to a straight breakwater at an angle to the shoreline, and is presented in Appendix B along with a sample output from the program. This numerical model served as the basis for comparison with the experimental results of the present study.



waves with truly deepwater characteristics. In addition, the requirement existed that the generated wave heights should be large enough so that small changes in the heights could be detectable, and at the same time the heights should be small enough so that comparisons with linear theories could be performed. Preliminary testing and experimental results of Bates (1980), indicated that for the area of major interest, and for the range of wave periods considered pertinent, the specific experimental conditions shown in Table I could be investigated with height changes remaining essentially linear, thus permitting comparisons with theoretical development.

43. Thirty-six wave-height sensors were used to determine the wave heights along the four sections parallel with the shoreline and downwave of the vertical breakwater (eight gages along two sections, nine gages along two sections, and two reference gages in the ocean region near the wave generator). The average of 90 wave heights recorded at each of the two ocean gages was considered to be the input wave height from the wave generator. The average of 90 wave heights recorded at the remaining 34 gages was normalized to this input wave height. All 36 gages were recorded simultaneously with each individual reading at all data stations consisting of the average of these 90 waves. Ten repeatability replication tests were conducted under identical test conditions to define the variability of the measurements (experimental scatter). The statistical measure of the variability was the square root of the variance or the standard deviation. The variance is defined as the sum of the squares of the deviates of each individual observation from their average, divided by one less than the total number of deviates. One standard deviation was usually only 1 to 3 percent of the average value of the observations.

44. The wave-height data were obtained with the wave sensors positioned at 2-ft intervals starting at the breakwater and extending along the sections parallel with the shoreline downwave from the breakwater. To provide better definition of the wave profile, the gages were offset a distance of 1 ft along the sections parallel with the shoreline. Hence, were repositioned at 2-ft intervals along the other sections. This provided information at 1-ft intervals for a distance of 16 ft from the breakwater along two sections and for a distance of 48 ft from the breakwater along the remaining two sections.

REFERENCES

Fig. 1. An independent wave train generated in the experimental facility.

were sufficiently small such that the waves were usually linear within the measurement region shown in Figure 1. The degree of linearity is summarized in Tables 2-19 for representative replicates of each different wave characteristic (period and height) tested. It was found that at the ocean gages, on the average, 97.32 percent of the energy of the wave form exists at the generated period (fundamental frequency). Of the remaining 2.68 percent of the energy, 2.39 percent exists at the first harmonic. The distribution of the wave energy throughout the model for these representative experiments is also displayed in Tables 2-19. Here is seen the manner in which nonlinear effects are detectable as the wave propagates shoreward past the various areas. A portion of the energy of the wave form is redistributed from the fundamental frequency to higher harmonics, and along the section at a distance of 0.10 from the shoreline only 89.05 percent exists (on the average) at the generated period. (This percentage increases with distance deep into the shallow zone protected by the breakwater.) However, of the remaining 10.95 percent of the energy, 8.32 percent exists (on the average) at the first harmonic.

46. The deviation from linearity, and hence the acceptability of comparisons of these experimental data with theoretical studies based on the small amplitude assumption, can be investigated by observing the rapidity with which the wave energy redistributes from the fundamental frequency as the waves shoal shoreward. For constant values of wave period, T , of 0.75 sec., 1.00 sec., and 1.50 sec., Figures 14-16, respectively, display the percent of total energy in the fundamental period with distance from the shoreline for three initial values of wave height each. In all cases, the nonlinearities are apparent as the waves propagate into shallower water with the least alteration occurring to the waves with the smaller period and the smaller initial generated wave height. As the wave height increases, the effect of the nonlinearity becomes increasingly greater for constant values of wave period. At the same time, the longer period waves appear to exhibit an even more rapid redistribution of energy from the fundamental period. This is due, in part, to reflection of long-period waves back to the source, and to a lesser degree, to resonance within the experimental basin. Use of the asymptotic theory used as a basis for comparison of these experimental data provides for a specific wave period analysis, although the comparison is not one regarding wave height and third harmonic coefficients.

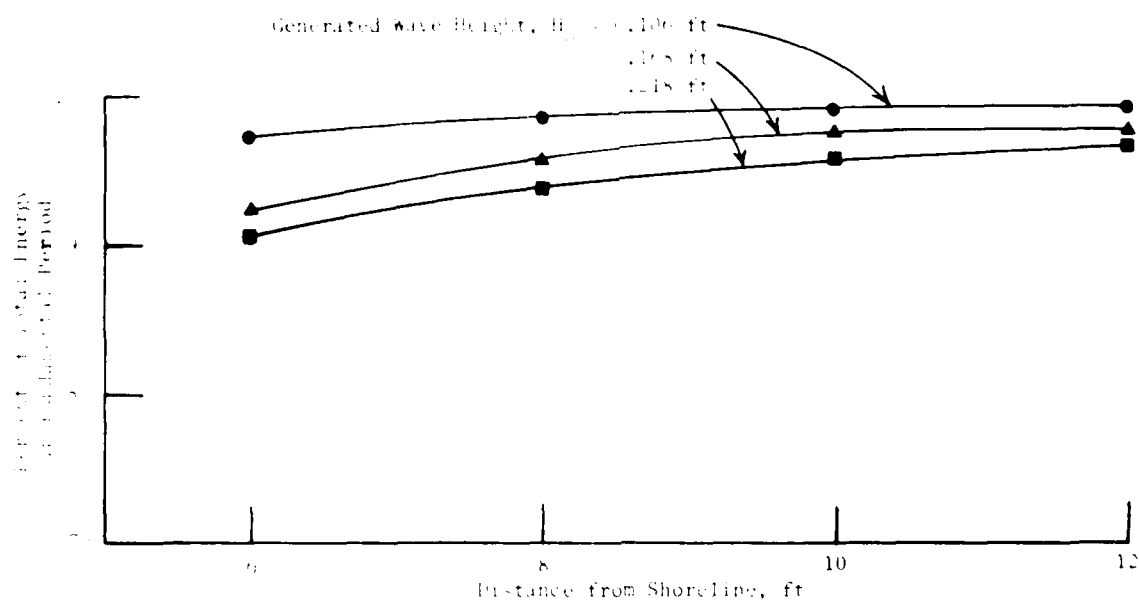


Figure 14. Effects of nonlinearities (initial wave height and shoaling effects) on percent of total energy in fundamental period, wave period = 0.75 sec

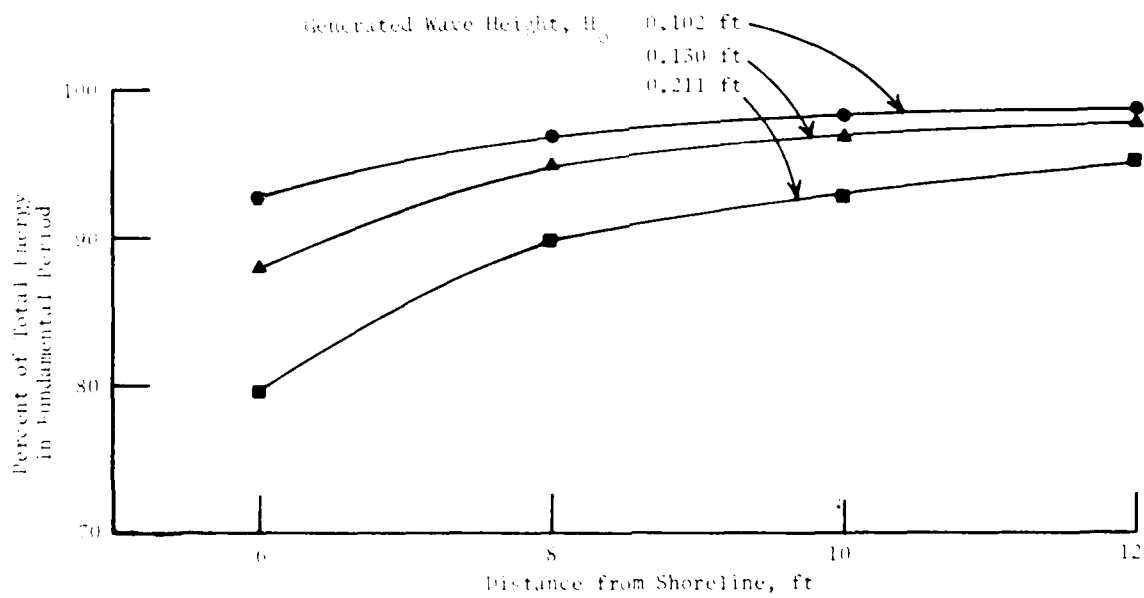


Figure 15. Effects of nonlinearities (initial wave height and shoaling effects) on percent of total energy in fundamental period, wave period = 1.00 sec

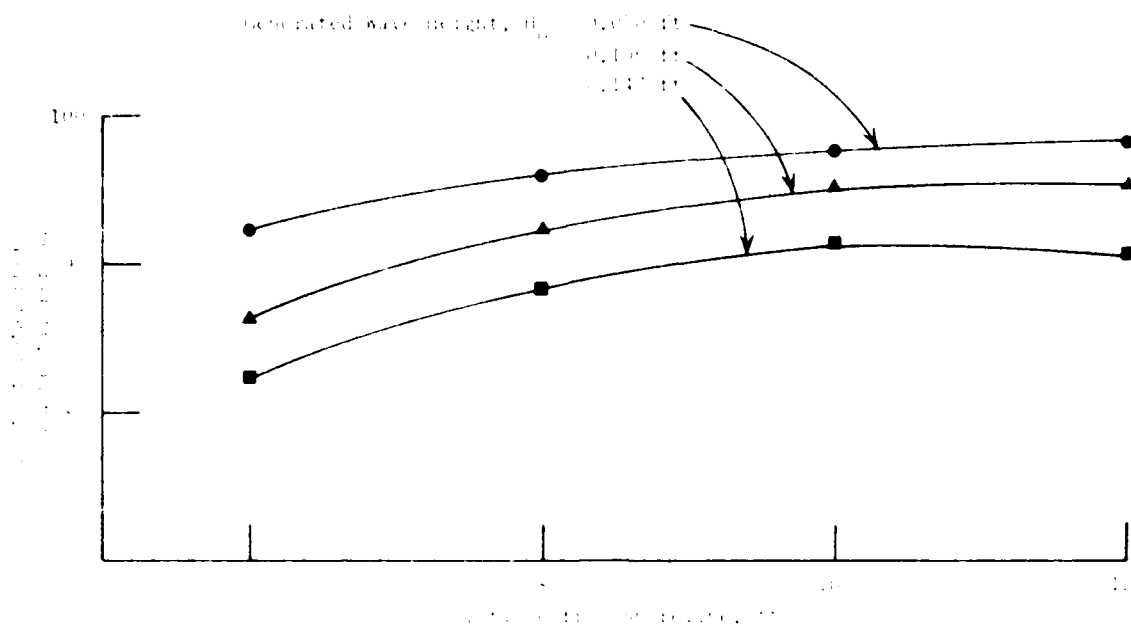


Figure 16. Effects of nonlinearities (initial wave height and shadowing effects) on percent of total energy in fundamental period, wave period = 1.50 sec

Wave-Height Data

47. Wave patterns, during the conditions tested in this experimental study, are shown in Photos 1-9. Wave-height amplification coefficients, H/H_0 , for all conditions tested are shown in Plates 1-36. Each of these plates constitutes a section parallel with the shoreline at distances from the shoreline of 6, 8, 10, or 12 ft. The corresponding scatter of the experimental data is indicated by the error bars of plus-or-minus one standard deviation. Also shown in these plates are the wave-height amplification due to diffraction alone (as if the basin were horizontal beyond the structure) and the wave-height amplification as indicated by the uniformly valid asymptotic theory.

Study Results

48. For small wave periods, small initial wave heights, and deep within the shadow zone (sections near the shoreline), both the diffraction theory and the uniformly valid asymptotic theory predict wave-height amplifications that

compare consistently well with the experimental data. Nearer the tip of the breakwater the diffraction theory tends to diverge rapidly from the experimental results, and the uniformly valid asymptotic theory more nearly approximates the experiments. As wave period increases, the deviation of the diffraction theory becomes more pronounced at all locations except very near the breakwater; however, the uniformly valid asymptotic theory continues to closely approximate the data from the experiments in all regions. The greatest deviation of the uniformly valid asymptotic theory from the experiments occurs outside the breakwater shadow zone in the area of the asymptotic undulations of the wave-height amplification factor. This can be attributed to reflection of longer period wave energy from the experimental beach breaker zone not accounted for in the analytical development, since the uniformly valid asymptotic theory consistently underpredicts the wave-height amplification in this area.

49. In general, it can be concluded that the uniformly valid asymptotic theory is superior to diffraction theory alone for estimating wave heights downcoast of nearshore structures subjected to combined refraction and diffraction. Particularly for longer period waves and for the region near the structures where scour and erosion are known to frequently occur, this theory provides an estimation that consistently approximates the results of this experimental study and that is significantly better than diffraction theory. At the same time, it appears desirable to incorporate into this theory a degree of nonlinearity that is not presently available.

50. Because the uniformly valid asymptotic theory compares favorably with the results of this experimental study (four sections parallel with the shoreline for three wave periods with three incident wave heights each), the numerical program developed from this theory and modified to fit the straight breakwater geometry was applied to the entire shadow zone region of the structure. These results are presented in Plates 37-50 for distances parallel to shoreline of 1 ft through 14 ft, respectively, in increments of 1-ft displacement seaward toward the tip of the breakwater (which was located 15 ft from the shoreline). The three wave periods utilized in the experimental phase of this study (0.75, 1.00, and 1.50 sec) are shown in these plates as the independent parameters. It is apparent near the shoreline that the longer period waves allow for the greater wave-height amplification at all locations (particularly within the shadow zone). With increase in distance from the

shoreline, the longer period waves continue to exhibit a greater wave-height amplification in the shadow zone; however, outside the shadow zone, the period effect becomes less apparent and eventually becomes entirely obscured as the undulations of the different periods engulf (overlap) each other.

PART VI: CONCLUSIONS

51. Based on results from the three-dimensional experimental investigation, reported herein, comparisons with existing diffraction theory, and a new uniformly valid asymptotic theory reported herein, it is concluded that:

- a. For short wave periods, small initial wave heights (linear waves), and locations well within the shadow zone of the structure, both the diffraction theory and the uniformly valid asymptotic theory predict wave-height amplifications that compare consistently well with the experimental data. However, nearer the tip of the structure, diffraction theory tends to diverge rapidly from the experimental results, and the uniformly valid asymptotic theory more nearly approximates the experiments.
- b. As the wave period increases, the deviation of the diffraction theory becomes more pronounced at all locations except very near the structure; however, the uniformly valid asymptotic theory continues to closely approximate the data from the experiments in all regions.
- c. The uniformly valid asymptotic theory is superior to diffraction theory for estimating wave heights downcoast of nearshore structures subjected to combined refraction and diffraction. Particularly for longer period waves and for the region near the structures where scour and erosion are known to occur, this theory consistently approximates the results of this experimental study.

REFERENCES

- Battjes, J. A., 1968 (Nov.), "Refraction of Water Waves," Journal, Waterways and Harbors Division, American Society of Civil Engineers, Vol. 94, No. WW4, pp. 437-454.
- Berkhoff, J. C. W., 1972 (Jan.), "Computation of Combined Refraction-Diffraction," Proceedings, Thirteenth Conference on Coastal Engineering, Vancouver, British Columbia, Canada, Vol. 1, pp. 471-490.
- Bretschneider, C. L., 1966, "Wave Refraction, Diffraction, and Reflection," Chapter 6, *Estuary and Coastline Hydrodynamics*, A. T. Ippen, ed., McGraw-Hill, New York.
- Carter, G. F., 1966 (April), "Gravity Waves on Water of Variable Depth," Journal of Fluid Mechanics, Vol. 24, Part 4, pp. 641-659.
- Chen, H. S., and Mei, C. C., 1974, "Oscillations and Wave Forces in an Off-shore Harbor," technical report No. 190, Massachusetts Institute of Technology, Cambridge, Mass.
- Dunham, J. W., 1951 (Oct.), "Refraction and Diffraction Diagrams," Proceedings, First Conference on Coastal Engineering, Long Beach, Calif., pp. 33-49.
- Burham, B. L., and Greer, R. C., III, 1976, "Automated Data Acquisition and Control Systems for Hydraulic Models," Proceedings, 1976 Army Numerical Analysis and Computer Conference, St. Louis, Mo., pp. 509-520.
- Hales, L. Z., 1980 (Sep.), "Erosion Control of Shore During Construction; Experimental Measurements of Refraction, Diffraction, and Current Patterns near Jetties," Technical Report HL-80-3, Report 3, US Army Engineer Waterways Experiment Station, Vicksburg, Miss.
- Harms, V. K., 1979 (Dec.), "Diffraction of Waves by Shore-Connected Breakwater," Journal, Hydraulics Division, American Society of Civil Engineers, Vol. 105, No. HY12, pp. 1301-1319.
- Houston, J. R., 1980 (May), "Modeling of Shore Waves Using the Finite Element Method," Proceedings, Third International Conference on Finite Elements in Water Resources, Vol. 2, pp. 5.181-5.196, University of Texas, Supply, Texas.
- Jonesen, E. G., and Brinkkjær, G., 1979, "A Comparison Between Two Reduced Wave Equations for Gradually Varying Depth," Technical Report No. 31, Technical University of Denmark.
- Keller, J. B., 1958, "Diffraction of Waves by a Semi-Infinite Wedge," Journal of Fluid Mechanics, Vol. 4, pp. 601-624.
- Kennedy, G. R., 1970, "Theory of the Propagation of Water Waves," Wiley, New York.
- Koide, M., 1970, "Diffraction of Water Waves by a Wedge," Proceedings of the First International Conference on Numerical Methods in the Solution of Nonlinear Problems, Stanford, Calif., pp. 101-107.
- Koide, M., 1971, "Diffraction of Water Waves by a Wedge," *Journal of Geophysical Research*, Vol. 76, No. 28, pp. 1701-1712.
- Koide, M., 1973, "Diffraction of Water Waves by a Wedge," *Journal, Waterways, Port, Coastal, and Ocean Engineering Division, American Society of Civil Engineers*, Vol. 99, No. 3, pp. 111-117.

- Liu, P. L. 1982 (Jul). "Combined Refraction and Diffraction: Comparison Between Theory and Experiments," Journal of Geophysical Research, Vol 87, No. C8, pp 5725-5730.
- Liu, P. L., and Lozano, C. J. 1979 (Mar). "Combined Wave Refraction and Diffraction," Proceedings, Coastal Structures 79, Alexandria, Va., Vol II, pp 978-997.
- Liu, P. L., and Mei, C. C. 1975 (Nov). "Effects of a Breakwater on Nearshore Currents due to Breaking Waves," Technical Memorandum No. 57, US Army Coastal Engineering Research Center, Washington, DC
- . 1976 (Jun). "Wave Motion on a Beach in the Presence of a Breakwater; I, Waves," Journal of Geophysical Research, Vol 81, No. 18, pp 3079-3084.
- Liu, P. L., Lozano, C. J., and Pantazaras, N. 1979. "An Asymptotic Theory of Combined Wave Refraction and Diffraction," Applied Ocean Research, Vol 1, No. 3, pp 137-146.
- Lozano, C. J., and Liu, P. L. 1980. "Refraction-Diffraction Model for Linear Surface Water Waves," Journal of Fluid Mechanics, Vol 101, Part 4, pp 705-720.
- Masch, F. D. 1964. "Cnoidal Waves in Shallow Water," Proceedings, Ninth Conference on Coastal Engineering, Lisbon, Portugal, pp 1-21.
- Mei, C. C., Tiapa, G. A., and Eagleson, P. S. 1968 (Jul). "An Asymptotic Theory for Water Waves on Beaches of Mild Slope," Journal of Geophysical Research, Vol 73, No. 14, pp 4555-4561.
- Mobarek, I. 1962 (Nov). "Effect of Bottom Slope on Wave Diffraction," Technical Report No. HEL-1-1, University of California, Berkeley, Calif.
- Pantazaras, N. 1979. "Combined Diffraction and Refraction of Water Waves," M.S. Thesis, Department of Environmental Engineering, Cornell University, Ithaca, N. Y.
- Penny, W. G., and Price, A. T. 1944. "Diffraction of Sea Waves by Breakwaters," Technical History Report No. 26, Directorate of Miscellaneous Weapons Development, Washington, DC.
- Putnam, J. A., and Arthur, R. S. 1948. "Diffraction of Water Waves by Breakwaters," Transactions, American Geophysical Union, Vol 29, No. 4, pp 481-490.
- Radder, A. C. 1979. "On the Parabolic Equation Method for Water-Wave Propagation," Journal of Fluid Mechanics, Vol 95, pp 159-176.
- Rayleigh, J. W. S. 1877. "On Progressive Waves," Proceedings, London Mathematical Society, Vol 9, pp 21-26.
- Schonfeld, J. 1972. "Propagation of Two-Dimensional Short Waves," Delft University of Technology, Delft, Netherlands.
- Smith R., and Sprinks, T. 1975. "Scattering of Surface Waves by a Conical Island," Journal of Fluid Mechanics, Vol 72, pp 373-384.
- Sommerfeld, A. 1896. "Mathematical Theory of Diffraction," Annals of Mathematics, Vol 47.
- Tsay, T. K., and Liu, P. L. 1982 (Sep). "Numerical Solution of Water-Wave Refraction and Diffraction Problems in the Parabolic Approximations," Journal of Geophysical Research, Vol 87, No. C10, pp 7932-7940.

- US Army Coastal Engineering Research Center, CE, 1977, Shore Protection Manual, Washington, DC.
- Whalin, R. W. 1972 (Jul). "Wave Refraction Theory in a Convergence Zone," Proceedings, Thirteenth Conference on Coastal Engineering, Vancouver, British Columbia, Canada, pp 451-470.
- Wiegel, R. L. 1962 (Jan). "Diffraction of Waves by Semi-Infinite Breakwaters," Journal, Hydraulics Division, American Society of Civil Engineers, Vol. 88, No. HY1, pp 27-44.

Table 1
Experimental Conditions Tested

Initial Wave Heights, H_o (ft) near Wave Generator	Wave Period, T (sec)	
0.75	1.00	1.50
0.106	0.102	0.070
0.168	0.130	0.106
0.218	0.211	0.147

Note: All experimental test conditions were replicated 10 times.

1

It is clear that the results of the fragment of the experimental trajectory, ending at the point $\tau = 10$, are in good agreement with the corresponding theoretical values.

¹ See also the discussion of the "new" or "revised" version of the theory of the firm by Williamson (1975).

Table 3
 Distribution of Wave Energy Throughout the Experimental Facility, 30-deg
 Incident Direction, Period = 0.75 sec, Ocean Wave Height = 0.106 ft
 60-deg Breakwater Angle with Shoreline
 Percent of Total Energy and Phase Angle (deg), Arrangement No. 2

Gage	Fundamental	First	Second	Third	Fourth
	Period 0.75 sec	Harmonic 0.38 sec	Harmonic 0.19 sec	Harmonic 0.19 sec	Harmonic 0.15 sec
1*	93.42(+99)	1.55(+161)	0.00(+155)	0.02(+76)	0.01(+86)
2*	93.51(+144)	1.30(-60)	0.09(+90)	0.00(+159)	0.00(+76)
3	96.63(-149)	0.35(-170)	0.02(+147)	0.00(-113)	0.00(-131)
4	99.38(-127)	0.06(+126)	0.04(-112)	0.01(-116)	0.01(-105)
5	93.93(-16)	1.01(-39)	0.04(-43)	0.01(-67)	0.00(-61)
6	99.35(+101)	0.60(-179)	0.02(+43)	0.02(+88)	0.01(+81)
7	99.70(-134)	0.26(+99)	0.02(-108)	0.01(-131)	0.01(-118)
8	90.01(-28)	0.95(-55)	0.03(-67)	0.01(-83)	0.00(-81)
9	99.30(+91)	0.66(+156)	0.01(+84)	0.02(+72)	0.01(+73)
10	99.57(-147)	0.40(+63)	0.03(-93)	0.01(-135)	0.00(-123)
11	99.64(-173)	0.35(-118)	0.01(+126)	0.00(-169)	0.00(-143)
12	99.68(+128)	0.27(+94)	0.02(+143)	0.02(+73)	0.01(+90)
13	99.81(+140)	0.17(-135)	0.00(+118)	0.01(+77)	0.00(+119)
14	99.86(-132)	0.10(+141)	0.02(-102)	0.01(-115)	0.01(-113)
15	93.53(-11)	1.39(-42)	0.07(-43)	0.01(-59)	0.00(-52)
16	99.05(+114)	0.92(-153)	0.01(+18)	0.02(+92)	0.01(+85)
17	99.28(-131)	0.67(+104)	0.04(-78)	0.01(-127)	0.01(-122)
18	93.46(-29)	1.44(-54)	0.08(-71)	0.02(-83)	0.01(-86)
19	99.19(+109)	0.69(+96)	0.08(+95)	0.02(+87)	0.02(+78)
20	99.84(+56)	0.04(+27)	0.08(+29)	0.04(+64)	0.01(+73)
21	99.35(+59)	0.57(+72)	0.04(+52)	0.03(+69)	0.01(+85)
22	99.63(+136)	0.33(-81)	0.03(+74)	0.01(+77)	0.00(+87)
23	93.73(-123)	1.17(+121)	0.03(-72)	0.02(-120)	0.01(-125)
24	96.77(-9)	3.05(-18)	0.15(-24)	0.03(-24)	0.00(-35)
25	97.45(+124)	2.47(-126)	0.07(+12)	0.01(+127)	0.00(+81)
26	93.45(-120)	1.46(+124)	0.05(-46)	0.03(-115)	0.01(-123)
27	97.22(-10)	2.62(-26)	0.13(-43)	0.02(-56)	0.01(-60)
28	99.35(+146)	0.13(-134)	0.01(-171)	0.02(+88)	0.01(+97)
29	99.64(+59)	0.25(+37)	0.07(+48)	0.04(+68)	0.02(+70)
30	99.57(+54)	0.11(+64)	0.01(-101)	0.00(-73)	0.00(-24)
31	99.63(+19)	0.31(+11)	0.01(-21)	0.01(-9)	0.00(+7)
32	97.44(+77)	2.42(+123)	0.04(+129)	0.03(+10)	0.02(+20)
33	93.42(+171)	1.16(-44)	0.02(+124)	0.00(+15)	0.00(+102)
34	95.20(-85)	4.71(-169)	0.03(+125)	0.01(-58)	0.01(-107)
35	93.25(+73)	7.04(+81)	0.60(+113)	0.04(+124)	0.01(+75)
36	94.11(+171)	5.54(-30)	0.35(+135)	0.02(-40)	0.00(+131)

* Ocean gage.

Table 4
Distribution of Wave Energy Throughout the Experimental Facility, 30-deg
Incident Direction, Period = 0.75 sec, Ocean Wave Height = 0.168 ft
60-deg Breakwater Angle with Shoreline
Percent of Total Energy and Phase Angle (deg), Arrangement No. 1

Gage	Fundamental	First	Second	Third	Fourth
	Period 0.75 sec	Harmonic 0.38 sec	Harmonic 0.25 sec	Harmonic 0.19 sec	Harmonic 0.15 sec
1*	93.66(+90)	6.00(+170)	0.29(-103)	0.05(+77)	0.00(+170)
2*	97.47(+141)	1.99(+11)	0.58(-173)	0.04(+12)	0.00(+156)
3	93.68(-122)	1.26(-44)	0.01(-119)	0.05(-125)	0.01(-116)
4	99.39(-160)	0.03(+179)	0.03(+116)	0.00(-126)	0.01(-113)
5	97.88(-92)	2.39(-153)	0.02(+178)	0.06(-140)	0.00(-124)
6	96.58(+30)	3.26(+39)	0.15(+86)	0.00(+97)	0.01(+52)
7	97.29(+144)	2.54(-74)	0.17(+82)	0.01(-107)	0.00(+147)
8	97.33(-93)	2.61(-178)	0.06(+117)	0.00(-74)	0.00(-112)
9	96.33(+18)	3.45(+33)	0.20(+54)	0.03(+80)	0.01(+60)
10	97.20(+134)	2.69(-165)	0.10(+39)	0.01(-173)	0.00(+114)
11	99.06(+146)	0.89(-178)	0.05(-122)	0.01(+35)	0.00(+132)
12	99.91(+119)	0.01(+134)	0.05(+105)	0.02(+12)	0.01(+110)
13	98.47(+163)	1.47(-32)	0.06(+143)	0.00(-96)	0.00(-132)
14	97.64(-94)	2.33(-175)	0.02(+174)	0.01(-50)	0.00(-120)
15	95.40(+21)	4.20(+43)	0.37(+76)	0.03(+80)	0.00(+43)
16	96.11(+154)	3.70(-59)	0.19(+161)	0.01(-86)	0.00(-108)
17	96.33(-102)	3.43(+166)	0.12(+55)	0.01(-48)	0.00(-90)
18	94.90(+15)	4.72(+26)	0.35(+56)	0.03(+73)	0.00(+34)
19	93.83(+162)	1.05(-77)	0.12(+90)	0.01(-179)	0.00(-6)
20	99.06(+77)	0.83(+61)	0.06(+58)	0.01(+31)	0.00(+73)
21	93.00(+41)	0.06(+79)	0.01(-3)	0.02(+95)	0.01(+63)
22	93.24(+36)	1.72(+123)	0.02(+176)	0.02(+58)	0.01(+74)
23	97.01(+173)	2.34(-15)	0.14(+157)	0.01(+7)	0.00(-129)
24	94.97(-93)	6.37(+173)	0.15(+93)	0.01(-49)	0.00(-122)
25	96.42(+31)	3.56(+64)	0.94(+51)	0.05(+116)	0.03(+39)
26	92.8(+163)	6.14(+49)	0.60(+112)	0.05(-65)	0.00(+33)
27	92.90(+31)	6.24(+18)	0.21(+135)	0.00(+39)	0.01(-117)
28	97.47(+173)	2.33(+167)	0.03(+131)	0.00(+35)	0.01(+60)
29	99.17(+77)	1.03(+39)	0.04(+57)	0.02(+36)	0.01(+56)
30	92.8(+17)	1.13(+17)	0.00(+133)	0.00(130)	0.00(-34)
31	93.07(+11)	1.17(+73)	0.05(+63)	0.01(+78)	0.00(+33)
32	94.18(+111)	1.17(+17)	0.23(-23)	0.04(+112)	0.01(+132)
33	91.13(-163)	1.17(+11)	0.79(-175)	0.03(+89)	0.01(-121)
34	91.17(-163)	1.17(+106)	2.03(-149)	0.05(-176)	0.01(+69)
35	91.17(+11)	1.17(+11)	2.72(-190)	0.33(-124)	0.04(-73)
36	91.17(+11)	1.17(+11)	2.06(-140)	0.16(+35)	0.04(-154)

Table 3
 Distribution of Wave Energy Throughout the Experimental Facility, 30-deg
 Incident Direction, Period = 0.75 sec, Ocean Wave Height = 0.168 ft
 90-deg Backwater Angle with Shoreline
 Percent of Total Energy and Phase Angle (deg), Arrangement No. 2

Gage	Fundamental	First	Second	Third	Fourth
	Period 0.75 sec	Harmonic 0.375 sec	Harmonic 0.25 sec	Harmonic 0.19 sec	Harmonic 0.15 sec
1*	94.84(+163)	4.50(+161)	6.40(-94)	0.12(+49)	0.03(+108)
2*	93.13(+146)	4.14(-2)	0.68(+138)	0.00(-31)	0.01(+102)
3	99.70(-160)	0.27(-102)	0.01(-168)	0.01(-110)	0.00(-162)
4	97.39(+137)	1.49(+92)	0.13(-45)	0.02(-124)	0.00(-125)
5	97.66(-23)	2.13(-55)	0.12(-74)	0.03(-67)	0.01(-75)
6	97.30(+99)	2.52(+162)	0.02(-92)	0.05(+83)	0.01(+80)
7	93.36(-142)	1.55(+78)	0.08(-75)	0.01(-131)	0.00(-128)
8	97.19(-36)	2.62(-73)	0.13(-91)	0.05(-96)	0.01(-93)
9	97.31(+80)	2.60(+154)	0.04(-168)	0.02(+54)	0.01(+31)
10	97.50(-166)	2.15(+34)	0.07(-123)	0.00(+143)	0.00(+140)
11	98.47(-177)	1.42(-3)	0.10(+26)	0.01(-144)	0.00(+49)
12	99.16(+127)	0.15(+150)	0.07(-152)	0.01(+36)	0.01(+76)
13	99.29(+134)	0.67(-120)	0.02(+48)	0.02(+113)	0.00(+83)
14	99.33(-142)	0.64(+104)	0.01(-9)	0.01(-144)	0.00(-173)
15	95.83(-36)	3.36(-66)	0.26(-63)	0.05(-102)	0.01(-75)
16	96.17(+103)	3.24(-171)	0.10(-47)	0.07(+82)	0.01(+79)
17	97.28(-142)	2.57(+69)	0.14(-36)	0.01(-146)	0.00(-134)
18	95.79(-36)	3.31(-69)	0.23(-92)	0.05(-91)	0.01(-92)
19	99.71(+110)	1.27(-137)	0.01(+115)	0.00(-16)	0.01(+77)
20	97.26(+55)	3.62(+82)	0.10(+59)	0.05(+52)	0.02(+74)
21	95.21(+54)	4.61(+68)	0.12(+65)	0.04(+68)	0.02(+68)
22	97.91(+129)	1.91(-91)	0.15(+51)	0.00(+144)	0.00(+67)
23	96.6(-138)	3.13(+85)	0.21(-59)	0.01(-144)	0.00(-167)
24	92.61(-21)	6.64(-43)	0.69(-57)	0.05(-58)	0.01(-77)
25	92.66(+104)	6.91(-159)	0.37(-36)	0.05(+73)	0.01(+101)
26	97.11(-176)	3.03(+95)	0.35(-53)	0.04(-124)	0.00(-114)
27	99.73(-26)	3.75(-57)	0.53(-75)	0.07(-85)	0.01(-99)
28	98.79(+162)	1.11(+89)	0.00(-76)	0.01(+162)	0.00(+102)
29	97.06(+117)	1.71(+99)	0.07(+54)	0.05(+88)	0.01(+110)
30	97.11(+96)	1.75(-24)	0.64(-103)	0.01(-110)	0.00(-102)
31	97.23(-177)	2.21(+35)	0.12(-25)	0.02(-13)	0.00(-19)
32	94.10(+127)	1.51(+131)	0.18(-169)	0.00(+60)	0.01(+81)
33	90.97(+151)	3.51(-54)	0.57(+115)	0.04(-68)	0.00(+141)
34	90.40(-99)	3.79(+159)	0.73(+52)	0.06(-46)	0.01(-128)
35	90.41(+151)	3.21(+117)	0.97(+43)	0.47(+51)	0.14(+52)
36	93.64(+147)	1.11(-37)	1.27(+48)	0.24(+176)	0.03(-70)

* Ocean wave.

Table I
Distribution of stress in the front horizontal facility, 30-deg
Incident angle, 30°, 30°, 30°, 30°, 30°, 30°, 30°, 30°, 30°, 30°
with the Aeronautics Research Institute

Percentages of the maximum stress at the Aeronautics Research Institute No. 1

edge	x	y	z	angle	Gage No.		Harm
					Element	Location	
1*	0.3	0.0	0.0	0.0	246	(+97)	0.02(+77)
2*	0.4	0.0	0.0	0.0	247	(+97)	0.00(+96)
3	0.5	0.0	0.0	0.0	248	(+93)	0.01(-113)
4	0.6	0.0	0.0	0.0	249	(+96)	0.00(+168)
5	0.7	0.0	0.0	0.0	250	(+91)	0.00(-145)
6	0.8	0.0	0.0	0.0	251	(+87)	0.02(-84)
7	0.9	0.0	0.0	0.0	252	(+72)	0.01(+59)
8	1.0	0.0	0.0	0.0	253	(+165)	0.00(-131)
9	1.1	0.0	0.0	0.0	254	(+90)	0.02(-93)
10	1.2	0.0	0.0	0.0	255	(+53)	0.01(+78)
11	0.3	0.1	0.0	0.0	256	(+14)	0.01(+76)
12	0.4	0.1	0.0	0.0	257	(+14)	0.01(+65)
13	0.5	0.1	0.0	0.0	258	(+36)	0.03(+96)
14	0.6	0.1	0.0	0.0	259	(+159)	0.03(-35)
15	0.7	0.1	0.0	0.0	260	(+104)	0.04(+100)
16	0.8	0.1	0.0	0.0	261	(+15)	0.01(+53)
17	0.9	0.1	0.0	0.0	262	(+11)	0.00(-153)
18	1.0	0.1	0.0	0.0	263	(-11)	0.02(-107)
19	1.1	0.1	0.0	0.0	264	(+18)	0.00(+101)
20	1.2	0.1	0.0	0.0	265	(+10)	0.00(+24)
21	0.3	0.2	0.0	0.0	266	(+34)	0.00(-49)
22	0.4	0.2	0.0	0.0	267	(+7)	0.02(+64)
23	0.5	0.2	0.0	0.0	268	(+32)	0.01(+112)
24	0.6	0.2	0.0	0.0	269	(+65)	0.01(-119)
25	0.7	0.2	0.0	0.0	270	(+22)	0.03(+124)
26	0.8	0.2	0.0	0.0	271	(+11)	0.02(+5)
27	0.9	0.2	0.0	0.0	272	(+100)	0.00(-110)
28	1.0	0.2	0.0	0.0	273	(+77)	0.02(+71)
29	1.1	0.2	0.0	0.0	274	(+26)	0.00(-80)
30	1.2	0.2	0.0	0.0	275	(+5)	0.00(-54)
31	0.3	0.3	0.0	0.0	276	(+31)	0.03(+41)
32	0.4	0.3	0.0	0.0	277	(+18)	0.03(+104)
33	0.5	0.3	0.0	0.0	278	(+34)	0.01(+167)
34	0.6	0.3	0.0	0.0	279	(+47)	0.04(-21)
35	0.7	0.3	0.0	0.0	280	(+13)	0.10(+98)
36	0.8	0.3	0.0	0.0	281	(+31)	0.10(+109)

Table 7
Distribution of Wave Energy Throughout the Experimental Facility, 30-deg
Incident Direction, Period = 0.75 sec., Ocean Wave Height = 0.218 ft
60-deg Breakwater Angle with Shoreline
Percent of Total Energy and Phase Angle (deg), Arrangement No. 2

<u>Gage</u>	<u>Fundamental</u> <u>Period</u> <u>0.75 sec</u>	<u>First</u> <u>Harmonic</u> <u>0.38 sec</u>	<u>Second</u> <u>Harmonic</u> <u>0.25 sec</u>	<u>Third</u> <u>Harmonic</u> <u>0.19 sec</u>	<u>Fourth</u> <u>Harmonic</u> <u>0.15 sec</u>
1*	94.49(+93)	4.86(+147)	0.61(-138)	0.03(-51)	0.02(+24)
2*	98.95(+143)	0.84(-7)	0.20(+176)	0.01(+60)	0.00(+113)
3	98.60(+162)	1.26(+75)	0.12(-149)	0.02(+47)	0.00(+146)
4	99.37(-172)	0.53(-29)	0.09(+128)	0.01(-30)	0.00(+100)
5	95.55(-73)	4.25(-134)	0.16(-179)	0.02(-161)	0.02(-99)
6	95.48(+38)	4.32(+76)	0.18(+117)	0.01(+85)	0.01(+33)
7	96.69(+158)	3.12(-54)	0.19(+127)	0.00(-17)	0.00(+39)
8	97.19(-98)	2.76(+175)	0.05(+118)	0.00(-120)	0.01(-134)
9	96.34(+20)	3.35(+41)	0.28(+56)	0.02(+78)	0.01(+53)
10	96.50(+131)	3.32(-95)	0.15(+57)	0.00(-171)	0.00(+174)
11	98.13(147)	1.83(-138)	0.04(-17)	0.01(+64)	0.01(+179)
12	99.52(+35)	0.32(+13)	0.14(+86)	0.01(+86)	0.01(+76)
13	99.09(+97)	0.20(+155)	0.09(+108)	0.01(+77)	0.01(+76)
14	96.33(+170)	3.43(-25)	0.24(+139)	0.01(-5)	0.00(+123)
15	94.48(-93)	5.31(-170)	0.19(+120)	0.00(+13)	0.01(-137)
16	92.46(+38)	6.81(+69)	0.63(+91)	0.07(+107)	0.03(+77)
17	94.57(+146)	5.12(-75)	0.31(+73)	0.00(-118)	0.00(-42)
18	95.25(-102)	4.59(+165)	0.15(+70)	0.01(-60)	0.00(-147)
19	97.71(+76)	2.13(+95)	0.11(+89)	0.04(+93)	0.01(+92)
20	99.99(+17)	0.01(-140)	0.00(-120)	0.00(+46)	0.00(+26)
21	99.62(+21)	0.36(+35)	0.00(-10)	0.01(+40)	0.00(+38)
22	95.75(+81)	4.05(+137)	0.15(+157)	0.03(+77)	0.01(+79)
23	92.23(+156)	7.23(-56)	0.54(+100)	0.01(-91)	0.00(+48)
24	90.02(-92)	9.59(+176)	0.36(+84)	0.02(-56)	0.01(-129)
25	84.85(+27)	12.65(+46)	2.06(+64)	0.33(+76)	0.10(+74)
26	89.60(+153)	9.35(-61)	0.99(+94)	0.06(-129)	0.01(+7)
27	91.80(-103)	7.94(+160)	0.23(+60)	0.03(-64)	0.01(-142)
28	98.06(+125)	1.92(-103)	0.02(+89)	0.00(+13)	0.00(+39)
29	98.77(+35)	1.18(+0.9)	0.03(-23)	0.01(-33)	0.01(+3)
30	99.67(-27)	0.32(-31)	0.01(+54)	0.01(-85)	0.00(-62)
31	98.77(-12)	1.19(-31)	0.04(+30)	0.01(-11)	0.00(-4)
32	91.39(+25)	7.80(+42)	0.70(+55)	0.10(+69)	0.02(+60)
33	87.77(+82)	11.39(+16)	0.78(-135)	0.03(-8)	0.03(+45)
34	83.33(+175)	14.65(-20)	1.78(+143)	0.22(-43)	0.03(+108)
35	81.49(-76)	16.60(-164)	1.75(+111)	0.12(-10)	0.04(-122)
36	80.89(+52)	15.36(+86)	3.01(+108)	0.59(+114)	0.15(+117)

* Ocean gage.

Table 8
Distribution of Wave Energy Throughout the Experimental Facility, 30-deg
Incident Direction, Period = 1.00 sec, Ocean Wave Height = 0.102 ft
60-deg Breakwater Angle with Shoreline
Percent of Total Energy and Phase Angle (deg), Arrangement No. 1

Gage	Fundamental	First	Second	Third	Fourth
	Period 1.00 sec	Harmonic 0.50 sec	Harmonic 0.33 sec	Harmonic 0.25 sec	Harmonic 0.20 sec
1*	99.19(+86)	0.65(+116)	0.16(+174)	0.01(-133)	0.00(-25)
2*	99.44(+122)	0.53(-96)	0.00(-125)	0.02(+13)	0.01(+119)
3	99.64(+163)	0.32(+156)	0.04(-56)	0.00(+128)	0.00(+27)
4	99.60(+137)	0.33(+147)	0.05(-141)	0.02(+10)	0.01(+113)
5	98.07(+176)	1.91(-13)	0.01(+146)	0.00(-147)	0.00(+51)
6	98.40(-103)	1.57(+165)	0.01(+74)	0.00(-116)	0.00(-130)
7	98.93(-25)	1.07(-58)	0.01(-72)	0.00(-171)	0.00(+38)
8	98.28(+57)	1.67(+93)	0.03(+111)	0.01(+101)	0.00(+116)
9	98.75(+125)	1.23(-119)	0.01(+54)	0.00(+68)	0.00(+106)
10	99.16(-156)	0.81(+32)	0.02(-136)	0.00(+99)	0.00(-136)
11	99.13(-15)	0.84(-22)	0.01(-60)	0.02(+142)	0.01(+142)
12	98.13(-27)	1.84(-50)	0.03(-98)	0.00(+105)	0.00(+65)
13	99.50(-6)	0.49(+19)	0.00(-169)	0.01(+179)	0.00(-142)
14	98.33(+64)	1.63(+105)	0.04(+106)	0.00(+140)	0.00(+79)
15	97.98(+144)	1.95(-84)	0.07(+54)	0.00(+156)	0.00(+61)
16	97.41(-130)	2.51(+94)	0.08(-49)	0.00(-150)	0.00(-144)
17	98.44(-63)	1.54(-121)	0.01(-159)	0.00(-57)	0.00(-77)
18	98.25(+18)	1.72(+30)	0.03(+35)	0.00(-0.5)	0.00(+22)
19	99.76(-115)	0.16(-41)	0.07(+177)	0.01(+151)	0.00(-82)
20	99.93(-171)	0.02(+125)	0.04(+16)	0.01(-131)	0.00(+94)
21	99.91(+170)	0.05(+8)	0.02(-18)	0.01(+146)	0.00(-15)
22	98.95(-166)	1.03(+1)	0.01(+54)	0.01(-106)	0.00(+78)
23	97.02(-109)	2.93(+138)	0.05(+7)	0.01(-126)	0.00(+127)
24	96.26(-40)	3.63(-83)	0.11(-113)	0.00(-109)	0.00(-141)
25	92.83(+46)	6.61(+79)	0.50(+118)	0.04(+133)	0.00(+152)
26	93.61(+124)	5.99(-123)	0.35(-6)	0.04(+113)	0.00(-92)
27	96.46(-153)	3.37(+36)	0.16(-125)	0.01(+83)	0.00(-91)
28	98.97(+93)	0.06(+162)	0.06(+140)	0.01(-165)	0.00(-17)
29	97.30(+63)	2.12(+33)	0.04(+13)	0.03(+62)	0.01(+93)
30	97.27(+41)	2.67(+47)	0.02(+35)	0.04(-6)	0.01(+24)
31	95.61(+59)	4.15(+03)	0.11(+123)	0.02(+100)	0.02(+102)
32	94.88(+105)	4.51(-165)	0.20(-70)	0.01(-6)	0.00(+59)
33	90.94(+172)	8.23(-36)	0.63(+120)	0.08(-77)	0.02(+103)
34	85.08(-110)	12.34(+124)	1.82(+2)	0.24(-112)	0.03(+154)
35	83.24(-31)	13.73(-82)	2.53(-121)	0.44(-153)	0.06(-168)
36	88.32(+55)	10.19(+90)	1.34(+123)	0.15(+159)	0.00(-164)

* Ocean gage.

Table 9

Distribution of Wave Energy Throughout the Experimental Facility, 30-deg

Incident Direction, Period = 1.00 sec, Ocean Wave Height = 0.102 ft

60-deg Breakwater Angle with Shoreline

Percent of Total Energy and Phase Angle (deg), Arrangement No. 2

Gage	Fundamental	First	Second	Third	Fourth
	Period 1.00 sec	Harmonic 0.50 sec	Harmonic 0.33 sec	Harmonic 0.25 sec	Harmonic 0.20 sec
1*	99.10(+80)	0.75(+112)	0.13(-141)	0.01(-81)	0.00(+128)
2*	99.54(+118)	0.39(-77)	0.03(-29)	0.03(-38)	0.01(+76)
3	99.23(+147)	0.73(+114)	0.03(-140)	0.01(+111)	0.00(-61)
4	99.28(+159)	0.71(-101)	0.01(+23)	0.00(-178)	0.00(-117)
5	98.21(-135)	1.75(+81)	0.04(-38)	0.00(+56)	0.00(-49)
6	93.41(-53)	1.53(-94)	0.05(-129)	0.00(+156)	0.00(-175)
7	93.09(+29)	1.83(+33)	0.03(+37)	0.00(+71)	0.00(+133)
8	93.02(+104)	1.96(-143)	0.02(-41)	0.00(+93)	0.00(+137)
9	99.00(+176)	0.99(-17)	0.01(+172)	0.00(-100)	0.00(+82)
10	98.37(-98)	1.11(+156)	0.01(+32)	0.00(-116)	0.00(-163)
11	93.39(+20)	1.47(+68)	0.10(-101)	0.03(-53)	0.01(-24)
12	97.92(-20)	2.06(-37)	0.02(+51)	0.00(+143)	0.01(+152)
13	93.57(-11)	1.37(+9)	0.02(-154)	0.03(-161)	0.01(-175)
14	99.65(+34)	0.35(+81)	0.00(+108)	0.00(-61)	0.00(-153)
15	93.41(+115)	1.54(-143)	0.03(-69)	0.02(+31)	0.10(+12)
16	96.27(-153)	3.54(+38)	0.20(-139)	0.01(+87)	0.00(-74)
17	97.29(-79)	2.71(+171)	0.15(+104)	0.01(-50)	0.00(-28)
18	97.41(-4)	2.71(-22)	0.11(-41)	0.01(-68)	0.00(-28)
19	99.50(-138)	0.48(-51)	0.02(+90)	0.03(-32)	0.01(-114)
20	99.37(-166)	0.61(+174)	0.03(+75)	0.03(-118)	0.01(+21)
21	99.66(-172)	0.29(-51)	0.01(+125)	0.03(+177)	0.01(+51)
22	97.48(-126)	2.44(+80)	0.07(-53)	0.00(+38)	0.00(-105)
23	96.08(-59)	3.80(-123)	0.11(-177)	0.00(+109)	0.00(-14)
24	93.64(+17)	5.96(+23)	0.36(+36)	0.03(+55)	0.01(+59)
25	93.03(+102)	6.42(-172)	0.50(-78)	0.05(+26)	0.00(+153)
26	94.37(-123)	5.23(-5)	0.34(-175)	0.03(-5)	0.01(-148)
27	95.59(-97)	4.23(+154)	0.11(+42)	0.01(-39)	0.00(-154)
28	99.01(+117)	0.89(-23)	0.03(-84)	0.06(+82)	0.00(-23)
29	93.47(+74)	1.17(+150)	0.07(+176)	0.02(+132)	0.00(-35)
30	94.37(+99)	1.53(+83)	0.09(+13)	0.05(+31)	0.01(+104)
31	96.17(+73)	1.16(+99)	0.11(+97)	0.03(+119)	0.02(+101)
32	95.97(+13)	3.89(+176)	0.13(-137)	0.00(-36)	0.00(+3)
33	92.66(+163)	6.87(-59)	0.11(+83)	0.05(-157)	0.01(+100)
34	86.81(-130)	11.24(+79)	1.69(-63)	0.24(+168)	0.02(+44)
35	82.93(-51)	14.31(-100)	2.32(-180)	0.38(+125)	0.05(+86)
36	83.81(+31)	13.74(+46)	2.05(+65)	0.34(+91)	0.05(+179)

Ocean gage.

table 10

Distribution of Wave Energy Throughout the Experimental Facility, 30-degIncident Direction, Period = 1.00 sec, Ocean Wave Height = 0.130 ft60-deg Breakwater Angle with ShorelinePercent of Total Energy and Phase Angle (deg), Arrangement No. 1

Gage	Fundamental	First	Second	Third	Fourth
	Period 1.00 sec	Harmonic 0.50 sec	Harmonic 0.33 sec	Harmonic 0.25 sec	Harmonic 0.20 sec
1*	99.22(+95)	0.59(+107)	0.18(+128)	0.01(+149)	0.00(+63)
2*	99.09(123)	0.89(-112)	0.01(-32)	0.01(+75)	0.00(-141)
3	99.82(+169)	0.15(+172)	0.01(-33)	0.02(+118)	0.00(-121)
4	99.91(+142)	0.09(-109)	0.01(+162)	0.04(+46)	0.00(+119)
5	99.44(-177)	0.58(+6)	0.00(-41)	0.00(+72)	0.00(+62)
6	96.35(-98)	3.49(+158)	0.14(+54)	0.02(-47)	0.01(-108)
7	96.99(-23)	2.86(-46)	0.17(-59)	0.03(-65)	0.01(-61)
8	97.21(+58)	2.69(+97)	0.10(+129)	0.01(-173)	0.00(+20)
9	97.22(+129)	2.69(-113)	0.08(+20)	0.01(+123)	0.00(+3)
10	98.27(-152)	1.63(+3)	0.05(-112)	0.00(+119)	0.00(-53)
11	98.28(-10)	1.67(-6)	0.00(+89)	0.04(+145)	0.01(+171)
12	97.95(-26)	2.04(-45)	0.00(-316)	0.00(+12)	0.00(+138)
13	98.78(+2)	1.20(+17)	0.01(-36)	0.01(+122)	0.01(-130)
14	97.08(+68)	2.84(+122)	0.08(+142)	0.00(-150)	0.01(+63)
15	96.10(+146)	3.65(-76)	0.23(+66)	0.02(-133)	0.00(+87)
16	94.54(+130)	5.05(+92)	0.36(-49)	0.06(-158)	0.00(+86)
17	95.69(-62)	4.07(-124)	0.21(-169)	0.01(-169)	0.00(-176)
18	96.73(+20)	3.08(+37)	0.16(+48)	0.03(+62)	0.01(+72)
19	99.59(-106)	0.37(+78)	0.05(-81)	0.01(+172)	0.00(-32)
20	99.92(-160)	0.01(-144)	0.06(-81)	0.01(-152)	0.00(+180)
21	99.69(+176)	0.30(-30)	0.01(+92)	0.00(+155)	0.00(+56)
22	97.90(-117)	2.03(-13)	0.06(-176)	0.01(-106)	0.00(-166)
23	95.57(-102)	4.29(+154)	0.12(+39)	0.02(-92)	0.00(+174)
24	94.03(-35)	5.34(-85)	0.47(+120)	0.03(-147)	0.05(-146)
25	87.22(+43)	10.39(+72)	1.66(+106)	0.22(+144)	0.02(+157)
26	87.90(+120)	10.95(-134)	0.97(-16)	0.16(+107)	0.02(-115)
27	92.87(-154)	6.17(+33)	0.51(-137)	0.06(+57)	0.10(-43)
28	97.20(+109)	1.77(-141)	0.01(+23)	0.00(+146)	0.00(+110)
29	96.49(+73)	1.17(+113)	0.15(+16)	0.01(+75)	0.00(+100)
30	95.04(+67)	4.19(+77)	0.41(+13)	0.01(+13)	0.02(+64)
31	94.41(+69)	1.19(+119)	0.13(+151)	0.01(+175)	0.02(+93)
32	92.29(+111)	7.15(-155)	0.40(-103)	0.01(+86)	0.00(-156)
33	83.77(+175)	13.77(+36)	2.10(+129)	0.39(-56)	0.04(+128)
34	77.46(-117)	1.17(+109)	0.01(+18)	0.02(-139)	0.09(+97)
35	74.52(-40)	19.14(-101)	4.91(-151)	0.01(+163)	0.12(+109)
36	79.41(+47)	19.17(+72)	3.49(+130)	0.61(+133)	0.07(+148)

* Ocean gage.

Table 11

Distribution of Wave Energy Throughout the Experimental Facility, 30-deg Incident Direction, Period = 1.00 sec, Ocean Wave Height = 0.130 ft
60-deg Breakwater Angle with Shoreline

Percent of Total Energy and Phase Angle (deg), Arrangement No. 2

Gage	Fundamental	First	Second	Third	Fourth
	Period 1.00 sec	Harmonic 0.50 sec	Harmonic 0.33 sec	Harmonic 0.25 sec	Harmonic 0.20 sec
1*	98.82(+91)	0.97(+110)	0.17(+137)	0.04(-141)	0.00(+25)
2*	99.03(+122)	0.94(-111)	0.01(-31)	0.02(+88)	0.00(-99)
3	99.51(+139)	0.42(+112)	0.07(-177)	0.00(-177)	0.00(+97)
4	99.22(+151)	0.75(-87)	0.02(+34)	0.01(-155)	0.00(-108)
5	98.06(-144)	1.30(+57)	0.14(-115)	0.00(+110)	0.00(-12)
6	95.54(-60)	4.21(-114)	0.24(-159)	0.01(+157)	0.00(-173)
7	96.69(+19)	3.09(+35)	0.18(+50)	0.03(+81)	0.00(+149)
8	97.13(+93)	2.78(+174)	0.07(-105)	0.02(+33)	0.00(+88)
9	97.41(+164)	2.52(-33)	0.07(+134)	0.01(-69)	0.00(+104)
10	98.07(-108)	1.88(+140)	0.03(+15)	0.01(-89)	0.00(-129)
11	98.38(+15)	1.55(+54)	0.04(-143)	0.02(-41)	0.01(-45)
12	97.35(-28)	2.10(-53)	0.06(-15)	0.00(-65)	0.00(+52)
13	98.49(-20)	1.48(-27)	0.03(-101)	0.00(+131)	0.00(+167)
14	98.25(+27)	1.69(+49)	0.05(+78)	0.00(+49)	0.00(+138)
15	96.94(+104)	2.88(-156)	0.16(-58)	0.02(+70)	0.00(-76)
16	94.21(-169)	5.27(+9)	0.47(-169)	0.04(+31)	0.00(-117)
17	94.33(-92)	5.36(+164)	0.27(+67)	0.03(-25)	0.01(-108)
18	95.31(-19)	3.97(-44)	0.19(68)	0.02(-73)	0.00(-81)
19	99.66(-140)	0.29(-73)	0.04(+85)	0.01(-16)	0.00(-149)
20	99.84(-180)	0.04(+90)	0.10(+9)	0.01(-98)	0.00(+10)
21	99.49(+178)	0.47(-29)	0.02(+25)	0.02(+143)	0.01(+16)
22	96.75(-135)	3.07(+70)	0.19(82)	0.00(+7)	0.00(-170)
23	93.83(-70)	5.91(-149)	0.24(+151)	0.03(+87)	0.00(-2)
24	89.48(+3)	9.50(-9)	0.84(-13)	0.15(-3)	0.03(+37)
25	88.38(+83)	10.37(+153)	1.12(-132)	0.11(-39)	0.02(+60)
26	91.54(+70)	7.73(-33)	0.65(+132)	0.08(-56)	0.01(+138)
27	93.51(-112)	6.03(+122)	0.40(-8)	0.05(-104)	0.01(+171)
28	97.23(+145)	2.74(-71)	0.01(-103)	0.01(+11)	0.00(-107)
29	97.09(+84)	2.77(+139)	0.11(+166)	0.03(+107)	0.01(+39)
30	96.65(+47)	3.24(+68)	0.06(+68)	0.03(+67)	0.03(+62)
31	93.73(+47)	5.75(+81)	0.45(+119)	0.04(+129)	0.03(+97)
32	93.23(+30)	6.32(+149)	0.42(-160)	0.02(-13)	0.01(+33)
33	86.99(+145)	11.76(-91)	1.03(+38)	0.21(+169)	0.01(+4)
34	77.45(-150)	13.10(+39)	3.71(-122)	0.66(+84)	0.08(-66)
35	74.82(-76)	19.69(-170)	4.41(+104)	0.90(+21)	0.18(-70)
36	75.96(+6)	13.54(-8)	4.34(-13)	0.98(-15)	0.18(-19)

* Ocean gage.

Distribution

Incident

Percent

Gage	Percent	Mean	SD	Min	Max
1*	0.0	0.00	0.00	0.00	0.00
2*	3.8	0.03	0.01	0.00	0.07
3	0.3	0.00	0.00	0.00	0.00
4	0.0	0.00	0.00	0.00	0.00
5	0.2	0.00	0.00	0.00	0.00
6	0.0	0.00	0.00	0.00	0.00
7	0.4	0.00	0.00	0.00	0.00
8	9.1	0.09	0.03	0.05	0.13
9	9.4	0.09	0.03	0.05	0.13
10	46.2	0.46	0.05	0.35	0.57
11	95.3	0.95	0.01	0.93	0.97
12	94.1	0.94	0.01	0.92	0.96
13	93.5	0.93	0.01	0.91	0.95
14	93.5	0.93	0.01	0.91	0.95
15	91.1	0.91	0.01	0.89	0.93
16	87.8	0.88	0.01	0.86	0.90
17	90.0	0.90	0.01	0.88	0.92
18	91.6	0.92	0.01	0.90	0.94
19	69.1	0.69	0.01	0.67	0.71
20	79.1	0.79	0.01	0.77	0.81
21	99.3	0.99	0.00	0.98	1.00
22	95.0	0.95	0.01	0.93	0.97
23	89.0	0.89	0.01	0.87	0.91
24	26.3	0.26	0.01	0.24	0.28
25	77.2	0.77	0.01	0.75	0.79
26	79.4	0.79	0.01	0.77	0.81
27	36.7	0.37	0.01	0.35	0.39
28	13.1	0.13	0.01	0.12	0.14
29	91.4	0.91	0.01	0.89	0.93
30	87.	0.87	0.01	0.85	0.89
31	8.3	0.08	0.01	0.07	0.09
32	80.4	0.80	0.01	0.78	0.82
33	73.2	0.73	0.01	0.71	0.75
34	67.0	0.67	0.01	0.65	0.69
35	67.3	0.67	0.01	0.65	0.69
36	69.4	0.69	0.01	0.67	0.71

* Ocean wave

Table 13
 Distribution of Wave Energy Through at the Experimental Facility, 30-deg
 Incident Direction, Period = 1.00 sec, Ocean Wave Height = 0.211 ft
 60-deg Breakwater Angle with Shoreline
 Percent of Total Energy and Phase Angle (deg), Arrangement No. 2

Gage	Fundamental	First	Second	Third	Fourth
	Period 1.00 sec	Harmonic 0.50 sec	Harmonic 0.33 sec	Harmonic 0.25 sec	Harmonic 0.20 sec
1*	95.87(+97)	0.14(-8)	0.06(-163)	0.12(-9)	0.01(+92)
2*	95.17(+129)	1.63(-105)	0.05(-27)	0.05(+105)	0.00(-137)
3	93.36(+138)	1.57(+103)	0.07(+121)	0.00(+25)	0.00(+161)
4	96.37(+155)	3.37(-117)	0.33(+8)	0.07(+158)	0.01(-39)
5	94.99(-150)	4.95(+58)	0.42(-92)	0.04(+131)	0.00(+2)
6	95.29(-71)	7.91(-142)	0.74(+162)	0.06(+125)	0.00(+52)
7	94.37(+6)	5.29(+6)	0.32(+16)	0.01(+17)	0.00(+4)
8	92.39(+14)	7.07(+146)	0.49(-136)	0.03(-7)	0.01(+111)
9	93.87(+164)	5.16(-50)	0.24(+109)	0.04(-66)	0.00(+114)
10	94.91(-115)	4.82(+115)	0.24(-8)	0.03(-106)	0.00(-154)
11	95.15(+13)	4.78(+57)	0.06(+89)	0.01(-104)	0.01(-2)
12	94.15(-29)	5.21(-58)	0.53(-76)	0.06(-116)	0.01(-129)
13	93.62(-15)	5.90(-27)	0.41(-36)	0.06(-52)	0.01(-50)
14	97.43(+18)	2.42(+51)	0.14(+87)	0.01(+38)	0.00(-159)
15	91.12(+39)	8.30(+168)	0.53(-105)	0.04(+22)	0.01(+83)
16	89.15(+174)	9.52(-32)	1.22(+135)	0.10(-64)	0.01(+36)
17	89.50(-193)	9.52(+135)	0.36(+19)	0.11(-81)	0.01(-170)
18	91.40(-30)	7.55(-63)	0.90(-92)	0.12(-105)	0.03(-104)
19	99.05(-141)	0.32(-64)	0.11(+41)	0.02(-110)	0.00(+161)
20	99.75(-178)	0.12(+36)	0.06(+46)	0.01(+151)	0.00(-32)
21	98.88(+114)	1.03(-45)	0.08(+128)	0.01(-103)	0.00(+157)
22	92.55(-147)	0.76(+33)	0.65(-122)	0.03(+92)	0.01(-64)
23	85.20(-39)	1.15(+172)	1.72(+80)	0.21(-19)	0.02(-121)
24	81.41(-22)	1.61(-57)	2.65(-88)	0.45(-104)	0.07(-127)
25	77.93(+57)	1.38(+101)	3.58(+147)	0.56(-167)	0.08(-129)
26	87.37(+147)	1.63(-36)	2.52(+60)	0.32(-157)	0.03(-21)
27	83.20(-176)	1.56(-84)	1.83(-51)	0.20(-177)	0.01(+48)
28	94.77(+148)	0.12(-253)	0.10(+38)	0.13(-79)	0.01(-104)
29	94.77(+148)	0.10(+149)	0.39(+178)	0.91(+166)	0.01(+59)
30	96.26(-117)	0.10(+13)	0.50(+124)	0.03(+59)	0.01(+79)
31	94.23(+147)	0.10(+14)	1.47(+96)	0.27(+111)	0.01(+171)
32	94.23(+147)	0.10(+14)	1.12(+171)	0.34(-130)	0.03(-21)
33	94.23(+147)	0.10(+14)	1.81(-51)	0.36(+61)	0.15(+166)
34	84.23(+147)	0.10(+14)	5.63(+115)	1.90(-90)	0.51(+59)
35	84.23(+147)	0.10(+14)	7.55(-39)	2.29(-177)	0.72(+33)
36	84.23(+147)	0.10(+14)	1.41(+135)	2.29(+175)	0.65(+171)

* Ocean gage.

Table I
Distribution of wave energy throughout the experimental Facility, 30-deg
Incident Direction, $T_{\text{sw}} = 1.50$ sec., Mean Wave Height ≈ 0.070 ft
Revised, Incident Angle with Shoreline
Percent of Total Incident Energy, Angle of deg., Arrangement No. 1

Gage	First Harmonic		Second Harmonic		Third Harmonic		Fourth Harmonic	
	Period 1.50 sec.	Phase Angle	Period 0.30 sec.	Phase Angle	Period 0.35 sec.	Phase Angle	Period 0.30 sec.	Phase Angle
1*	97.41(+27)	-1.1(+17)	0.10(+70)	0.08(+45)	0.03(+158)			
2*	99.13(+1)	-1.1(+17)	0.19(+33)	0.11(-168)	0.00(+66)			
3	98.86(+17)	-1.1(+17)	0.10(+11)	0.02(-117)	0.00(+96)			
4	98.11(+1)	-1.1(+17)	0.17(+11)	0.07(+95)	0.01(+78)			
5	98.11(+1)	-1.1(+17)	0.18(+17)	0.03(+175)	0.00(+178)			
6	97.83(+1)	-1.1(+17)	0.10(+41)	0.06(-121)	0.01(+111)			
7	99.13(+1)	-1.1(+17)	0.11(+15)	0.01(+123)	0.01(+23)			
8	99.56(+6)	-1.1(+168)	0.12(-53)	0.00(+58)	0.01(-24)			
9	99.49(+11)	-1.1(+17)	0.31(-172)	0.04(+22)	0.01(+51)			
10	99.14(+1)	-1.1(+17)	0.04(+14)	0.10(-84)	0.01(-103)			
11	93.33(+1)	-1.1(+17)	0.00(-171)	0.04(+123)	0.01(+52)			
12	98.56(+3)	-1.1(+17)	0.24(+146)	0.07(-91)	0.08(+111)			
13	99.13(+1)	-1.1(+17)	0.01(-89)	0.04(-7)	0.02(-91)			
14	99.56(+6)	-1.1(+168)	0.04(-65)	0.04(-3)	0.00(-104)			
15	99.88(+1)	-1.1(+17)	0.04(+152)	0.01(-40)	0.00(-74)			
16	99.48(+1)	-1.1(+17)	0.09(+11)	0.04(-111)	0.01(-159)			
17	93.11(+1)	-1.1(+17)	0.11(-15)	0.01(-131)	0.00(+164)			
18	97.11(+1)	-1.1(+14)	0.18(-68)	0.03(-167)	0.00(-106)			
19	97.20(+1)	-1.1(+17)	0.31(-136)	0.06(-39)	0.01(+30)			
20	99.13(+1)	-1.1(+17)	0.01(+30)	0.09(+141)	0.01(+107)			
21	98.11(+1)	-1.1(+17)	0.07(+11)	0.04(-91)	0.02(-16)			
22	93.13(+1)	-1.1(+17)	0.11(-15)	0.16(+119)	0.06(-99)			
23	99.13(+1)	-1.1(+17)	0.04(+1)	0.13(+107)	0.06(+168)			
24	99.13(+1)	-1.1(+17)	0.13(-17)	0.07(+92)	0.00(-99)			
25	99.13(+1)	-1.1(+17)	0.24(+9)	0.03(-89)	0.00(+177)			
26	93.11(+1)	-1.1(+17)	0.80(+10)	0.68(+156)	0.01(+91)			
27	89.81(+1)	-1.1(+17)	1.15(+1)	0.08(+5)	0.01(+24)			
28	99.13(+1)	-1.1(+17)	1.12(+1)	0.01(-35)	0.02(-2)			
29	98.11(+1)	-1.1(+17)	0.73(-15)	0.10(-79)	0.01(-2)			
30	99.13(+1)	-1.1(+17)	0.12(+17)	0.01(-60)	0.01(-114)			
31	93.63(+1)	-1.1(+17)	0.13(+6)	0.06(-69)	0.02(-31)			
32	91.66(+1)	-1.1(+17)	0.37(+17)	0.10(+162)	0.02(+119)			
33	93.11(+1)	-1.1(+17)	0.96(+1)	0.01(-48)	0.01(+173)			
34	94.91(+1)	-1.1(+17)	1.71(+10)	0.17(+96)	0.06(+135)			
35	79.56(+1)	-1.1(+17)	4.87(+93)	0.87(-6)	0.16(+86)			
36	78.11(+1)	-1.1(+17)	3.42(+55)	0.47(+178)	0.12(-50)			

Table 15
 Distribution of Wave Energy Throughout the Experimental Facility, 30-deg
 Incident Direction, Period = 1.50 sec, Ocean Wave Height = 0.070 ft
 60-deg Breakwater Angle with Shoreline
 Percent of Total Energy and Phase Angle (deg), Arrangement No. 2

Gage	Fundamental	First	Second	Third	Fourth
	Period 1.50 sec	Harmonic 0.75 sec	Harmonic 0.50 sec	Harmonic 0.38 sec	Harmonic 0.30 sec
1*	97.22(+81)	2.77(-87)	0.00(+146)	0.00(-75)	0.01(-173)
2*	99.17(+97)	0.6n(-9)	0.17(+131)	0.00(-79)	0.00(+98)
3	95.38(-94)	3.95(+177)	0.11(+91)	0.01(-174)	0.06(+55)
4	94.18(-39)	5.73(-1/4)	0.06(+99)	0.01(+77)	0.03(+118)
5	98.05(-55)	1.90(-66)	0.02(+16)	0.02(+57)	0.00(+77)
6	99.47(-16)	0.46(+16)	0.07(-11)	0.00(-43)	0.00(+146)
7	99.34(+34)	0.07(+127)	0.09(-89)	0.01(-38)	0.00(+50)
8	99.77(+86)	0.15(+9)	0.08(-169)	0.00(+82)	0.00(-2)
9	99.95(+137)	1.03(+171)	0.01(-157)	0.02(-127)	0.00(-37)
10	97.60(+175)	2.17(-89)	0.23(+26)	0.00(+70)	0.00(-77)
11	96.62(+56)	3.29(+129)	0.02(-139)	0.05(+134)	0.01(-99)
12	96.38(+27)	3.53(+67)	0.01(-115)	0.03(-36)	0.06(-21)
13	98.04(+33)	1.81(+97)	0.02(+143)	0.02(+168)	0.12(+42)
14	98.67(+52)	1.18(+152)	0.13(-148)	0.01(+80)	0.01(+41)
15	99.52(+94)	0.27(+149)	0.20(+119)	0.00(+145)	0.00(-97)
16	98.19(+144)	1.70(-126)	0.11(-17)	0.01(+170)	0.00(-124)
17	96.83(-163)	3.11(-34)	0.05(+71)	0.01(+177)	0.00(+27)
18	94.35(-116)	5.07(+61)	0.54(-103)	0.04(+92)	0.00(+23)
19	97.45(-177)	2.50(+35)	0.02(-111)	0.02(+17)	0.01(+64)
20	96.62(+163)	3.29(-2)	0.06(+120)	0.02(-163)	0.02(-8)
21	97.41(+161)	2.32(-4)	0.05(-122)	0.11(-69)	0.12(-29)
22	99.74(+177)	0.21(+6)	0.02(-35)	0.00(+115)	0.02(-56)
23	99.65(-145)	0.93(+2)	0.35(-164)	0.02(+103)	0.00(+10)
24	94.24(-104)	5.71(+93)	0.03(-19)	0.02(+113)	0.01(-14)
25	92.18(-47)	6.65(-156)	1.08(+122)	0.07(+37)	0.02(-21)
26	89.57(+3)	9.71(-42)	0.67(-45)	0.05(-71)	0.01(-152)
27	88.49(+49)	10.99(+55)	0.50(+72)	0.03(+77)	0.00(+85)
28	99.20(+4)	0.67(+106)	0.06(+158)	0.02(-100)	0.05(-147)
29	93.92(-41)	1.00(-9)	0.01(+60)	0.01(+168)	0.00(+94)
30	99.33(-51)	0.50(-107)	0.03(-91)	0.01(+116)	0.03(+5)
31	99.16(-43)	0.17(-34)	0.14(+103)	0.06(-10)	0.03(-60)
32	93.08(-33)	1.67(-101)	0.11(+152)	0.10(+98)	0.02(+93)
33	94.69(-2)	0.23(+54)	0.45(-89)	0.03(-128)	0.00(+125)
34	86.31(+37)	11.12(+23)	1.75(+14)	0.22(+23)	0.02(+5)
35	78.76(+92)	16.53(-131)	3.97(-162)	0.61(-99)	0.14(-30)
36	75.21(+139)	0.23(-126)	3.57(-21)	0.75(+93)	0.23(-157)

* Ocean gage.

Table I
Distribution of Wave Energy Throughout the Experiment at Four Incident
Incident Periodicity Period = 1.50 sec., Mean Wave Height = 0.05 m.
Standing Breakwater Angle with Shoreline
Percent of Total Energy and Phase Angle (deg.) At Angle θ

Gage	Wavelength		Period		Percent
	0.10 sec	0.20 sec	0.50 sec	0.88 sec	
1*	94.8 (+0.4)	1.10 (-100)	0.14 (-20)	0.05 (+145)	0.04 (+0.3)
2*	94.7 (-+1.0)	1.10 (+43)	0.14 (+35)	0.02 (-36)	0.01 (+26)
3	94.7 (-+0.7)	1.10 (+14)	0.16 (-110)	0.04 (+133)	0.01 (-113)
4	94.7 (-+0.7)	1.10 (+141)	0.14 (+2)	0.03 (+50)	0.03 (+13)
5	94.7 (-+0.7)	1.10 (-161)	0.64 (+127)	0.04 (+54)	0.01 (-110)
6	94.7 (-+1.7)	1.10 (-61)	0.37 (-73)	0.02 (-134)	0.01 (-118)
7	95.0 (-+0.7)	1.10 (+33)	0.12 (+32)	0.03 (-36)	0.00 (-141)
8	94.8 (-+0.7)	1.10 (+154)	0.21 (-148)	0.02 (-33)	0.00 (+36)
9	94.7 (-+0.7)	1.10 (+153)	0.16 (+97)	0.01 (-131)	0.00 (+86)
10	94.7 (-+0.7)	1.10 (-123)	0.00 (-36)	0.03 (+152)	0.00 (-81)
11	94.7 (-+0.7)	0.70 (+63)	0.23 (+101)	0.03 (+121)	0.03 (-121)
12	94.80 (+19)	0.78 (+81)	0.41 (+84)	0.01 (+98)	0.00 (-111)
13	94.98 (+32)	0.74 (+56)	0.15 (+159)	0.02 (+182)	0.01 (+13)
14	94.91 (+50)	0.75 (+169)	0.36 (-161)	0.04 (-127)	0.00 (-95)
15	94.97 (+108)	0.73 (-114)	0.29 (+55)	0.02 (-109)	0.01 (-42)
16	94.53 (+163)	0.29 (+10)	0.14 (-9)	0.04 (+101)	0.01 (-11)
17	94.81 (-+149)	1.10 (-11)	0.09 (+152)	0.01 (-26)	0.01 (-+16)
18	95.61 (-+0.8)	1.10 (+83)	0.44 (-79)	0.03 (+147)	0.01 (+73)
19	94.89 (-+161)	1.10 (+0)	0.01 (+69)	0.01 (-37)	0.01 (+157)
20	94.677 (+158)	1.10 (-26)	0.09 (+158)	0.06 (-142)	0.01 (-7)
21	94.61 (+144)	5.34 (-44)	0.03 (+150)	0.00 (-127)	0.02 (-10)
22	95.61 (+161)	4.91 (-31)	0.37 (+145)	0.01 (-103)	0.00 (+7)
23	94.21 (-+173)	2.01 (+7)	0.14 (-98)	0.01 (+45)	0.00 (-33)
24	94.87 (-+136)	0.92 (+44)	0.48 (-173)	0.03 (+54)	0.00 (+145)
25	94.60 (-+84)	5.42 (+131)	0.42 (+13)	0.02 (-116)	0.03 (+161)
26	94.62 (-+84)	1.10 (-129)	1.34 (-131)	0.32 (+35)	0.09 (+25)
27	94.56 (-+1.3)	1.10 (-64)	3.50 (-13)	0.67 (-62)	0.15 (-72)
28	94.7 (-+0.7)	1.10 (+0)	0.36 (-7)	0.02 (-164)	0.00 (+54)
29	94.7 (-+0.7)	1.10 (-+13)	0.15 (-113)	0.01 (-11)	0.01 (-6)
30	94.7 (-+0.7)	1.10 (-113)	1.30 (-103)	0.31 (-159)	0.01 (-135)
31	94.7 (-+0.7)	1.10 (-+13)	0.15 (-93)	0.01 (-126)	0.01 (-10)
32	94.7 (-+0.7)	1.10 (-128)	0.79 (+127)	0.16 (+70)	0.04 (+8)
33	94.7 (-+0.7)	1.10 (-+64)	0.56 (-97)	0.13 (-136)	0.00 (-157)
34	94.7 (-+0.7)	1.10 (-+13)	0.15 (+12)	0.11 (+33)	0.17 (+18)
35	94.7 (-+0.7)	1.10 (-+140)	0.83 (-161)	0.10 (+43)	0.11 (+163)
36	94.7 (-+0.7)	1.10 (-+127)	1.13 (-113)	0.13 (+105)	0.13 (-133)

Incident wave

Periodicity = 1.50 sec., Mean wave height = 0.05 m., Standing breakwater angle = 45°, Incident wave angle = 0°, Incident wave height = 0.05 m.

Table 1
Distribution of wave Energy throughout the Experimental Facility, 30-deg
Incident Direction, Period = 1.50 sec, Ocean Wave Height = 0.106 ft
nearby Breakwater Angle with Shoreline
Percent of Total Energy and Phase Angle (deg), Arrangement No. 2

Gage	Fundamental	First	Second	Third	Fourth
	Period 1.50 sec	Harmonic 0.75 sec	Harmonic 0.50 sec	Harmonic 0.38 sec	Harmonic 0.30 sec
1*	93.35(+89)	5.01(-76)	0.08(+11)	0.01(-86)	0.03(+90)
2*	97.13(+103)	1.94(-19)	0.24(+110)	0.03(-4)	0.01(+48)
3	91.03(-83)	3.85(+179)	0.06(-175)	0.03(-53)	0.03(+7)
4	89.31(-87)	9.57(-162)	0.83(+88)	0.02(+26)	0.00(+153)
5	93.09(-84)	6.18(-68)	0.15(-75)	0.00(+102)	0.00(+74)
6	97.43(-13)	2.31(+30)	0.14(+8)	0.01(-52)	0.00(-115)
7	98.67(+39)	1.04(+132)	0.26(-133)	0.03(-115)	0.00(+111)
8	99.71(+91)	0.17(-85)	0.10(+81)	0.01(-165)	0.00(-19)
9	98.99(+139)	0.16(+49)	0.15(-75)	0.01(+97)	0.00(-14)
10	95.47(+179)	3.03(-89)	0.19(+12)	0.03(+133)	0.00(-27)
11	93.72(+56)	6.15(+138)	0.12(-130)	0.03(-11)	0.02(+104)
12	89.84(+34)	9.13(+75)	0.85(+112)	0.16(+125)	0.01(-74)
13	90.68(+35)	8.72(+93)	0.57(+162)	0.01(-40)	0.02(+12)
14	96.35(+56)	3.51(+164)	0.13(-160)	0.01(-135)	0.00(-102)
15	99.18(+95)	0.17(-139)	0.42(+82)	0.02(+133)	0.01(-23)
16	98.38(+147)	1.33(-115)	0.24(-40)	0.04(+87)	0.00(+20)
17	97.54(-159)	2.13(-35)	0.12(+138)	0.02(-56)	0.00(+73)
18	93.08(-112)	6.51(+64)	0.35(-106)	0.07(+98)	0.01(-56)
19	94.73(-175)	5.23(+39)	0.01(-102)	0.00(-152)	0.03(+70)
20	94.85(+161)	5.00(+11)	0.05(+23)	0.01(93)	0.06(-151)
21	94.97(+167)	4.29(+4)	0.16(+107)	0.04(-128)	0.03(-58)
22	99.49(+175)	0.34(+35)	0.13(-75)	0.04(+125)	0.01(+3)
23	98.42(-142)	1.13(+11)	0.38(+177)	0.07(+31)	0.00(-161)
24	93.46(-94)	5.08(+93)	0.84(-46)	0.02(+178)	0.00(+39)
25	87.53(-46)	10.19(-159)	2.10(+112)	0.19(+38)	0.04(-38)
26	90.15(+61)	15.14(-47)	3.33(-68)	0.63(-81)	0.11(-105)
27	78.40(+13)	1.13(+49)	3.13(+83)	0.45(+108)	0.10(+144)
28	93.64(+27)	0.17(-113)	0.76(+46)	0.00(+152)	0.01(+103)
29	97.17(+31)	1.13(+11)	1.11(-46)	0.00(-67)	0.00(-19)
30	94.25(+11)	0.17(+11)	0.13(-114)	0.00(-57)	0.09(+99)
31	94.25(+11)	0.17(+11)	0.17(-113)	0.01(+121)	0.02(-13)
32	97.17(+31)	1.13(+11)	0.12(+144)	0.13(+40)	0.03(-7)
33	90.15(+61)	6.05(-68)	1.93(-108)	0.51(-152)	0.11(+164)
34	87.53(+46)	10.19(+112)	3.19(+3)	1.60(+18)	0.32(+30)
35	90.15(+61)	15.14(-159)	3.19(+30)	1.73(-120)	1.01(-26)
36	90.15(+61)	15.14(-159)	3.19(+31)	3.55(+79)	1.16(-120)

TABLE 18
Distribution of wind shear throughout the aircraft for lifting, 0° leading
Incident flow angle, $\alpha = 10^\circ$, $U_\infty = 100 \text{ ft/sec}$, $Re = 10^6$
Cylinder diameter, $D = 10 \text{ ft}$, $W = 10 \text{ ft}$, $L = 10 \text{ ft}$
Percent of maximum value of ΔC_x at $x = 0$ and $y = 0$

Case	Forward flow		Reverse flow		ΔC_x at $x = 0$
	Leading edge	Trailing edge	Leading edge	Trailing edge	
1*	0.13 (+0.0)	-0.03 (-0.3)	0.13 (+0.0)	-0.03 (-0.3)	0.01 (-1.7)
2*	0.13 (+0.0)	-0.03 (-0.3)	1.13 (+0.0)	-0.03 (-0.3)	0.01 (-1.3)
3	0.13 (+0.0)	-0.03 (-0.3)	0.13 (+0.0)	-0.03 (-0.3)	0.01 (-1.3)
4	0.13 (+0.0)	-0.03 (-0.3)	0.13 (+0.0)	-0.03 (-0.3)	0.01 (-1.3)
5	0.13 (+0.0)	-0.03 (-0.3)	0.13 (+0.0)	-0.03 (-0.3)	0.01 (-1.3)
6	84.83 (+1.0)	-0.03 (-0.3)	1.75 (+0.0)	-0.03 (-0.3)	0.01 (+2.0)
7	89.83 (+1.0)	-0.03 (-0.3)	1.75 (+0.0)	-0.03 (-0.3)	0.01 (+2.0)
8	94.13 (+1.0)	-0.03 (-0.3)	0.13 (+0.0)	-0.03 (-0.3)	0.01 (+1.0)
9	94.23 (+1.0)	-0.03 (-0.3)	0.13 (+0.0)	-0.03 (-0.3)	0.01 (+1.0)
10	99.27 (+1.0)	-0.03 (-0.3)	0.41 (+0.0)	-0.03 (-0.3)	0.01 (+1.0)
11	30.23 (+1.0)	-0.03 (-0.3)	0.41 (+0.0)	-0.03 (-0.3)	0.01 (-0.7)
12	34.01 (+1.0)	-0.03 (-0.3)	1.54 (+0.0)	-0.03 (-0.3)	0.01 (-1.0)
13	36.53 (+1.0)	-0.03 (-0.3)	0.77 (+0.0)	-0.03 (-0.3)	0.01 (+1.0)
14	51.13 (+1.0)	-0.03 (-0.3)	0.76 (+0.0)	-0.03 (-0.3)	0.01 (+1.0)
15	98.53 (+1.0)	-0.03 (-0.3)	0.43 (+0.0)	-0.03 (-0.3)	0.01 (+1.0)
16	69.13 (+1.0)	-0.03 (-0.3)	0.02 (+0.0)	-0.03 (-0.3)	0.01 (-0.3)
17	98.33 (+1.0)	-0.03 (-0.3)	0.13 (+0.0)	-0.03 (-0.3)	0.01 (+1.0)
18	98.33 (+1.0)	-0.03 (-0.3)	1.11 (+0.0)	-0.03 (-0.3)	0.02 (-0.3)
19	91.13 (+1.0)	-0.03 (-0.3)	0.72 (+0.0)	-0.03 (-0.3)	0.01 (-1.0)
20	97.13 (+1.0)	-0.03 (-0.3)	0.74 (+0.0)	-0.03 (-0.3)	0.01 (+1.0)
21	38.03 (+1.0)	-0.03 (-0.3)	0.63 (+0.0)	-0.03 (-0.3)	0.01 (-1.0)
22	92.33 (+1.0)	-0.03 (-0.3)	0.73 (+0.0)	-0.03 (-0.3)	0.01 (-1.0)
23	98.13 (+1.0)	-0.03 (-0.3)	0.13 (+0.0)	-0.03 (-0.3)	0.01 (+1.0)
24	97.13 (+1.0)	-0.03 (-0.3)	0.13 (+0.0)	-0.03 (-0.3)	0.01 (+1.0)
25	91.13 (+1.0)	-0.03 (-0.3)	0.13 (+0.0)	-0.03 (-0.3)	0.01 (-1.0)
26	98.13 (+1.0)	-0.03 (-0.3)	0.13 (+0.0)	-0.03 (-0.3)	0.01 (-1.0)
27	98.13 (+1.0)	-0.03 (-0.3)	0.13 (+0.0)	-0.03 (-0.3)	0.01 (-1.0)
28	98.13 (+1.0)	-0.03 (-0.3)	0.13 (+0.0)	-0.03 (-0.3)	0.01 (-1.0)
29	98.13 (+1.0)	-0.03 (-0.3)	0.13 (+0.0)	-0.03 (-0.3)	0.01 (-1.0)
30	98.13 (+1.0)	-0.03 (-0.3)	0.13 (+0.0)	-0.03 (-0.3)	0.01 (-1.0)
31	98.13 (+1.0)	-0.03 (-0.3)	0.13 (+0.0)	-0.03 (-0.3)	0.01 (-1.0)
32	98.13 (+1.0)	-0.03 (-0.3)	0.13 (+0.0)	-0.03 (-0.3)	0.01 (-1.0)
33	98.13 (+1.0)	-0.03 (-0.3)	0.13 (+0.0)	-0.03 (-0.3)	0.01 (-1.0)
34	98.13 (+1.0)	-0.03 (-0.3)	0.13 (+0.0)	-0.03 (-0.3)	0.01 (-1.0)
35	98.13 (+1.0)	-0.03 (-0.3)	0.13 (+0.0)	-0.03 (-0.3)	0.01 (-1.0)
36	98.13 (+1.0)	-0.03 (-0.3)	0.13 (+0.0)	-0.03 (-0.3)	0.01 (-1.0)

TABLE 19
Distribution of Wave Energy Throughout the Experimental Facility, $\theta = 90^\circ$
Incident Direction, Period = 1.50 sec., Ocean Wave Height = 0.147 ft
Incidence or Downwater Angle with Shoreline
Percent of Total Energy and Phase Angle (deg.), Arrangement No. 2

Gage	Fundamental	First	Second	Third	Fourth
	Period 1.50 sec.	Harmonic 0.75 sec	Harmonic 0.50 sec	Harmonic 0.38 sec	Harmonic 0.30 sec
1*	93.12(+101)	6.30(-49)	0.48(+41)	0.02(-54)	0.01(+2)
2*	94.63(+113)	4.16(-2)	1.13(+130)	0.02(-51)	0.02(+55)
3	84.68(-78)	14.82(-169)	0.17(+171)	0.29(+172)	0.03(+173)
4	79.57(-78)	19.13(-144)	1.16(+100)	0.12(+59)	0.01(-65)
5	36.51(-45)	11.91(-57)	1.42(-87)	0.11(-112)	0.05(-127)
6	92.23(-6)	7.21(+40)	0.47(+73)	0.04(+107)	0.00(+119)
7	95.50(+47)	3.63(+142)	0.74(-142)	0.11(-95)	0.00(-58)
8	98.34(+101)	0.82(-97)	0.30(+77)	0.04(-158)	0.00(-51)
9	98.90(+150)	0.45(+176)	0.58(-69)	0.07(+73)	0.00(-178)
10	93.30(-170)	6.23(-70)	0.43(+101)	0.02(+173)	0.01(+32)
11	87.96(+68)	10.30(+156)	0.90(-94)	0.17(-55)	0.09(-45)
12	84.00(+44)	13.63(+93)	2.28(+128)	0.05(+176)	0.03(-169)
13	83.40(+45)	14.81(+102)	1.53(+163)	0.23(-120)	0.03(-37)
14	90.10(+60)	9.61(+171)	0.25(-115)	0.03(+12)	0.00(-171)
15	97.69(+102)	1.66(-102)	0.57(+37)	0.06(+140)	0.01(-116)
16	93.27(+155)	1.39(-73)	0.21(-93)	0.11(+57)	0.01(-162)
17	96.38(-152)	2.53(+10)	0.44(+149)	0.09(-21)	0.01(+177)
18	91.17(-102)	7.30(+82)	1.29(-59)	0.22(+165)	0.02(+12)
19	89.36(-165)	10.45(+60)	0.04(+2)	0.04(-84)	0.11(-38)
20	87.32(+169)	12.30(+16)	0.09(-102)	0.29(+48)	0.00(-50)
21	91.72(+171)	8.02(+18)	0.24(+168)	0.01(+89)	0.00(-148)
22	97.91(-171)	1.37(+33)	0.52(-109)	0.19(+66)	0.01(-135)
23	97.97(-136)	1.18(+45)	0.61(+138)	0.19(-29)	0.04(-168)
24	92.36(-92)	5.12(+107)	1.93(-31)	0.42(-139)	0.13(+135)
25	83.74(-36)	11.68(-147)	3.82(+140)	0.64(+75)	0.13(+11)
26	73.74(+13)	11.19(-36)	6.76(-56)	1.91(-69)	0.40(-83)
27	67.50(+67)	11.71(+63)	3.40(+94)	1.84(+129)	0.55(+168)
28	97.91(+19)	1.15(+58)	0.65(+151)	0.08(+155)	0.07(+109)
29	93.61(-19)	1.83(-10)	1.49(-22)	0.02(+106)	0.15(-133)
30	94.74(-4)	3.93(-67)	0.92(-124)	0.32(-139)	0.05(-167)
31	94.03(-17)	4.17(-62)	1.41(-109)	0.09(-157)	0.22(-137)
32	95.00(-17)	4.20(-58)	0.01(+134)	0.01(+54)	0.33(+7)
33	87.72(+3)	6.00(+127)	4.11(-106)	1.84(-129)	0.33(+153)
34	70.49(+5)	16.95(+21)	0.91(+26)	2.73(+63)	0.83(+42)
35	53.53(-17)	21.11(+17)	12.30(+175)	1.17(+27)	0.33(+14)
36	47.77(+13)	17.17(+17)	1.14(+178)	1.17(+27)	0.22(+14)

Overall peak



Report
for

showing of breakwater at 60 deg to shoreline
near the wave generator approaching from an
angle of 30 deg

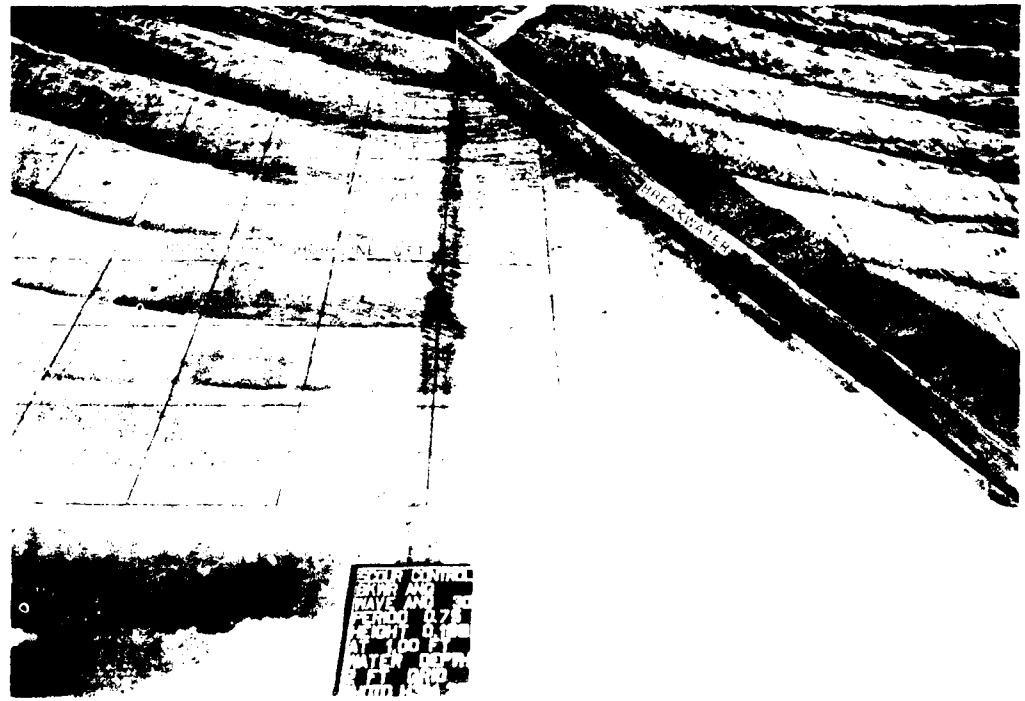


Photo 2. Typical wave pattern downwave of breakwater at 60 deg to shoreline for 0.75-sec., 0.168-ft high wave near the wave generator approaching from an incident direction of 30 deg

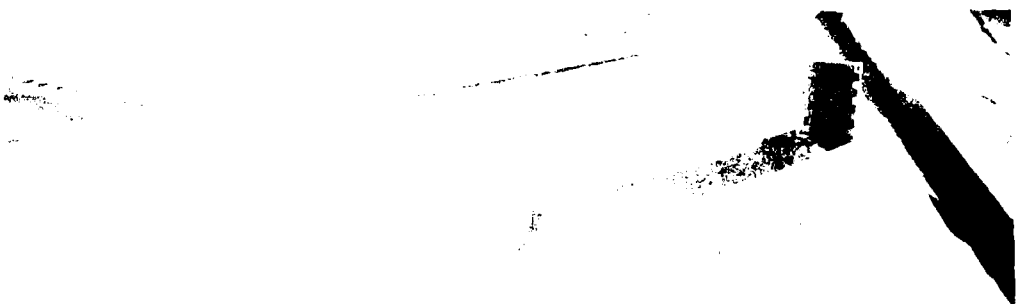


Photo
Series

measured at 60 deg to shoreline
at point of separation approaching from an
angle of 30 deg.

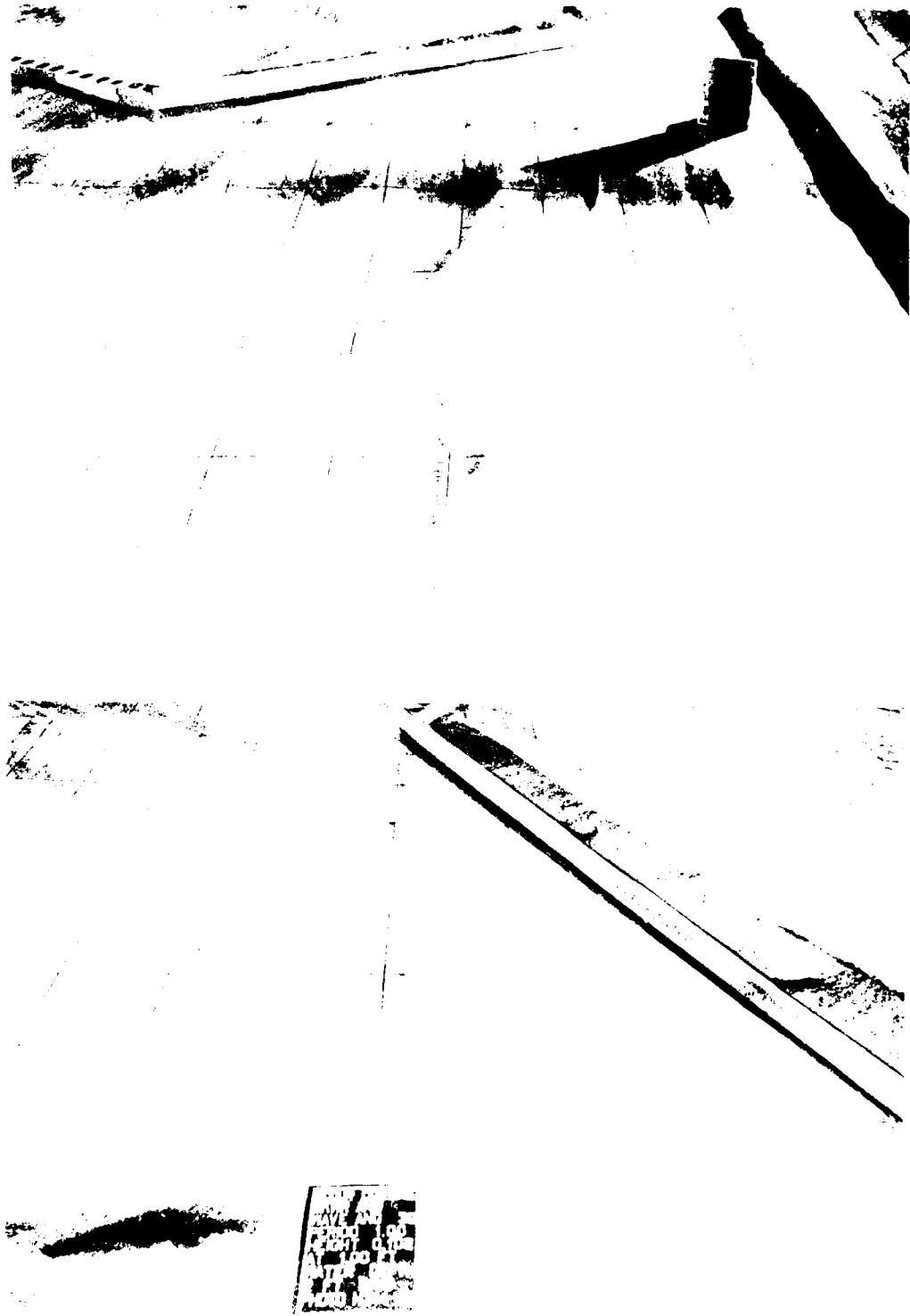


Photo 4 - typical wave pattern downwave of breakwater at 60 deg to shoreline for 1.0m sec^{1/2} 10° irregular wave near the wave generator approaching from an incident direction of 30 deg



Photo 5. (Top) Photograph of wave patterns downwave of breakwater at 60 deg to shoreline and (bottom) photograph of wave patterns downwave of the wave generator approaching from an angle of 30 deg to the direction of 30 deg.

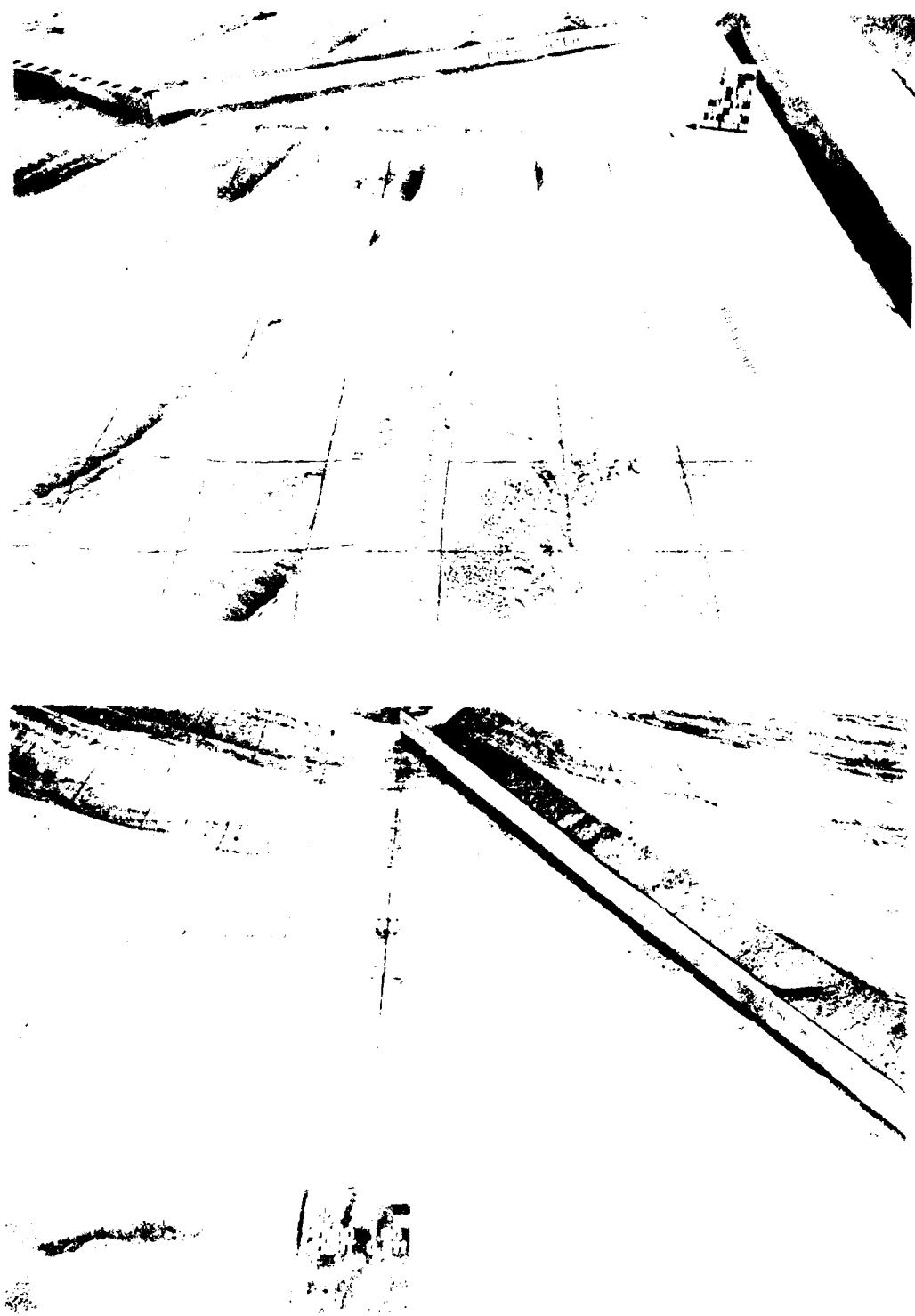
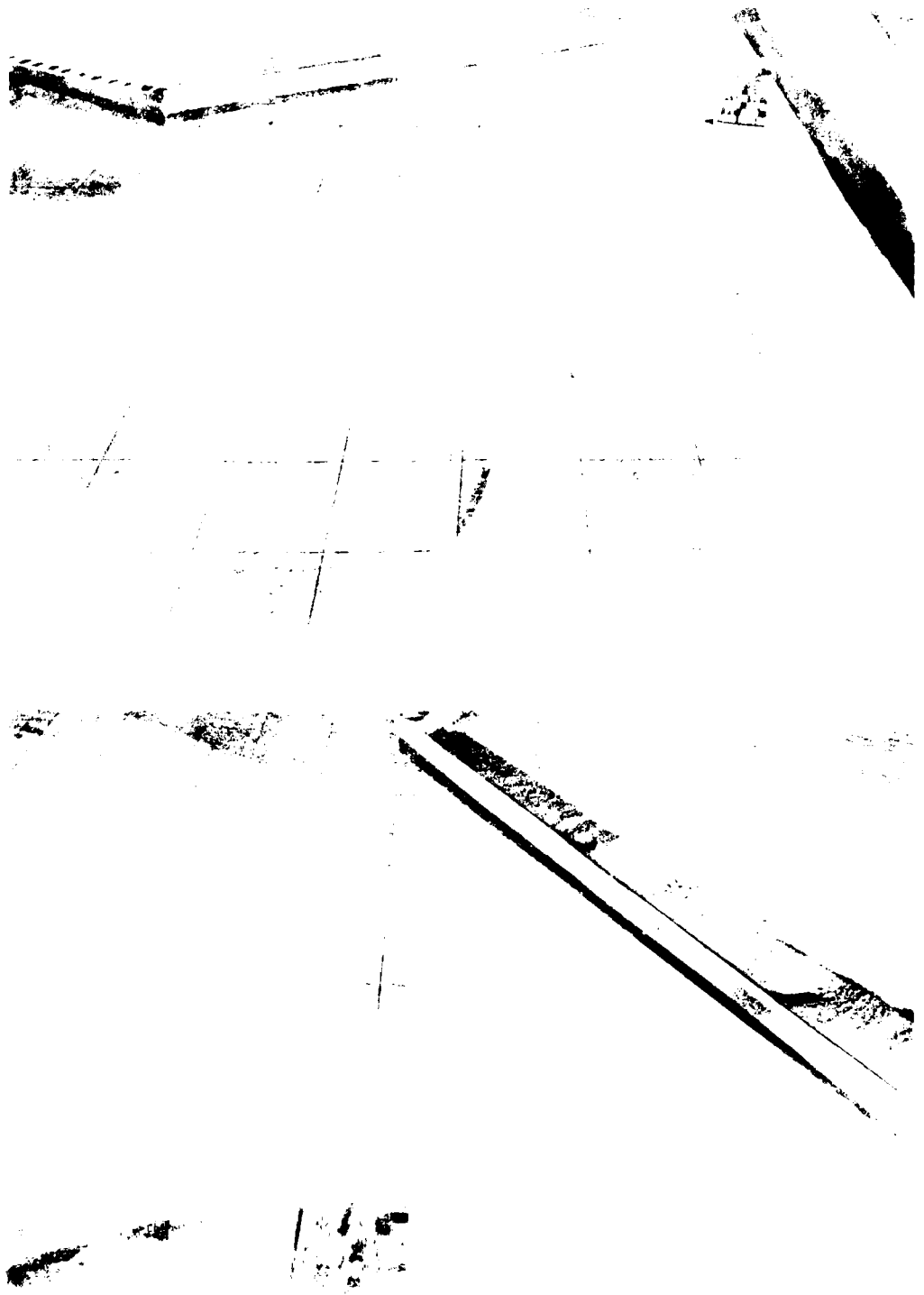


Photo 6. Wake zone around the end of a breakwater at 60 deg to shoreline for 1.0 sec. The wave generator approaching from an incident direction of 30 deg



Photo 7. Shoreline
for Figure 1.

Photo 7. Shoreline at or near the shoreline
of the regeneration approaching from an
upland area.



Photos 1 through 5 showing wave patterns around a breakwater at 60 deg to shoreline for 15° wave generation approaching from an angle of 30° deg

Photo
from

the original negative

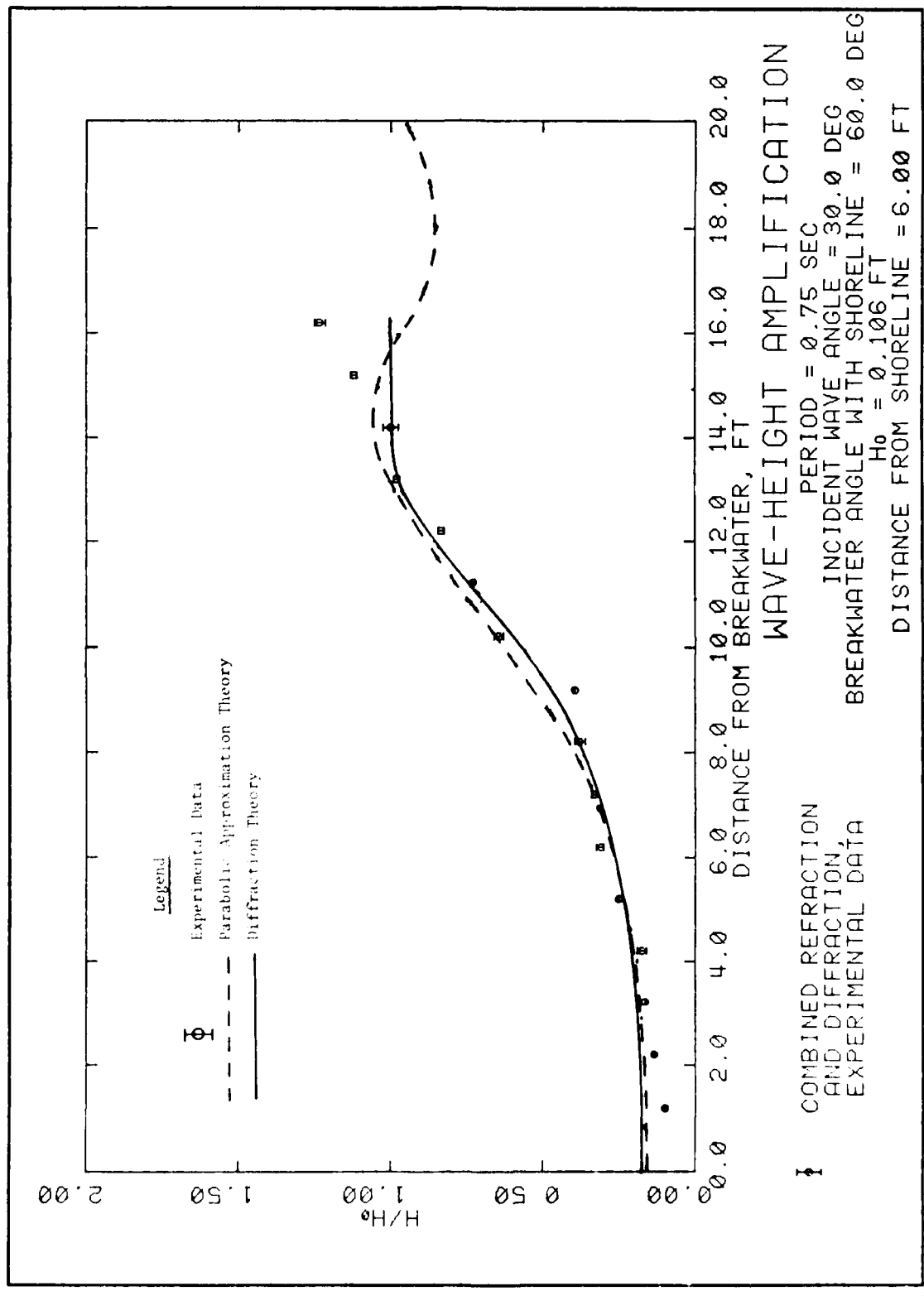
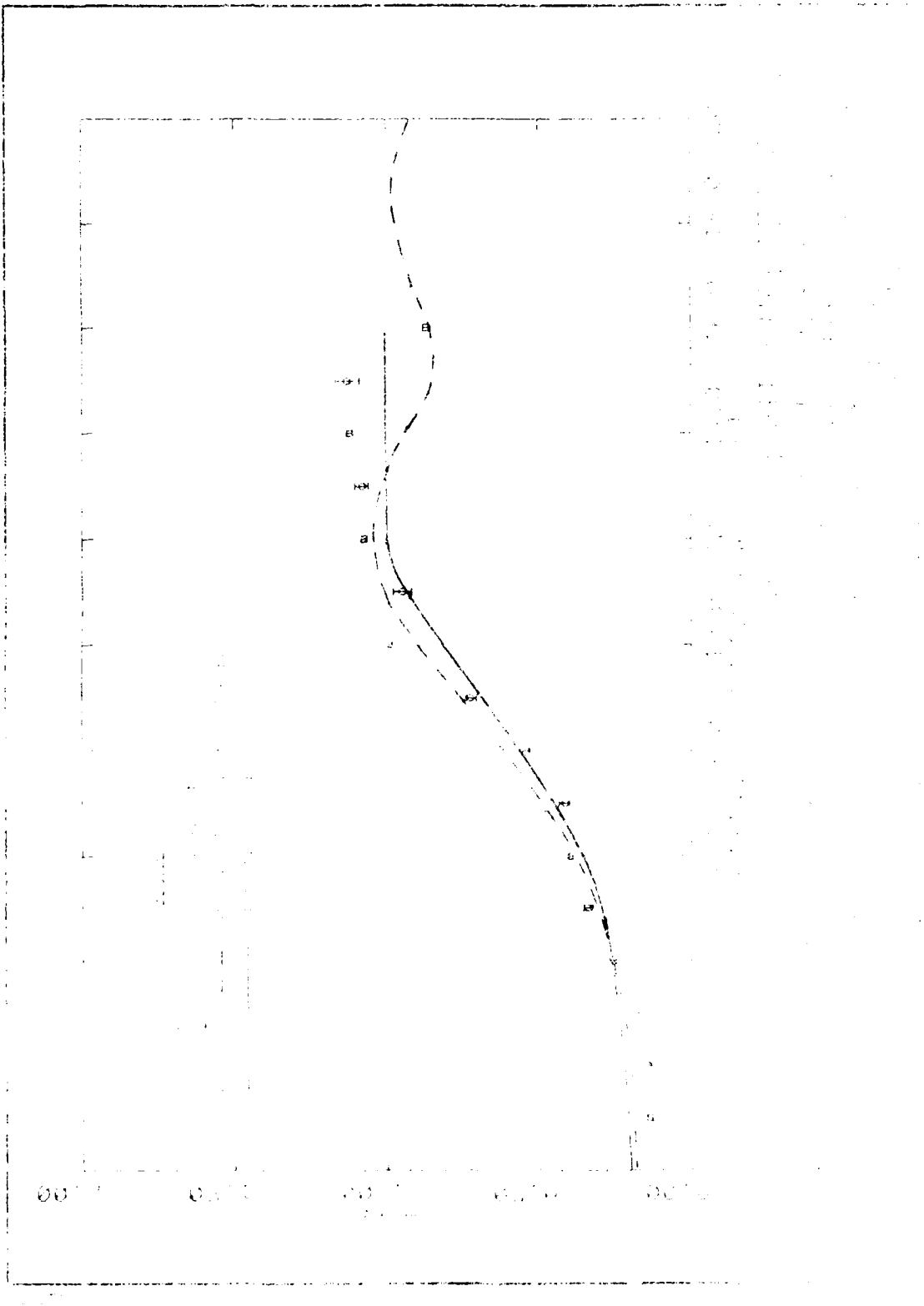
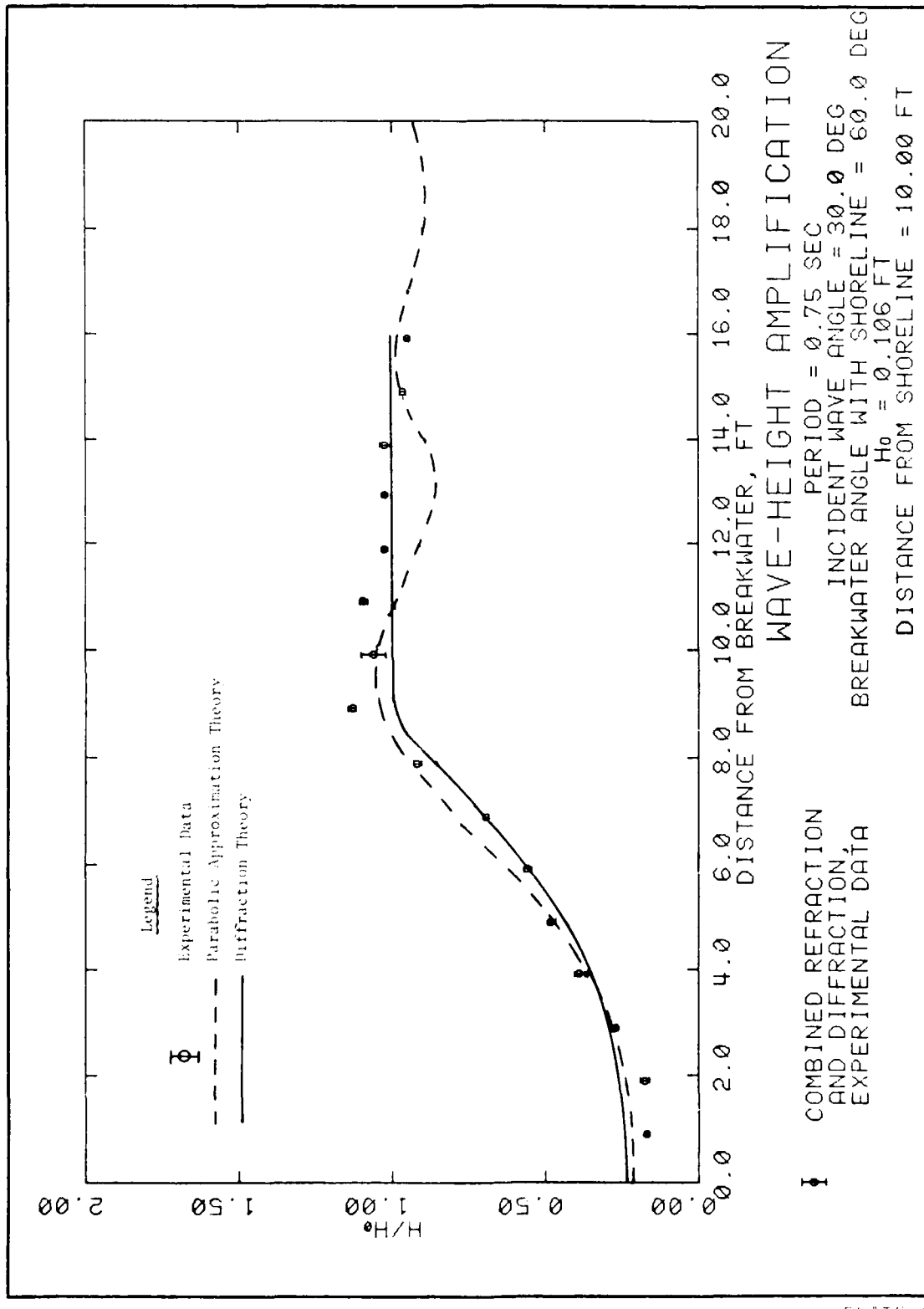


PLATE 1







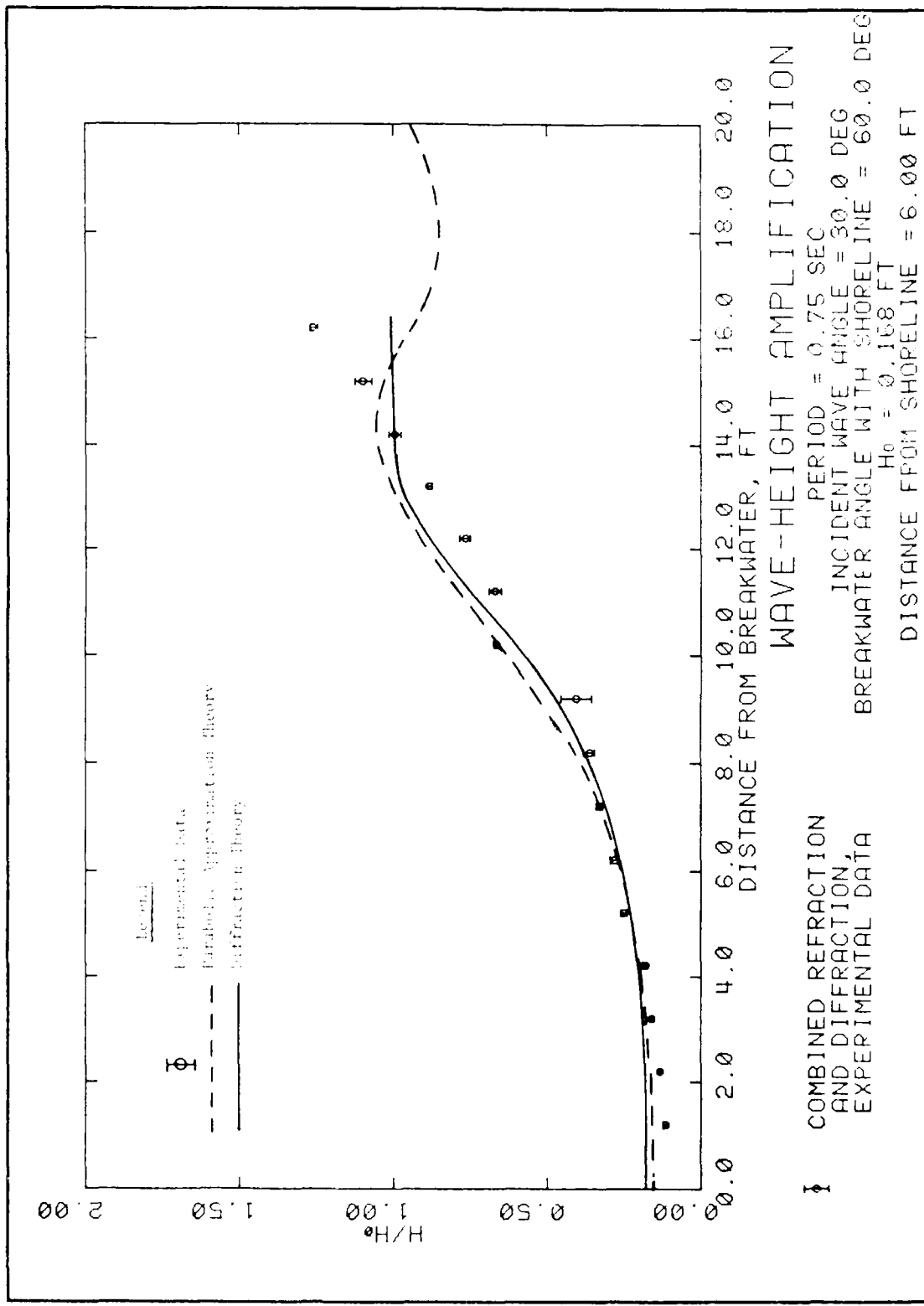
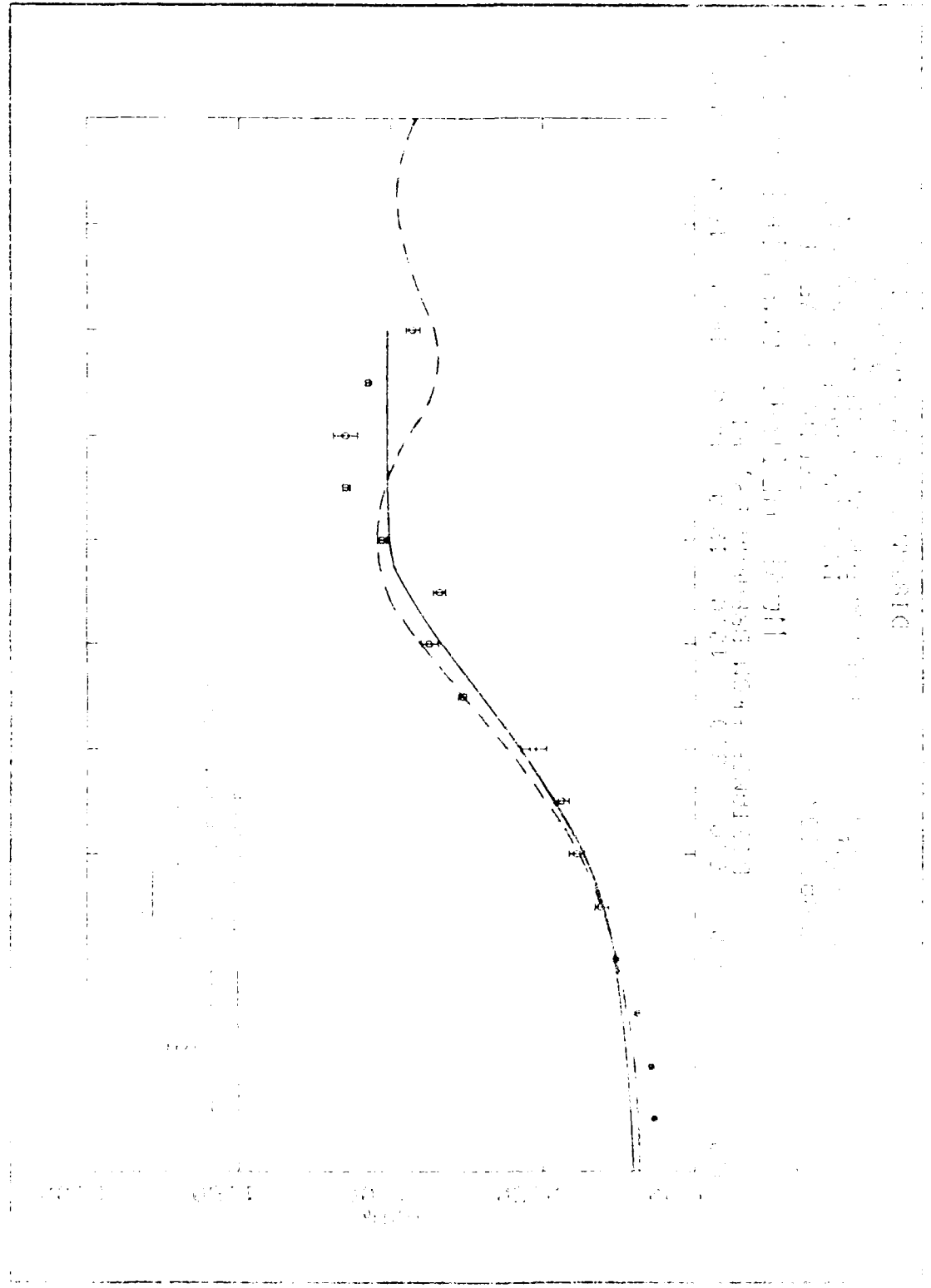
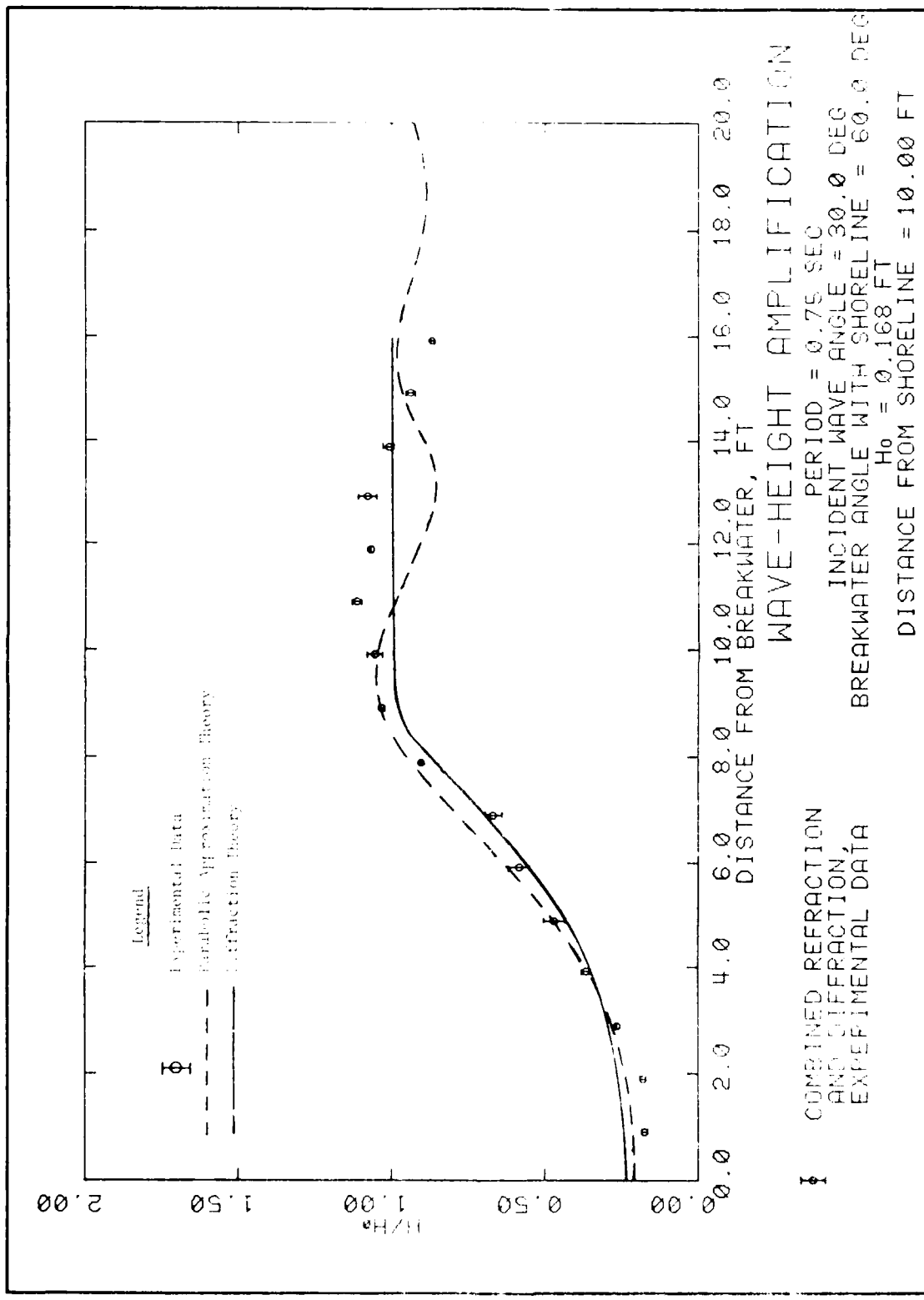


PLATE 6





WAVE-HEIGHT AMPLIFICATION

COEFFICIENTS OF
REFRACTION AND
REFLECTION

INVESTIGATION OF THE
REFRACTION AND REFLECTION
OF SURFACE WAVES BY A
SUBMERGED PLATE

BY
J. W. WESTERHOFF
AND
R. J. M. VAN DER HORST

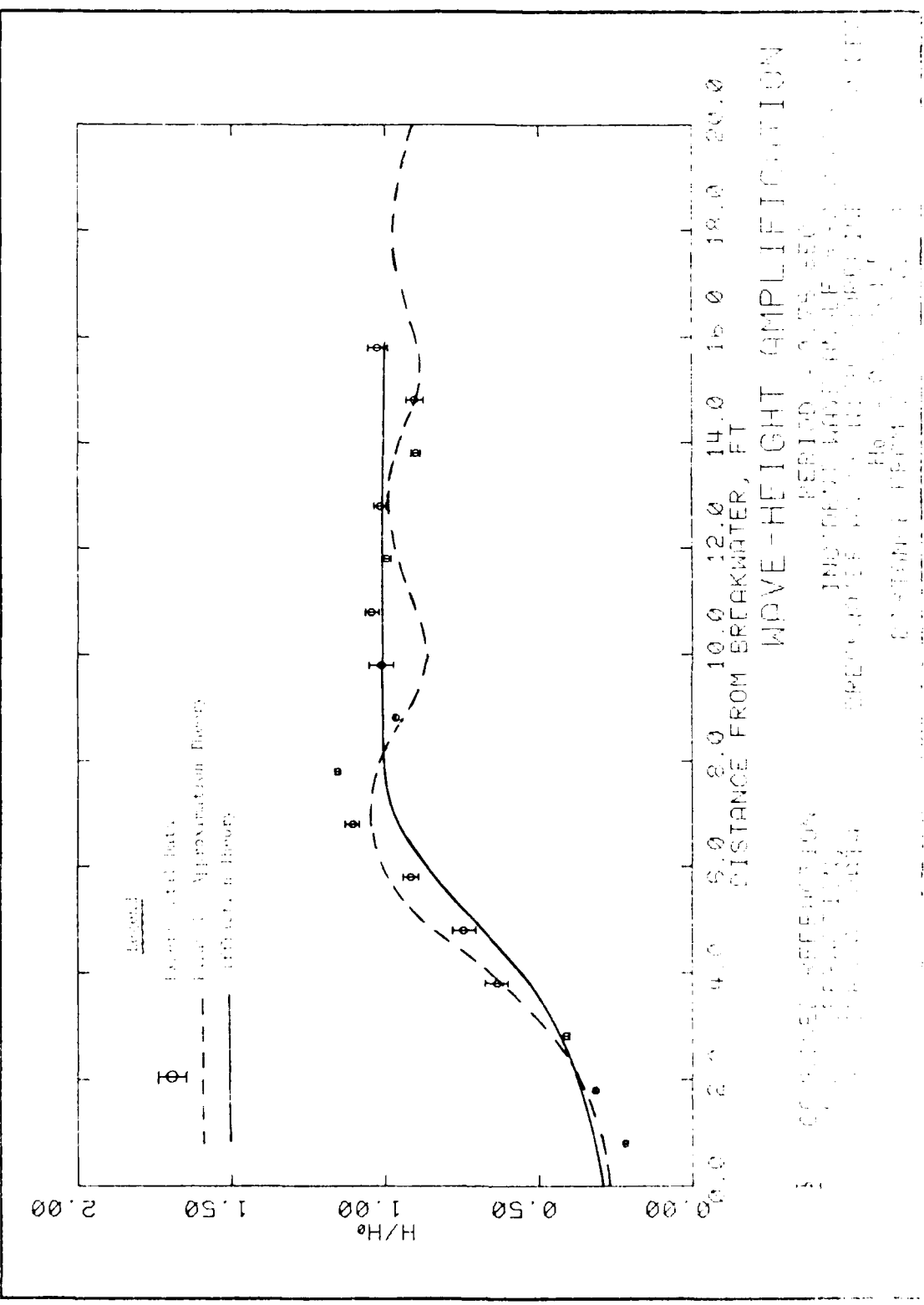


PLATE 8

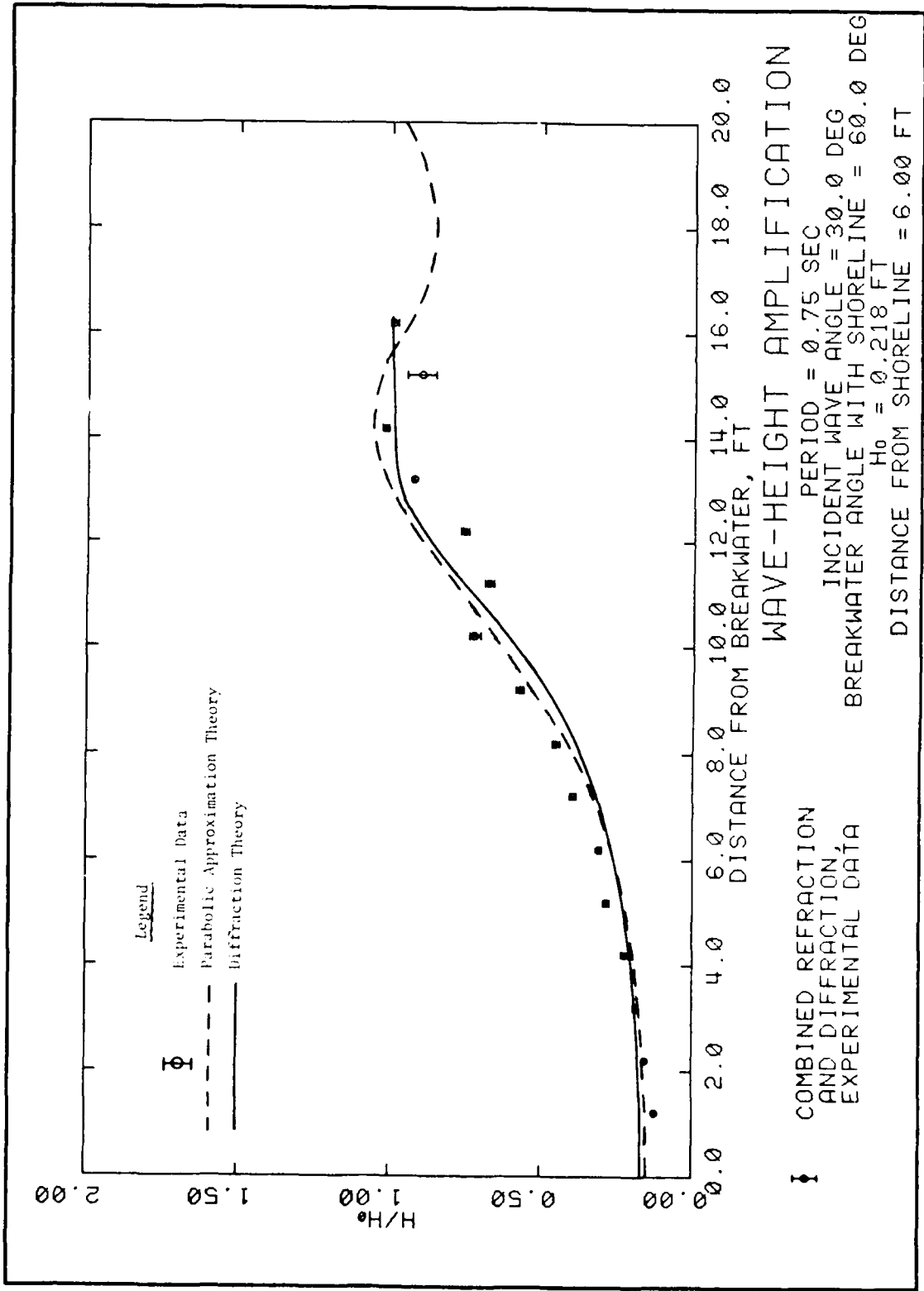
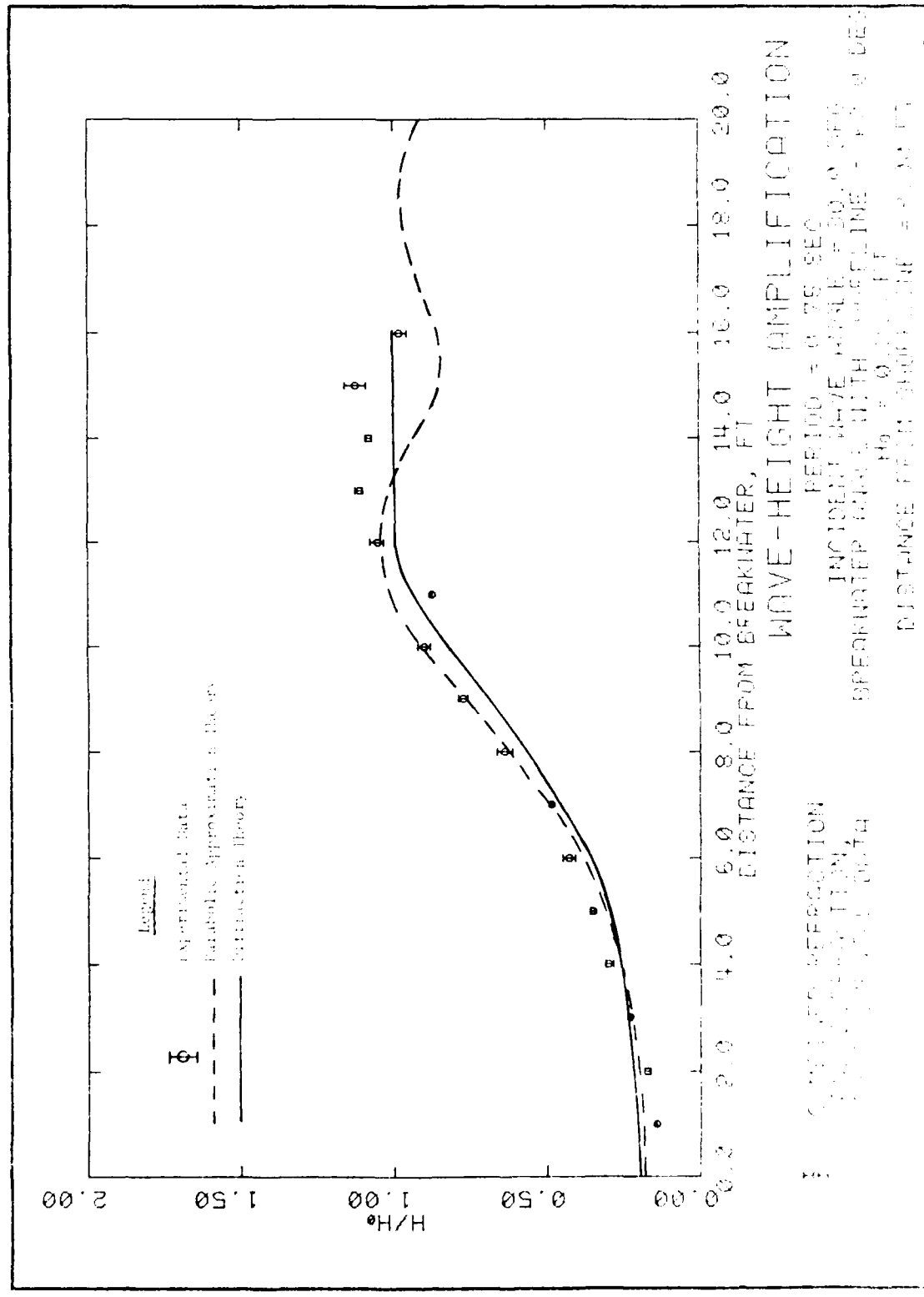
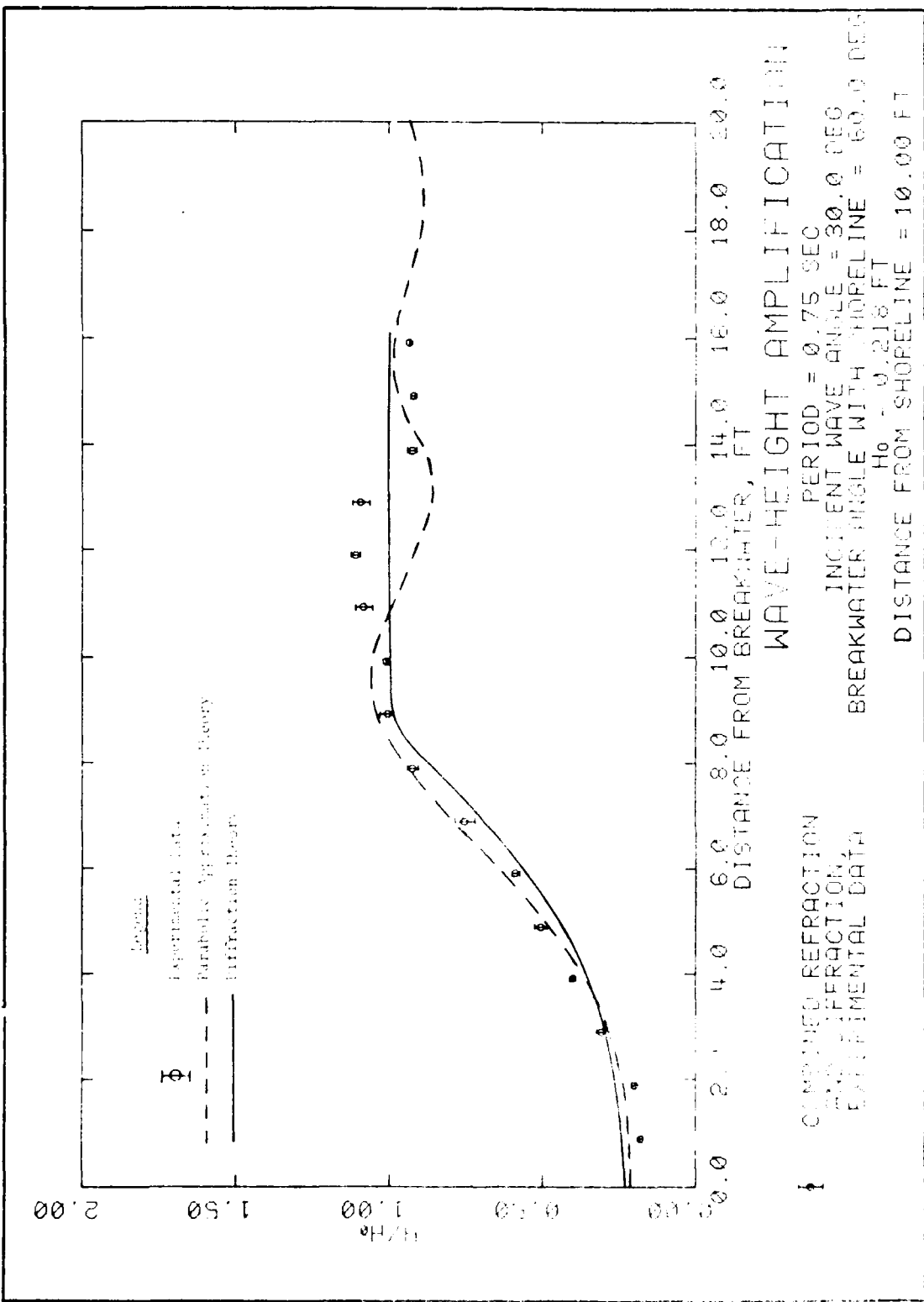


PLATE 9



STATE 10



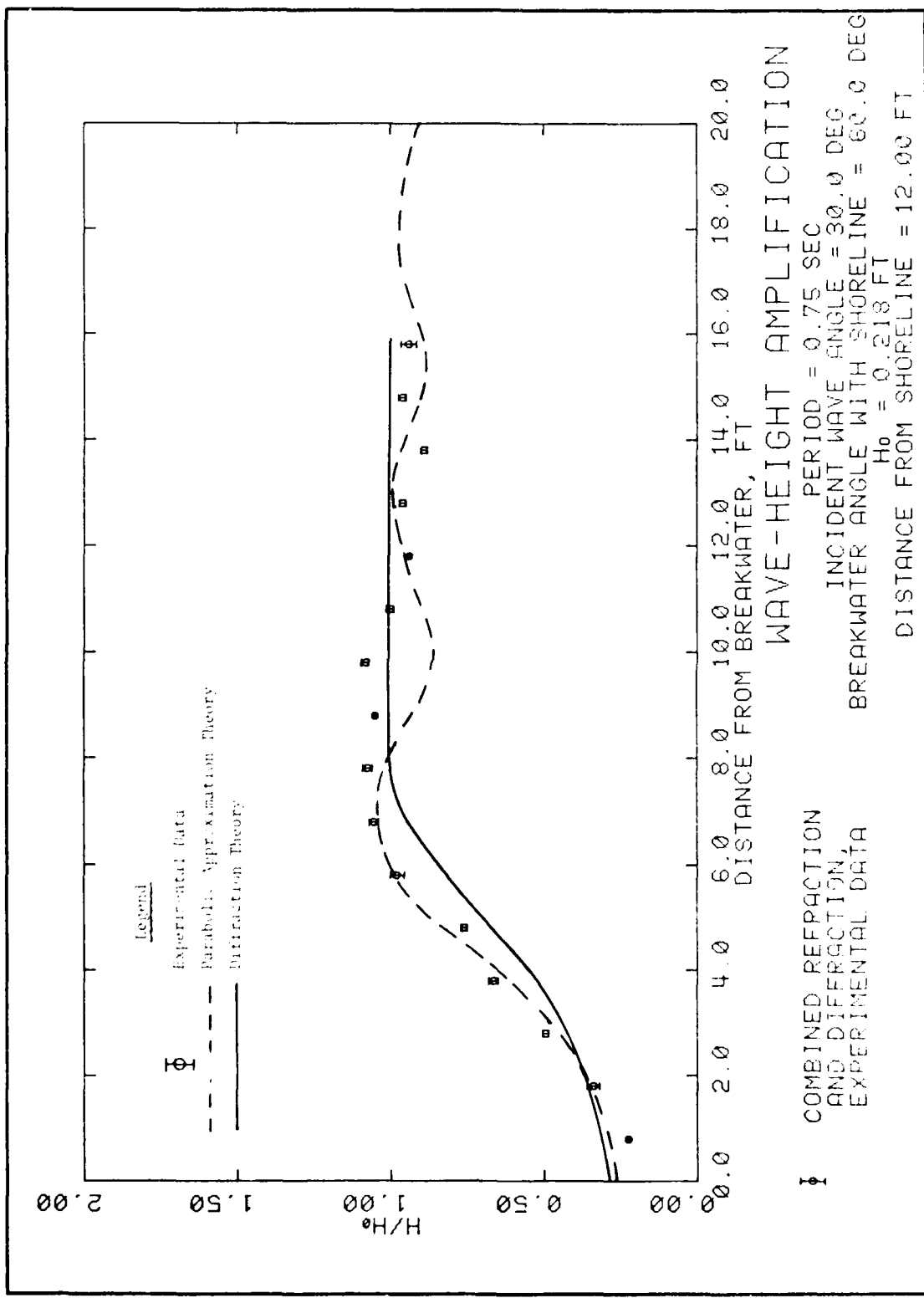
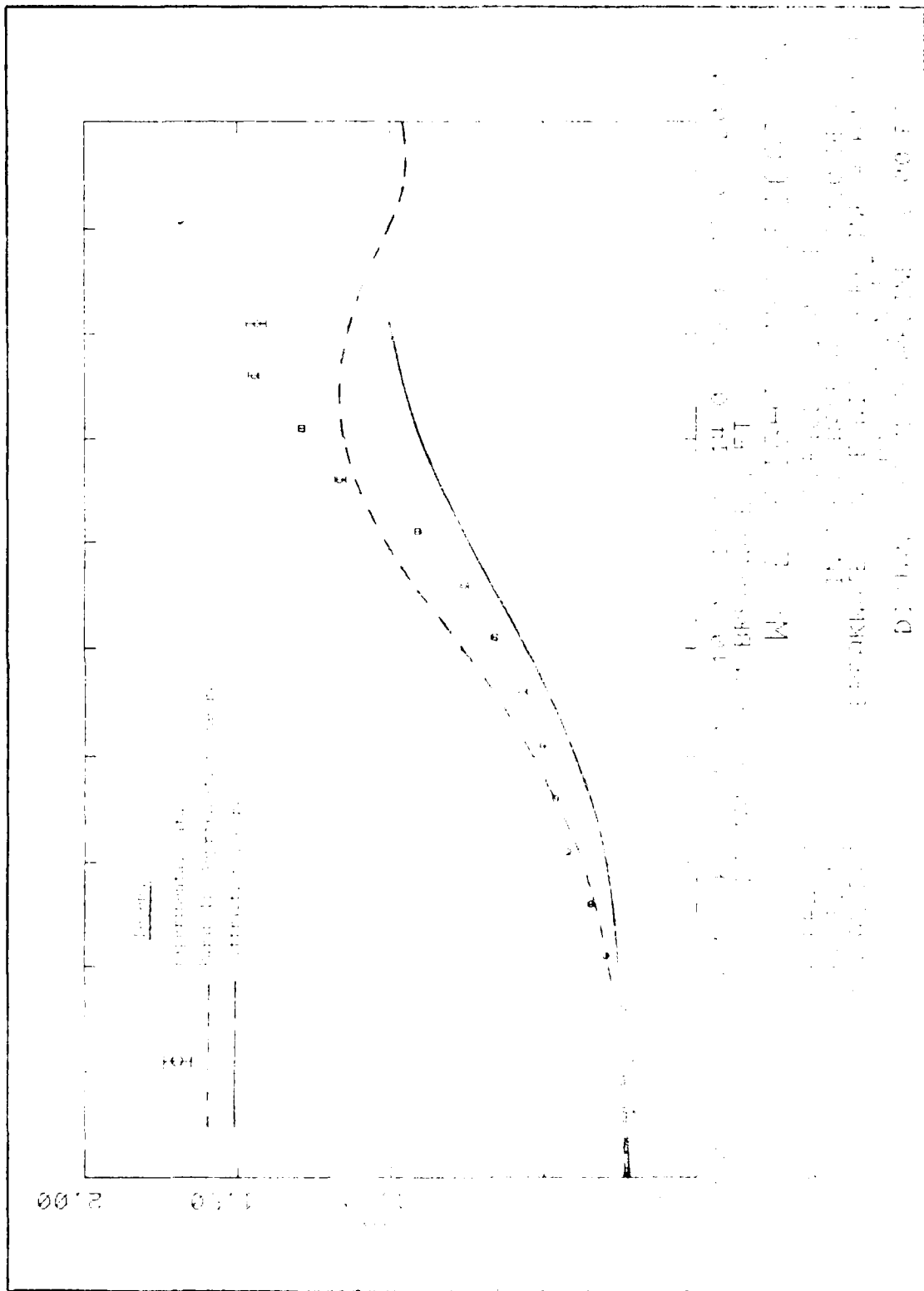


PLATE 12



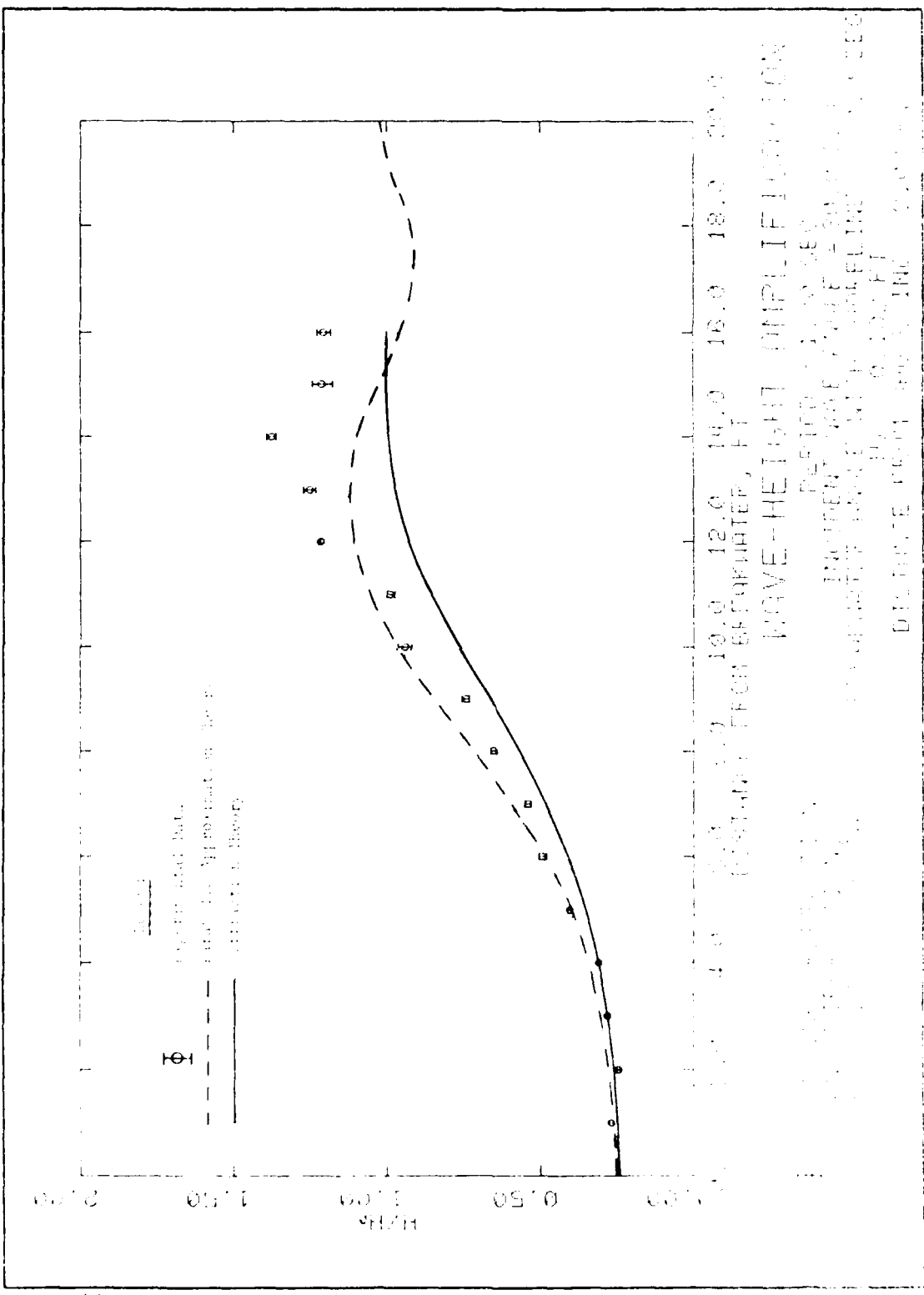
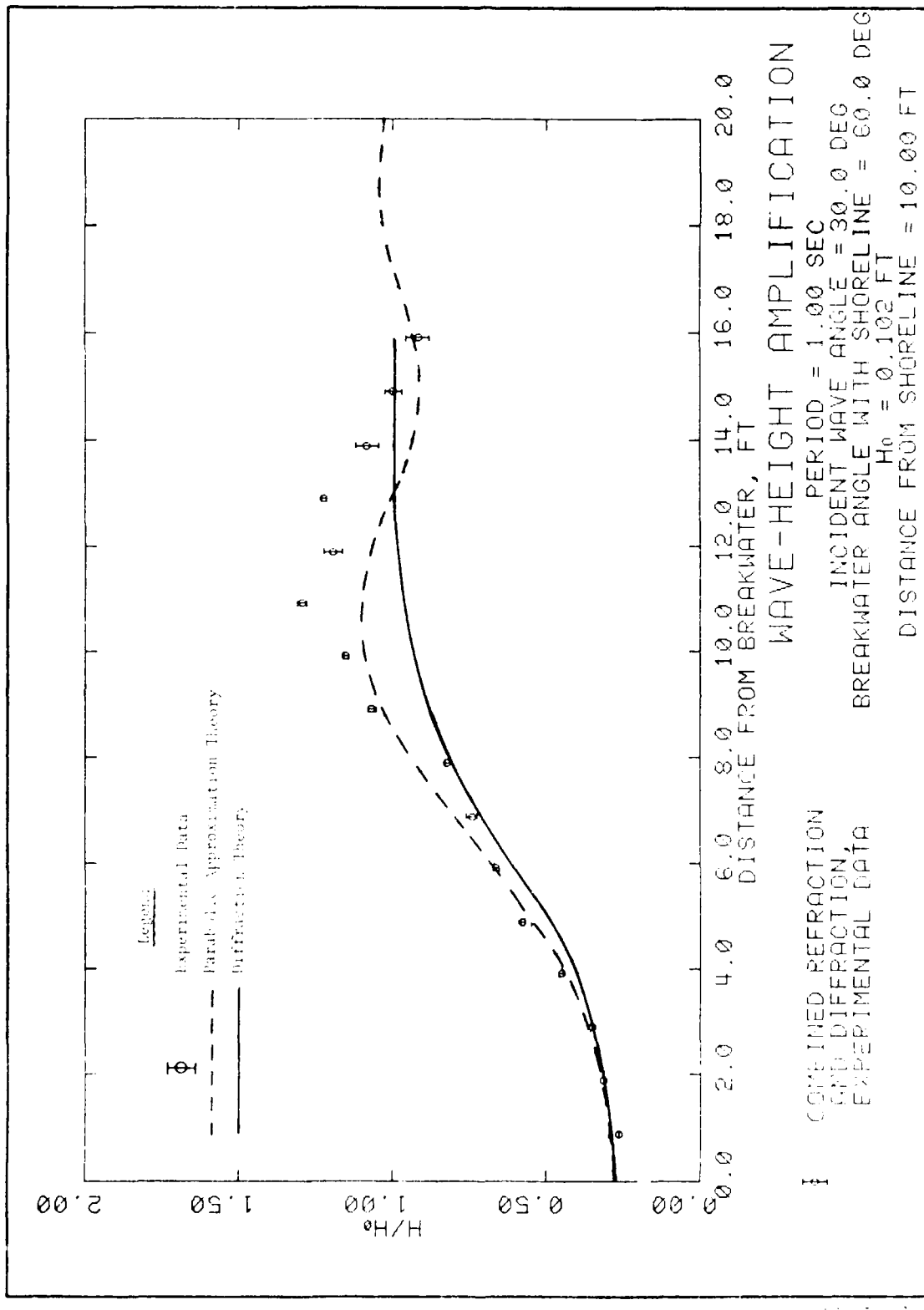


Fig. 1. (a) Plot of Φ_1 versus H/H_0 obtained from experiments on the five- μ magnet.

Five- μ magnet, $H_0 = 10^4$ oersteds.



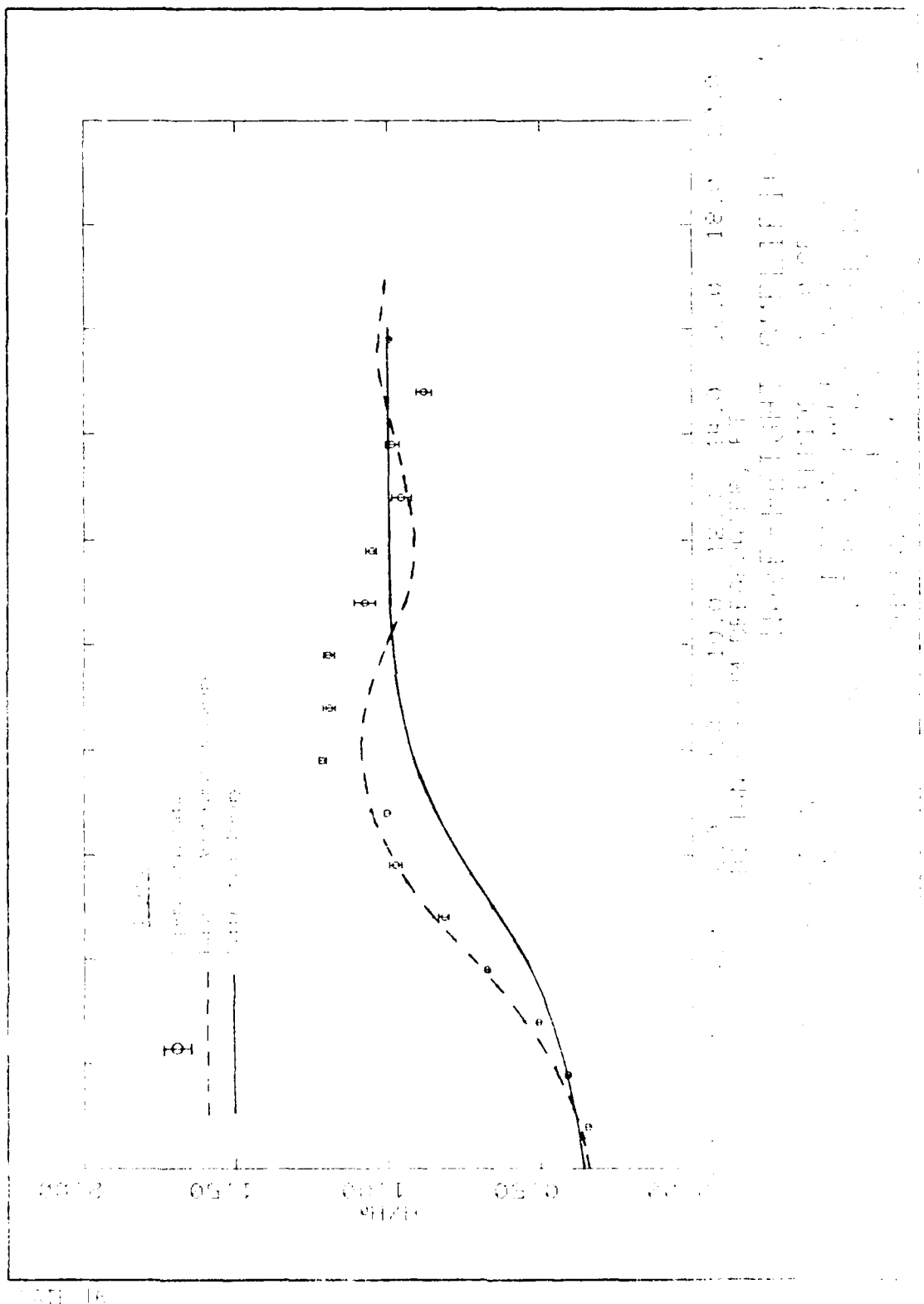
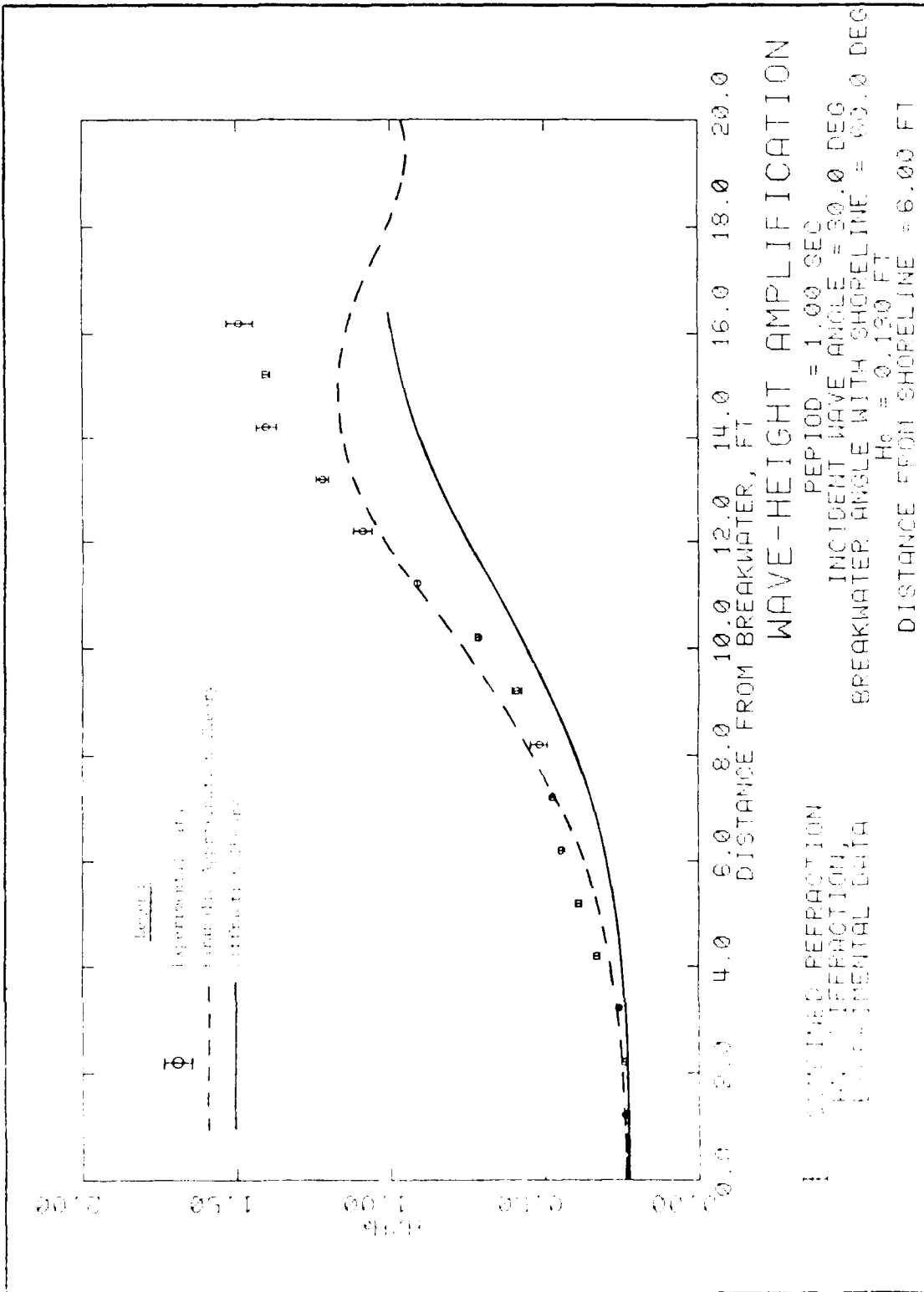


FIGURE 16



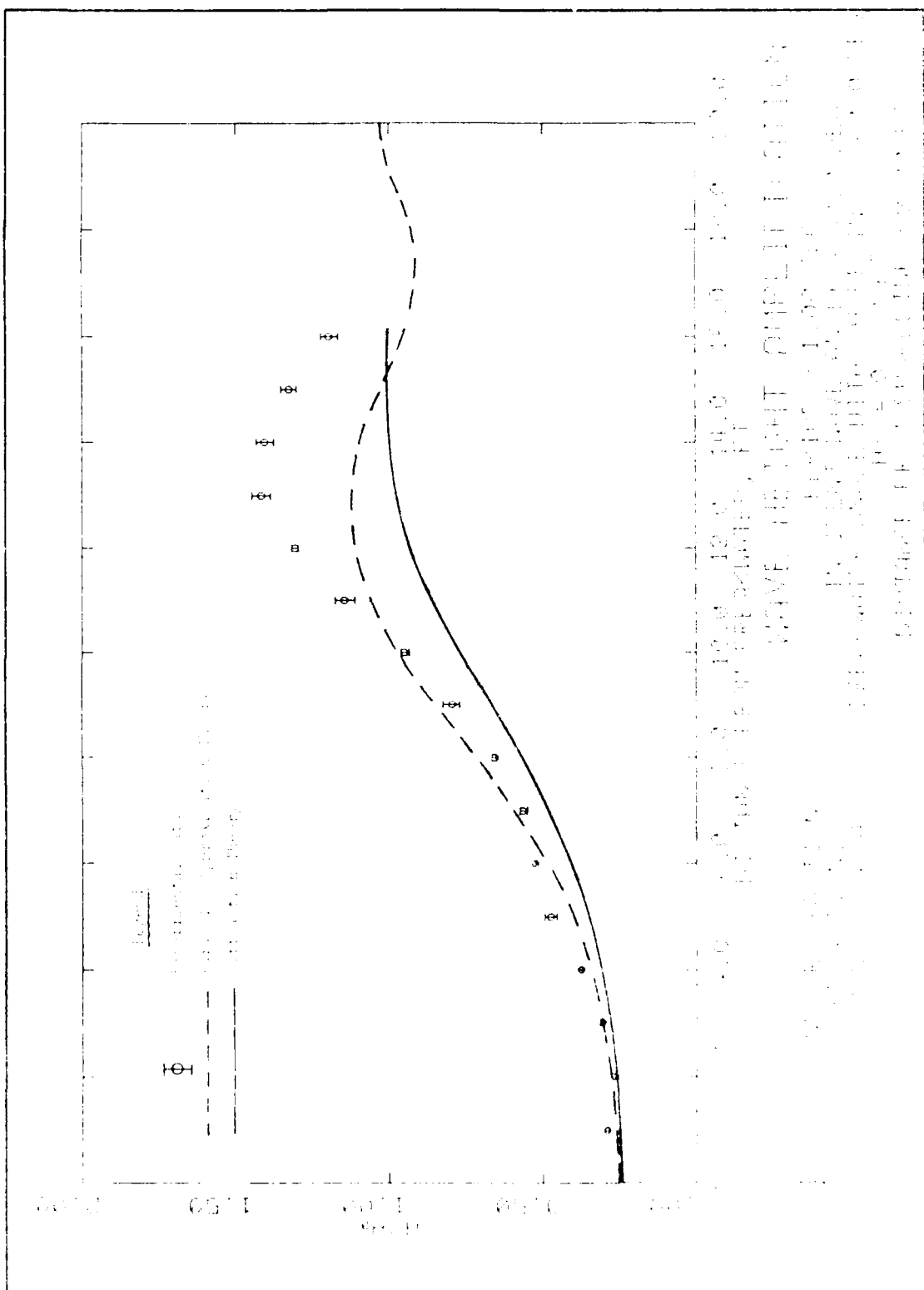
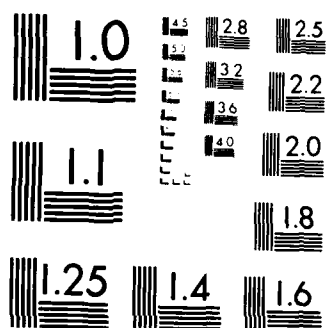


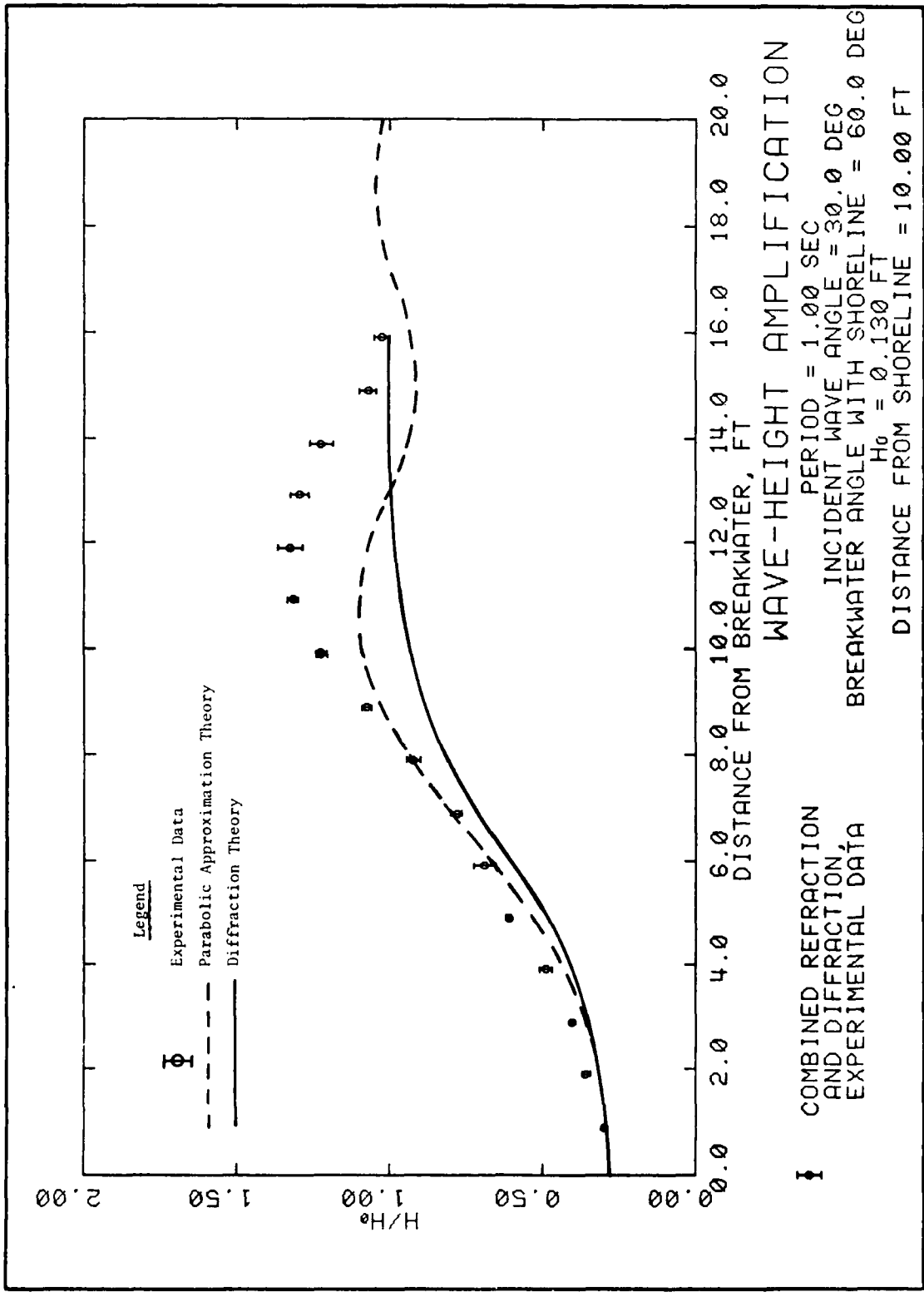
FIGURE 1.

AD-A149 743 EROSION CONTROL OF SCOUR DURING CONSTRUCTION REPORT 5 2/2
EXPERIMENTAL MEASUR. (U) ARMY ENGINEER WATERWAYS
EXPERIMENT STATION VICKSBURG MS HYDRA. L Z HALES
UNCLASSIFIED SEP 84 WES/TR/HL-80-3-5 F/G 13/2 NL

END
PAGE
13



MICROCOPY RESOLUTION TEST CHART
NATIONAL BUREAU OF STANDARDS 1964 A



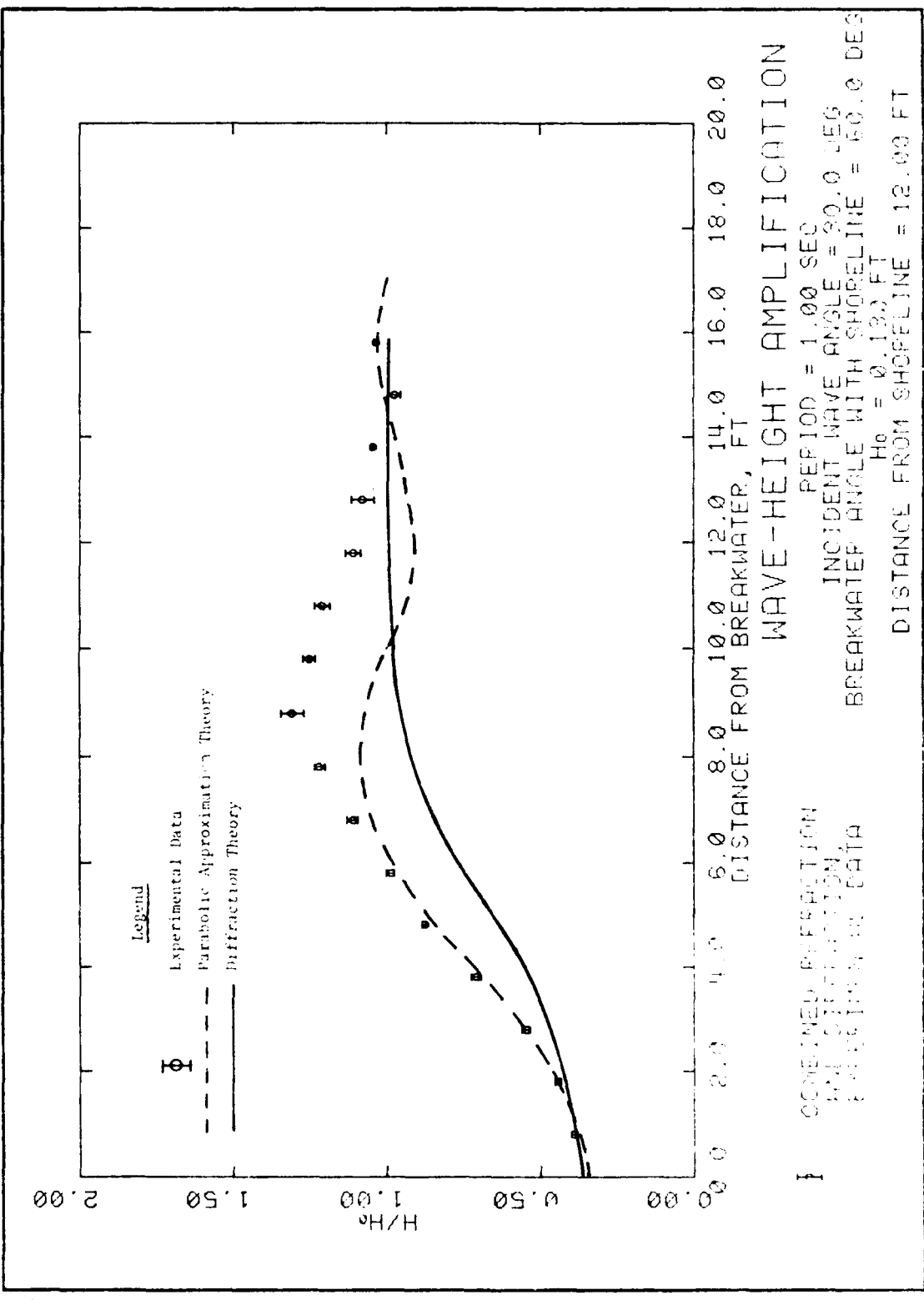


PLATE 20

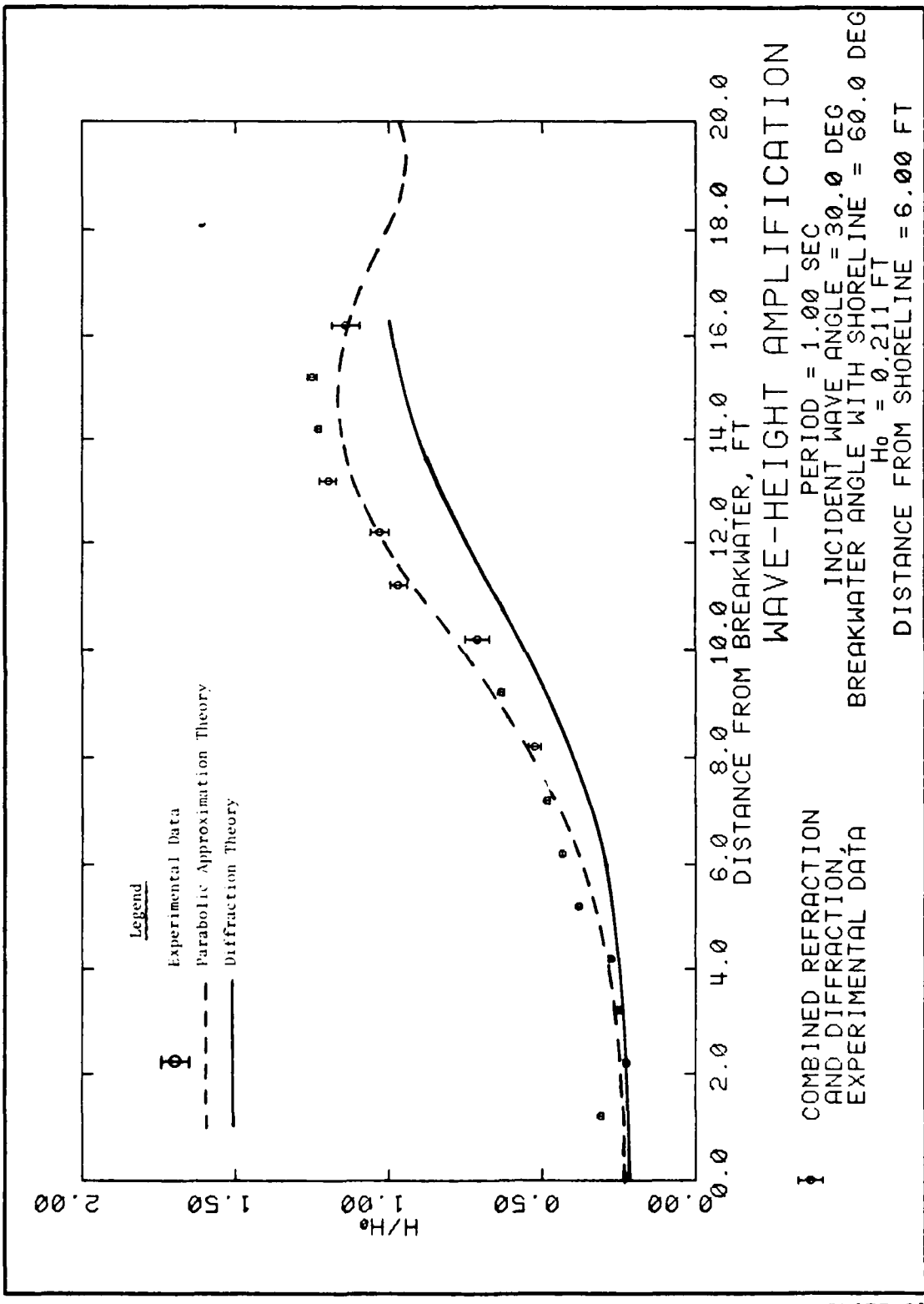


PLATE 21

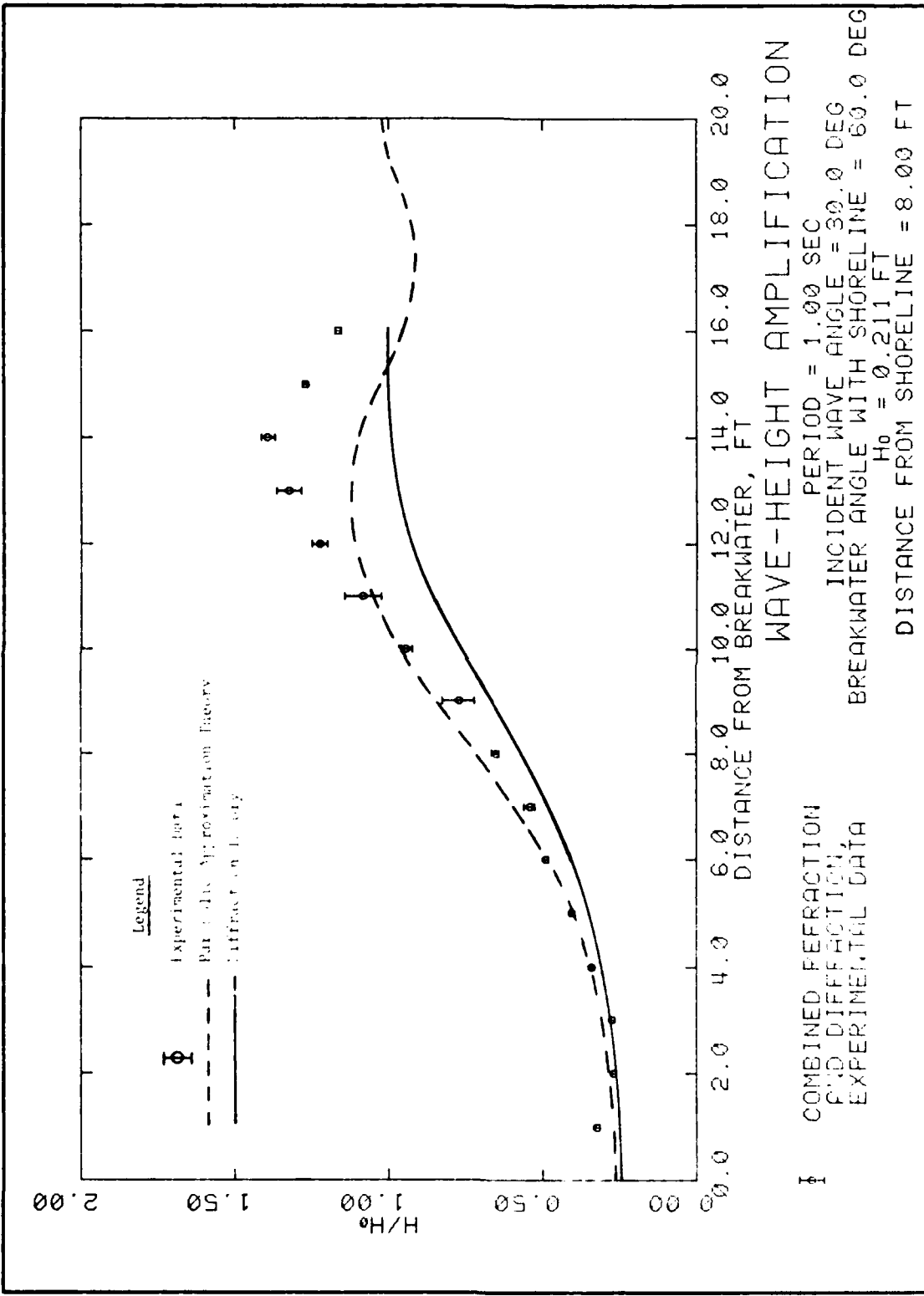
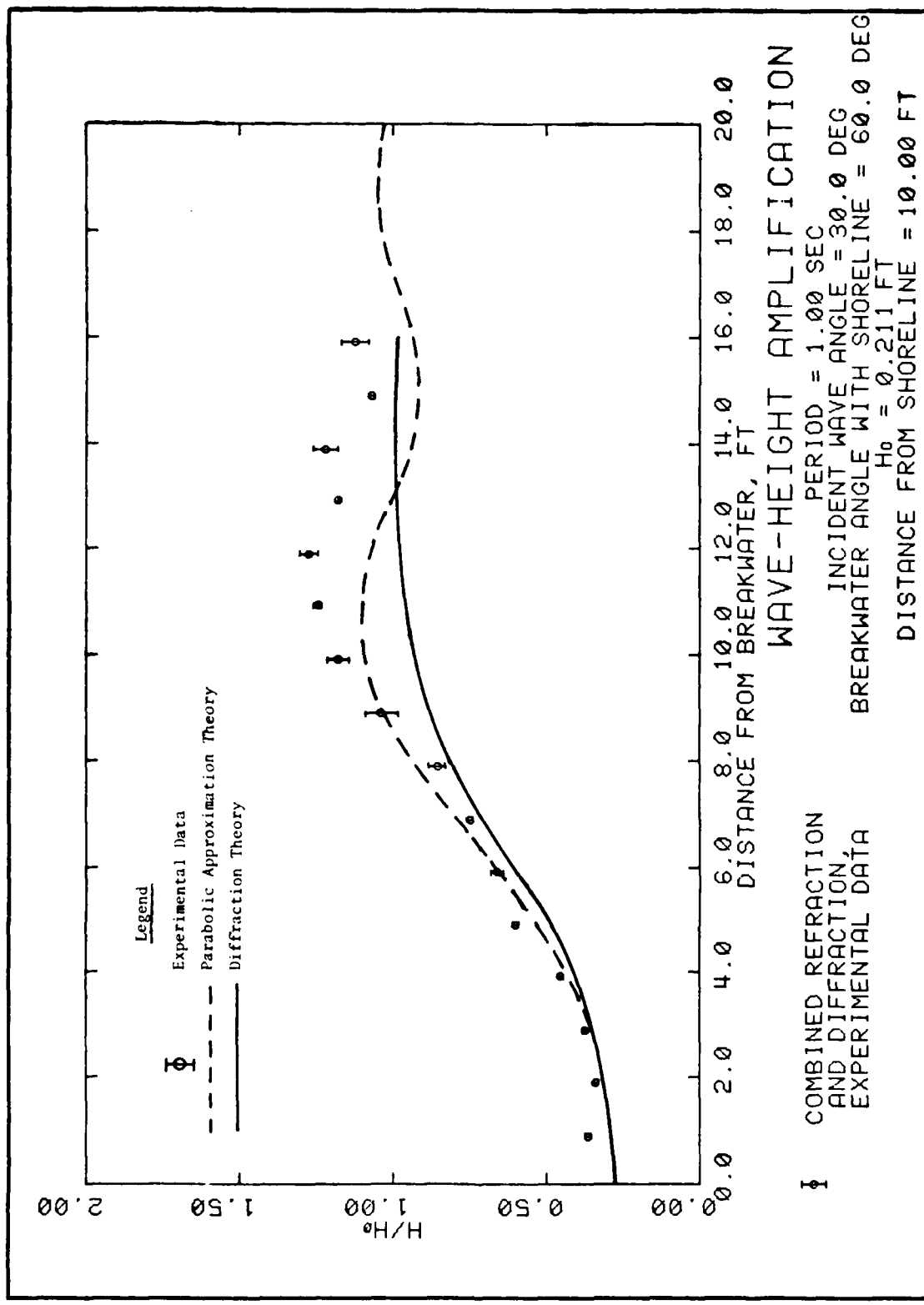


PLATE 22



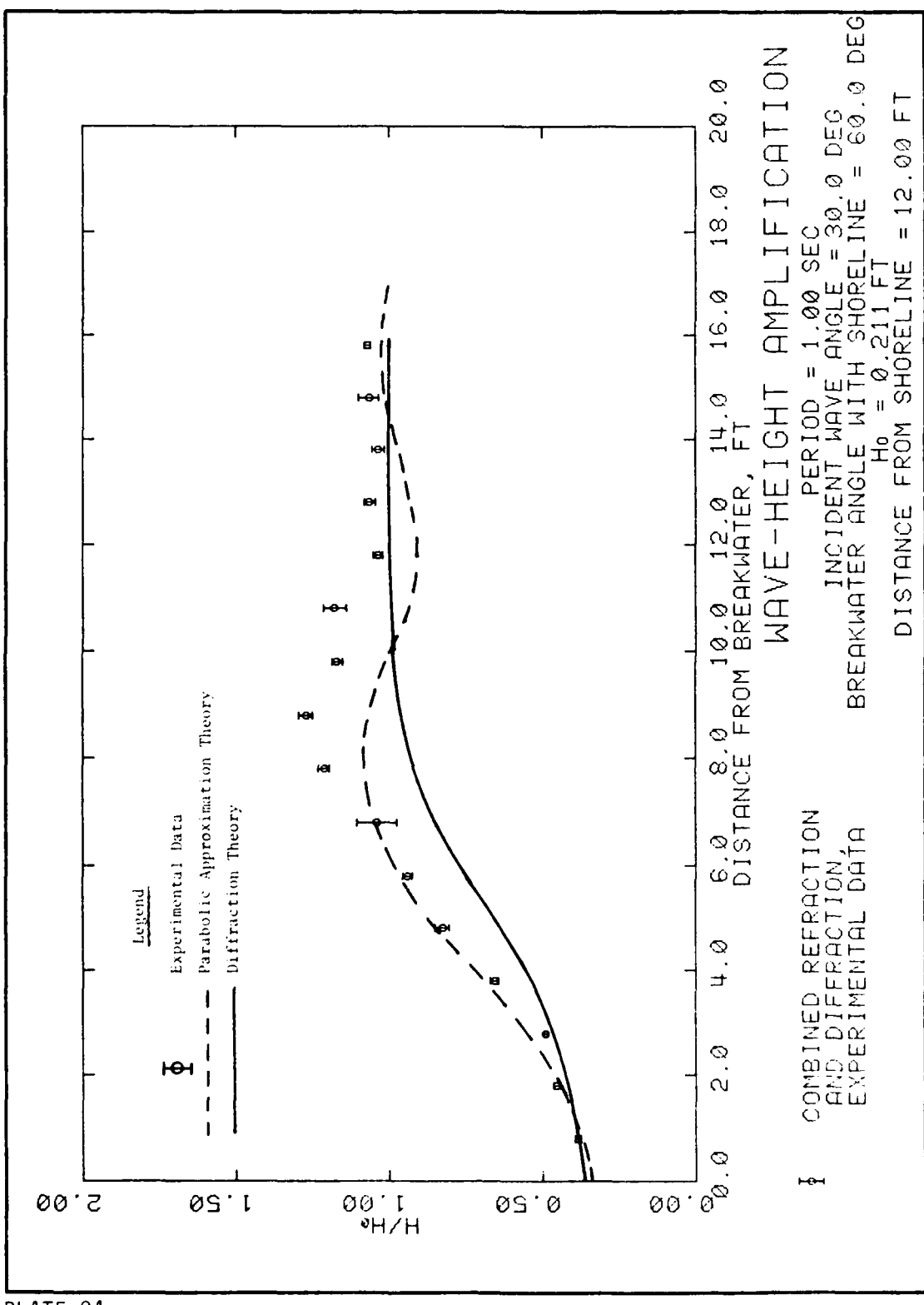


PLATE 24

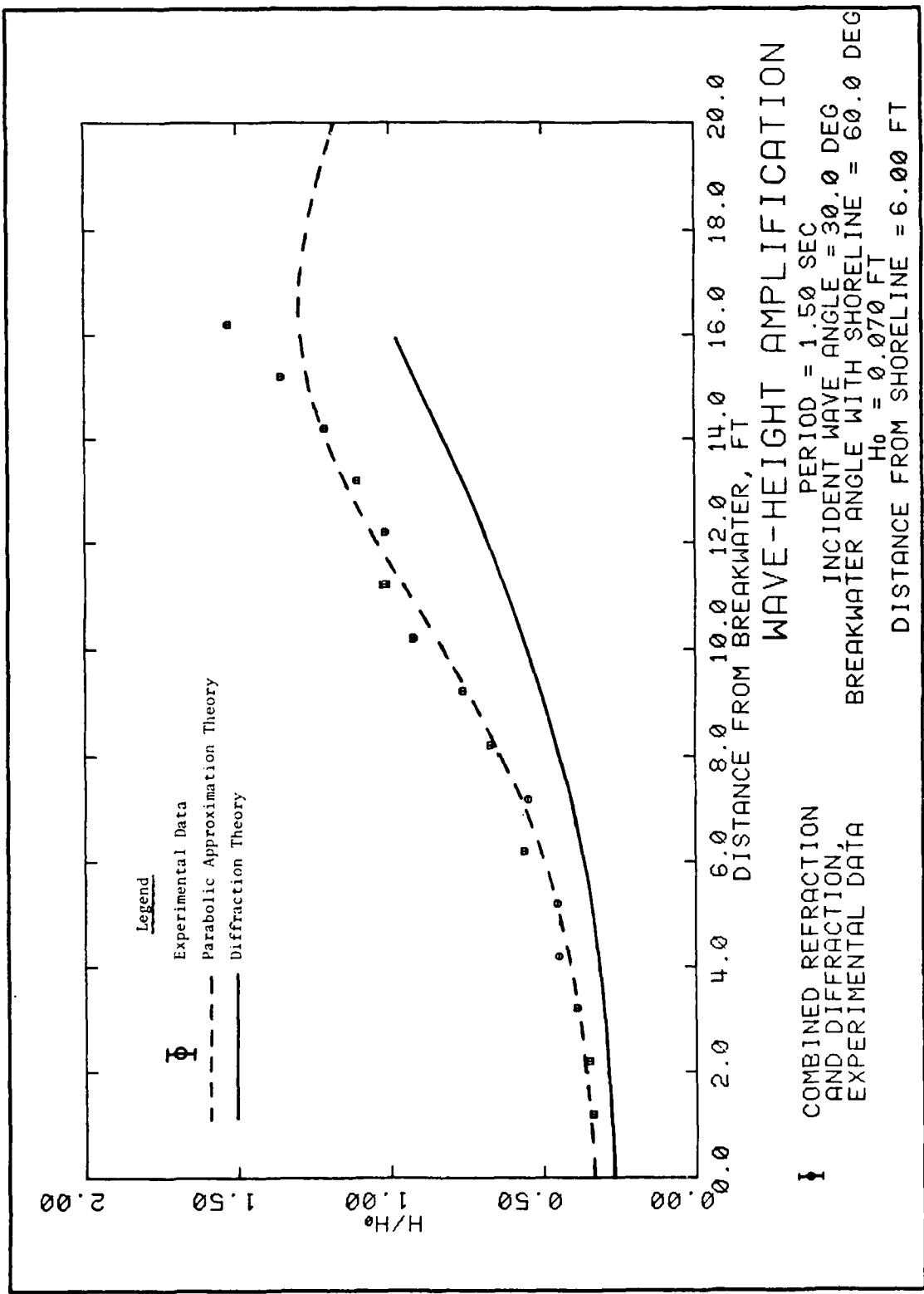


PLATE 25

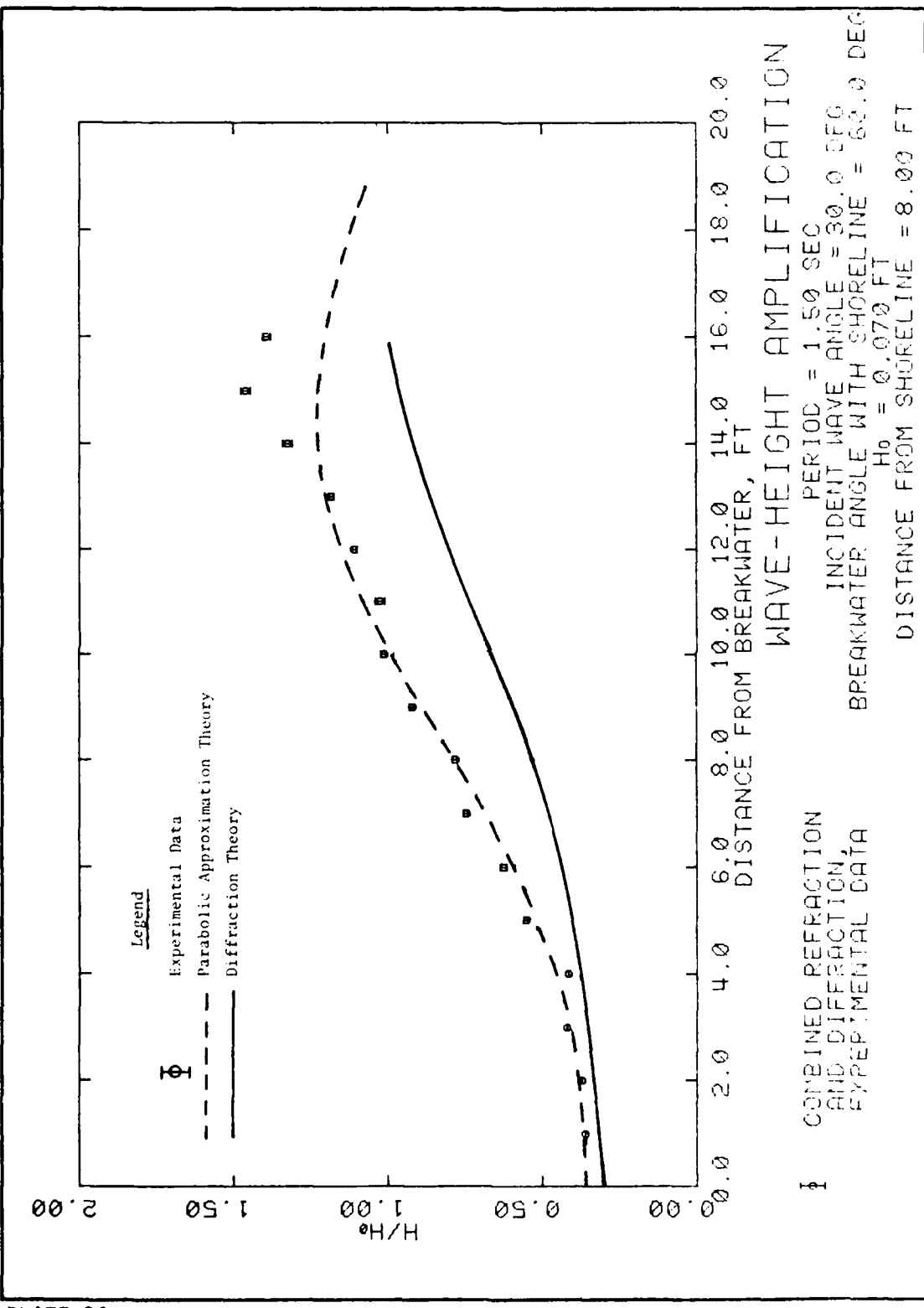
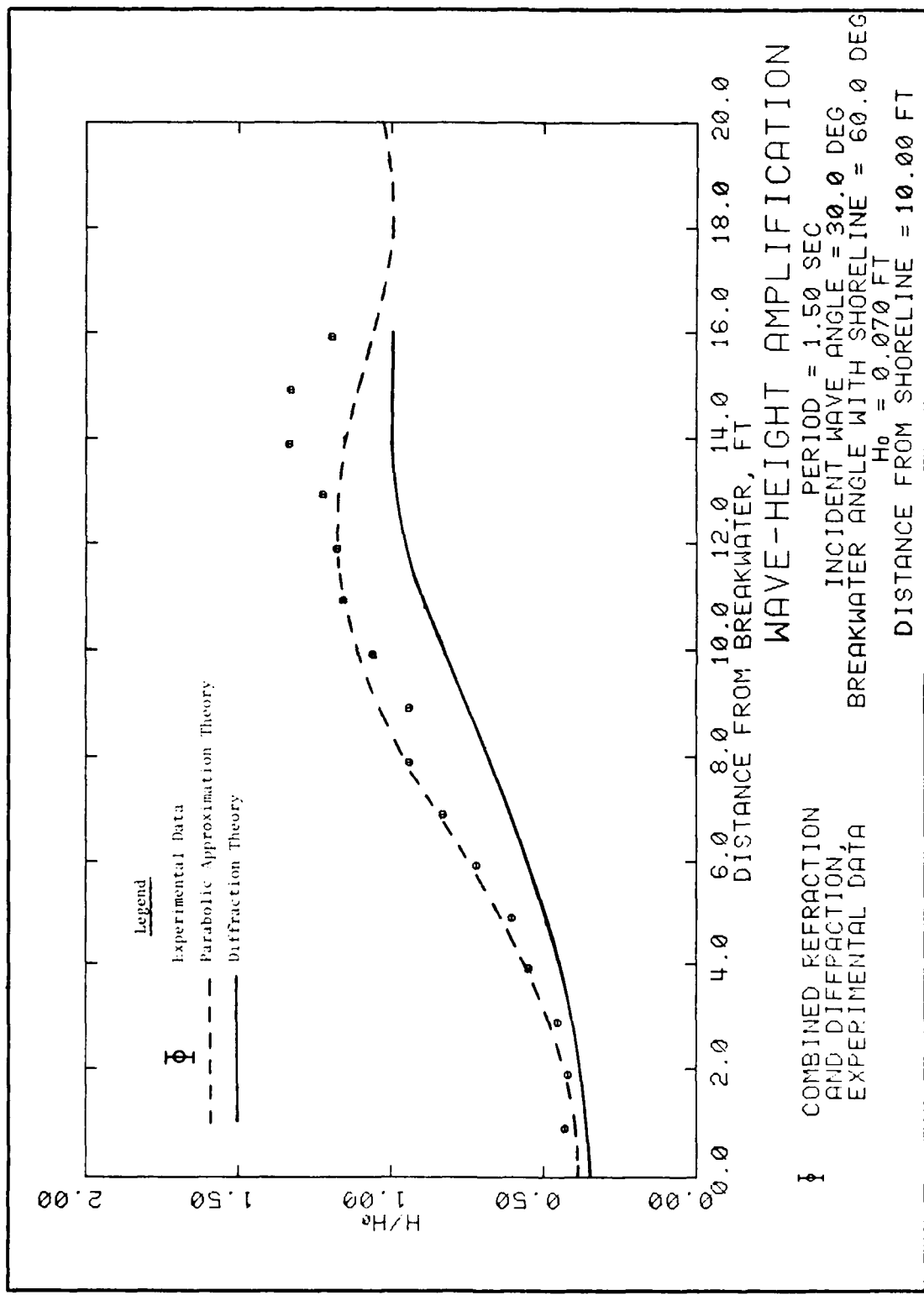


PLATE 26



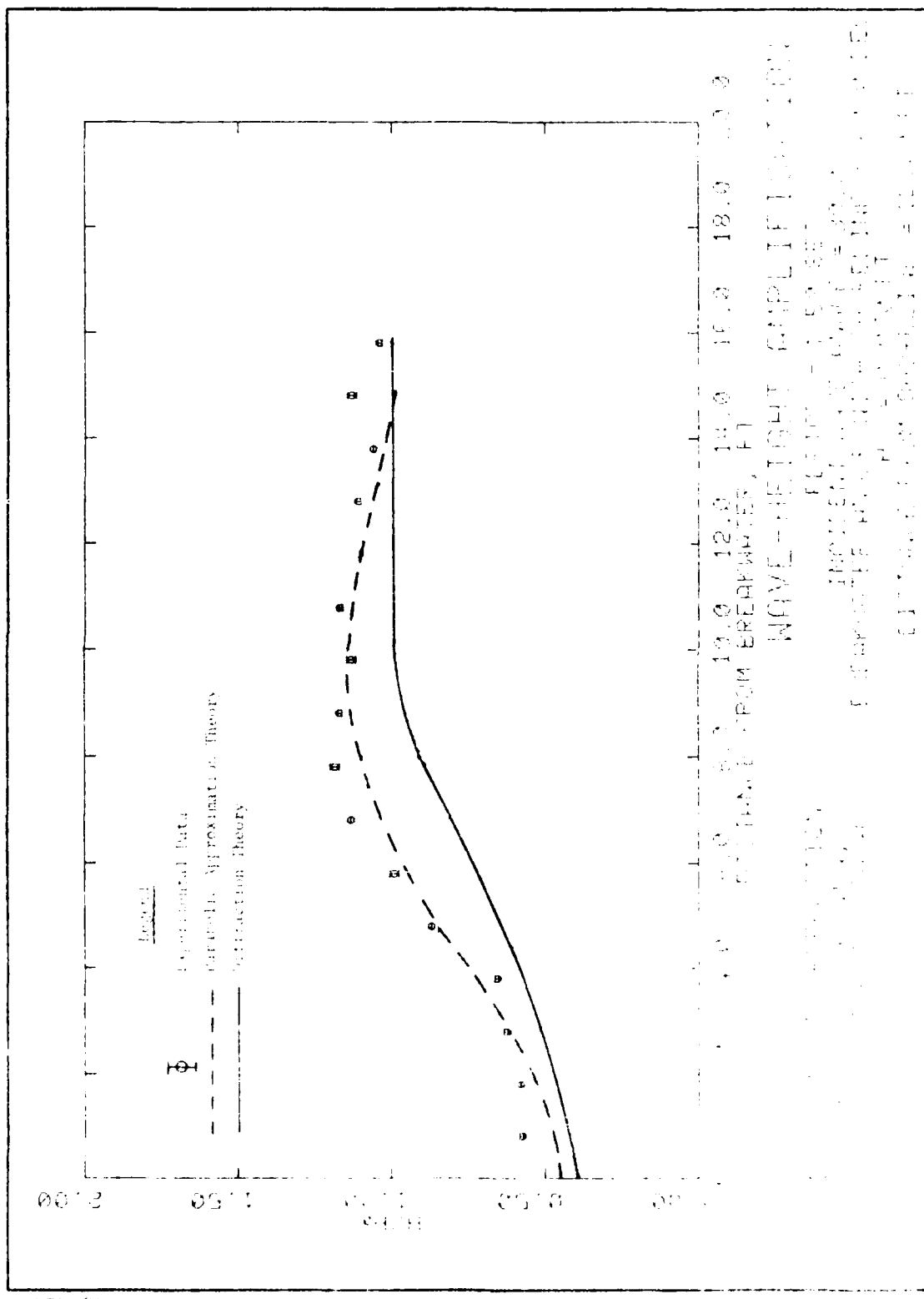
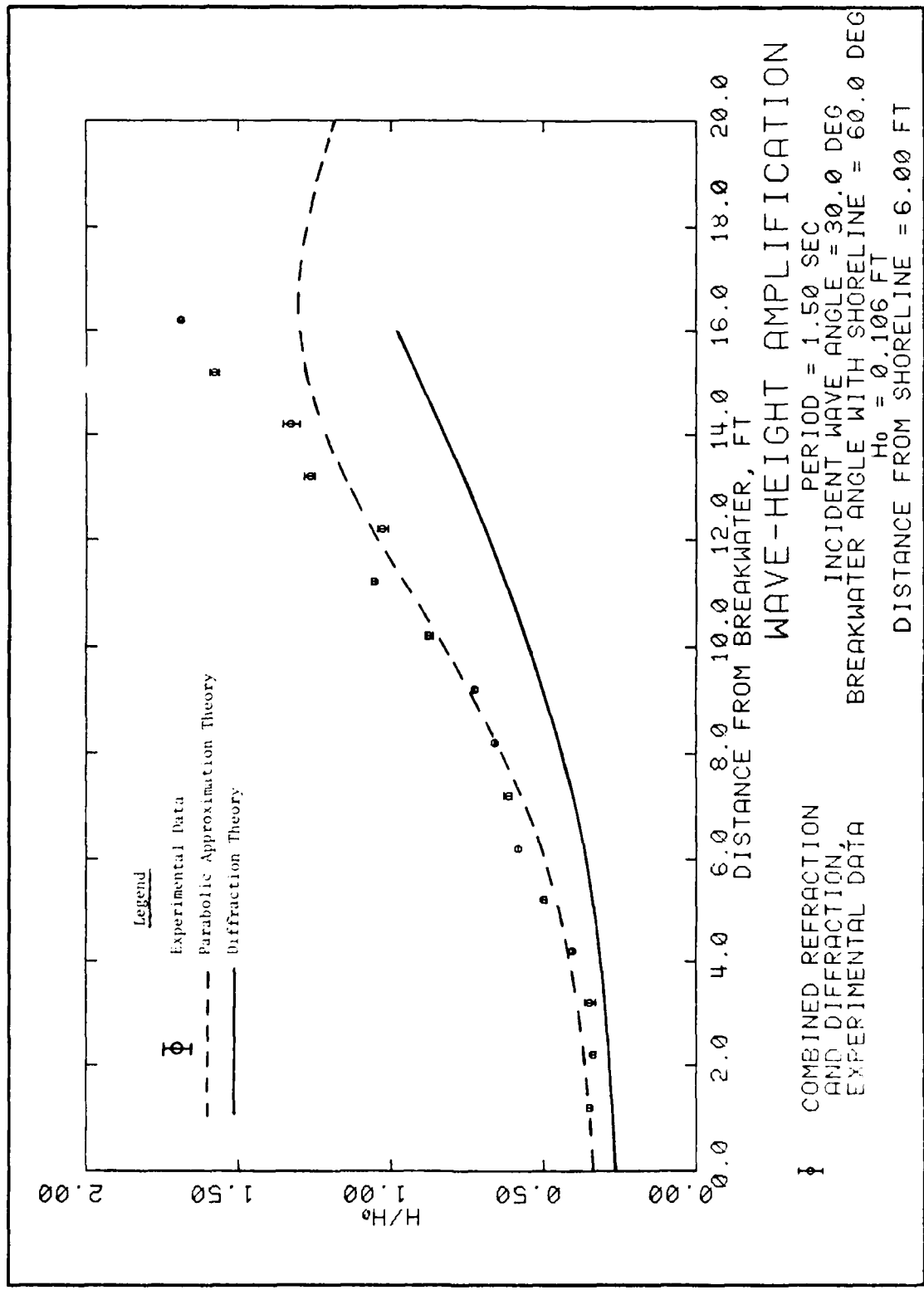


PLATE 26



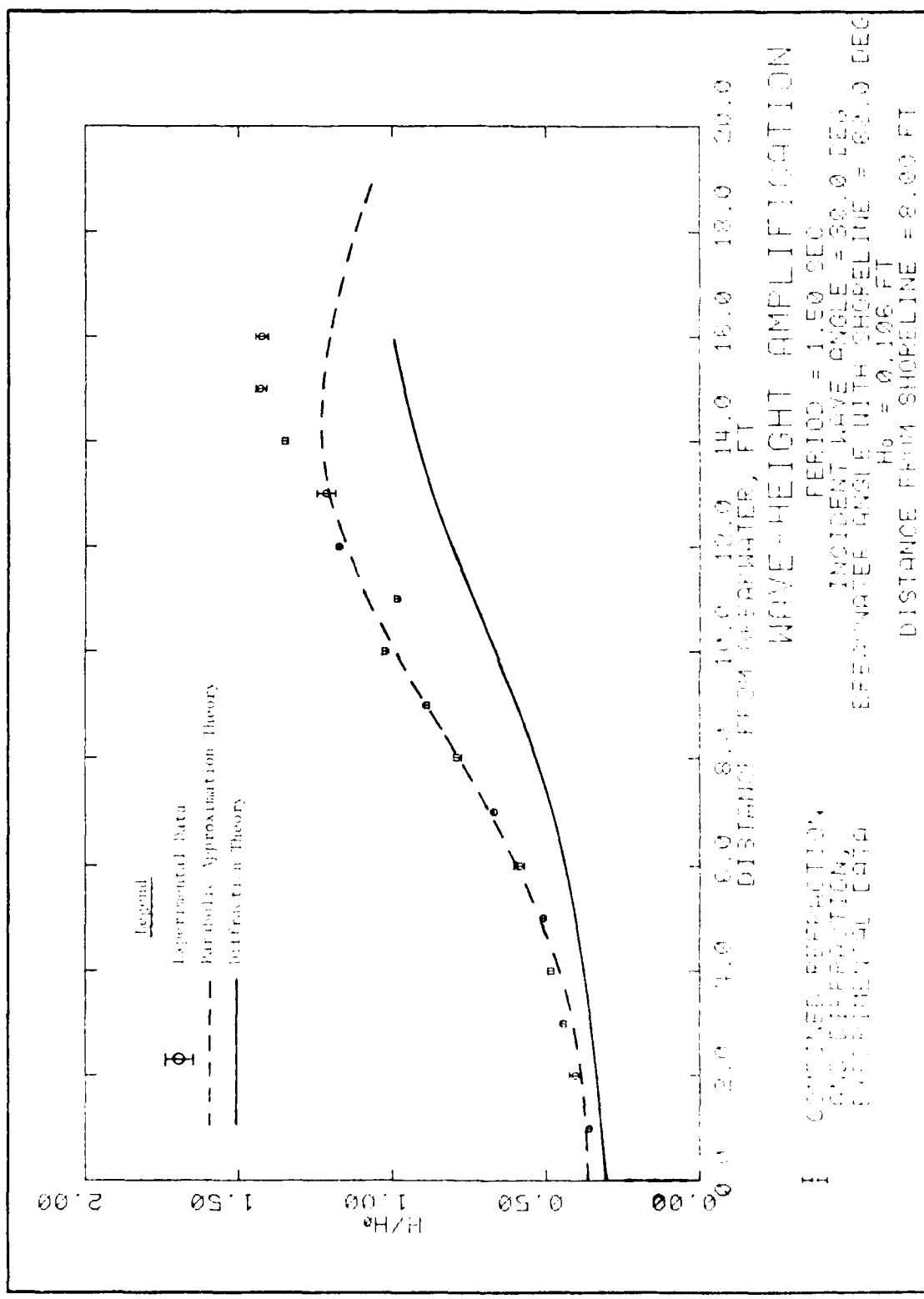


PLATE 30

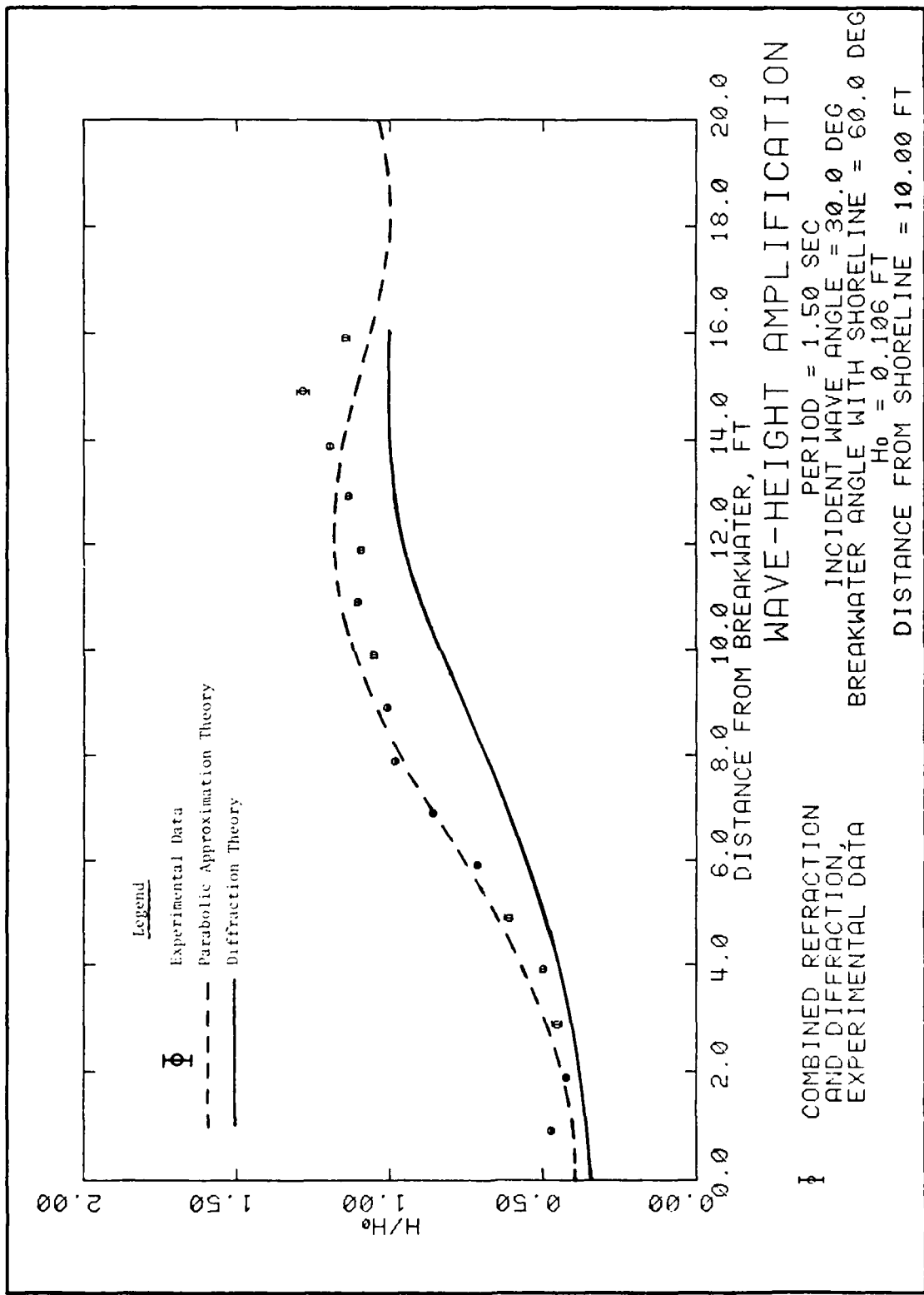


PLATE 31

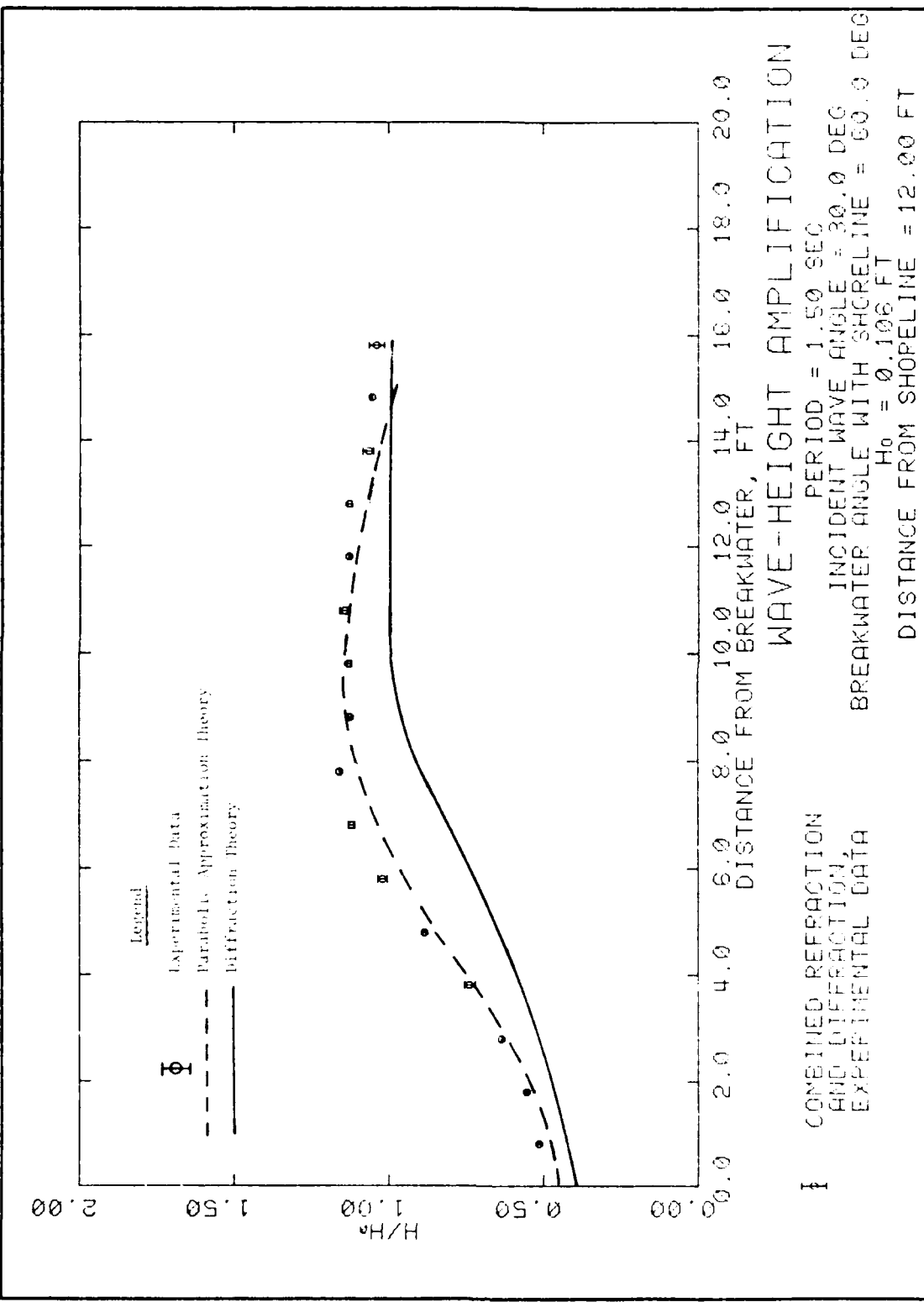
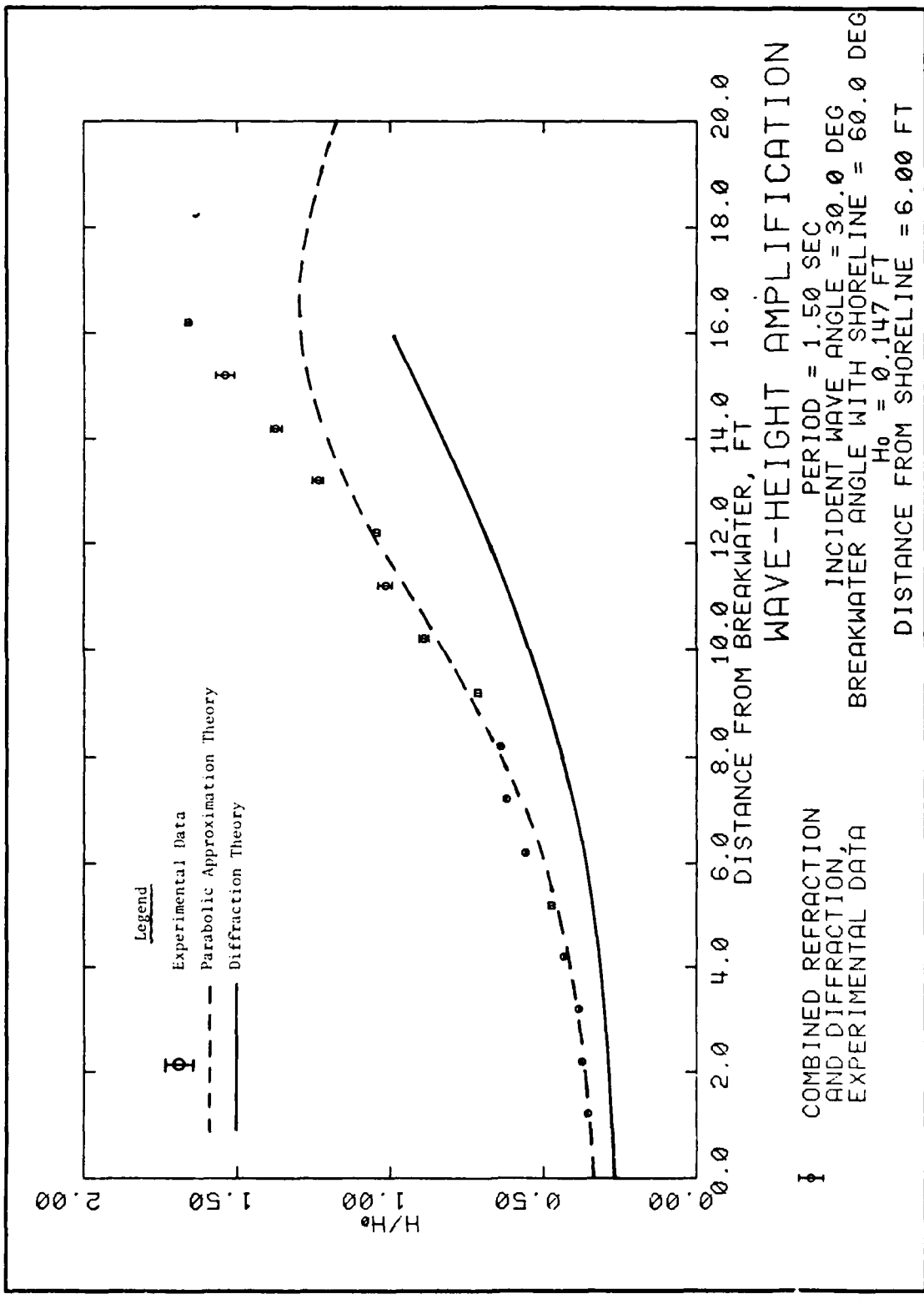


PLATE 32



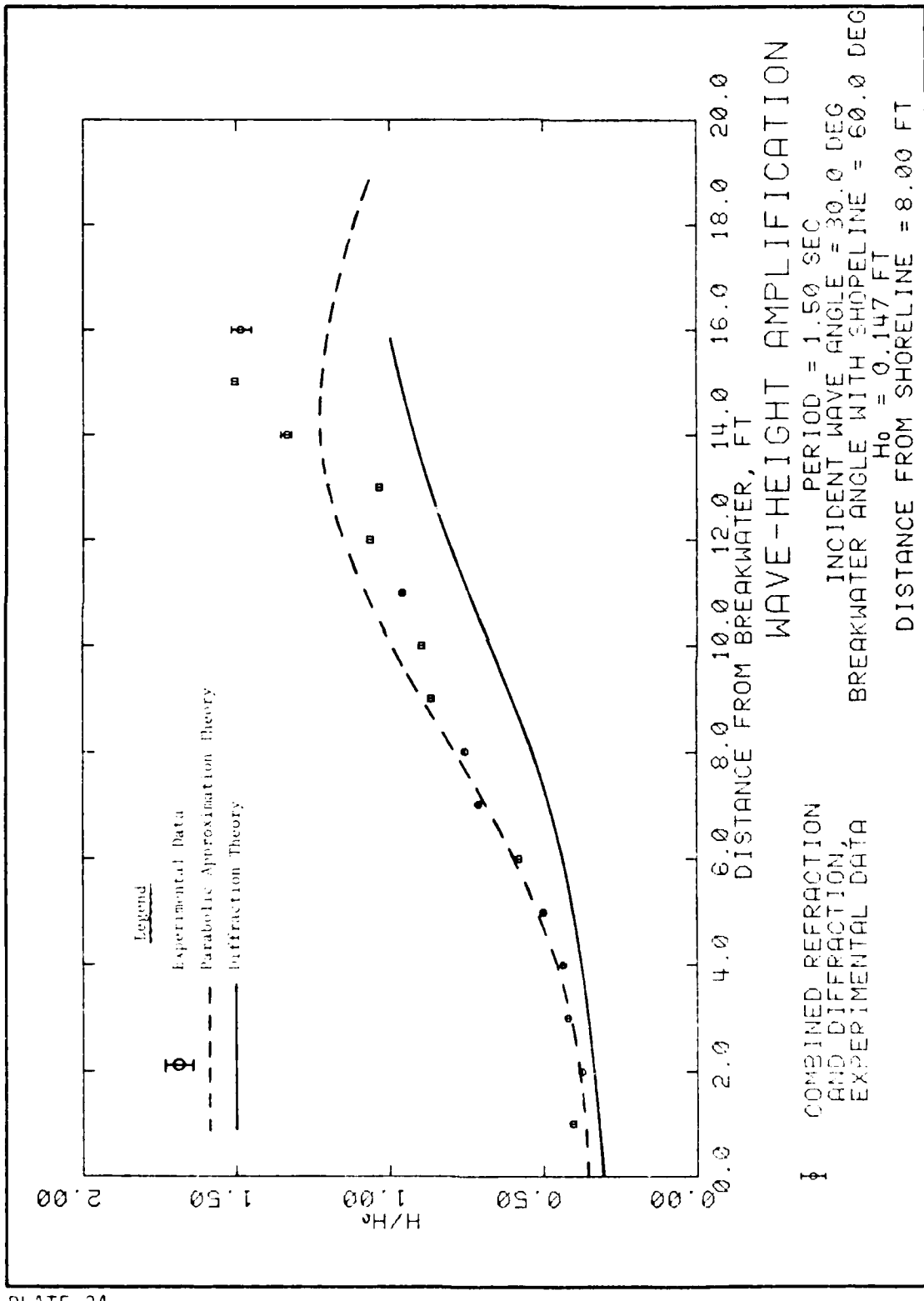
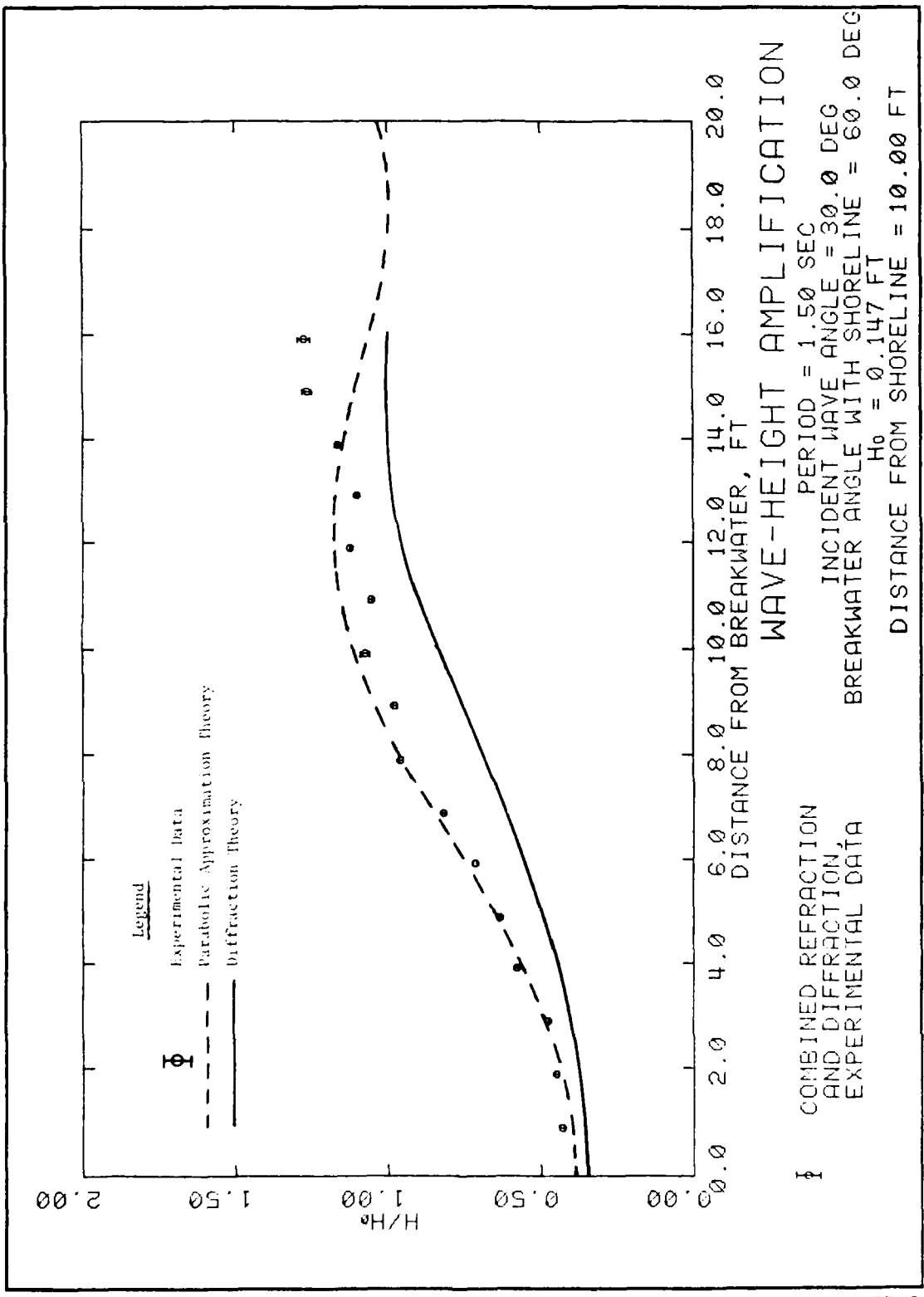


PLATE 34



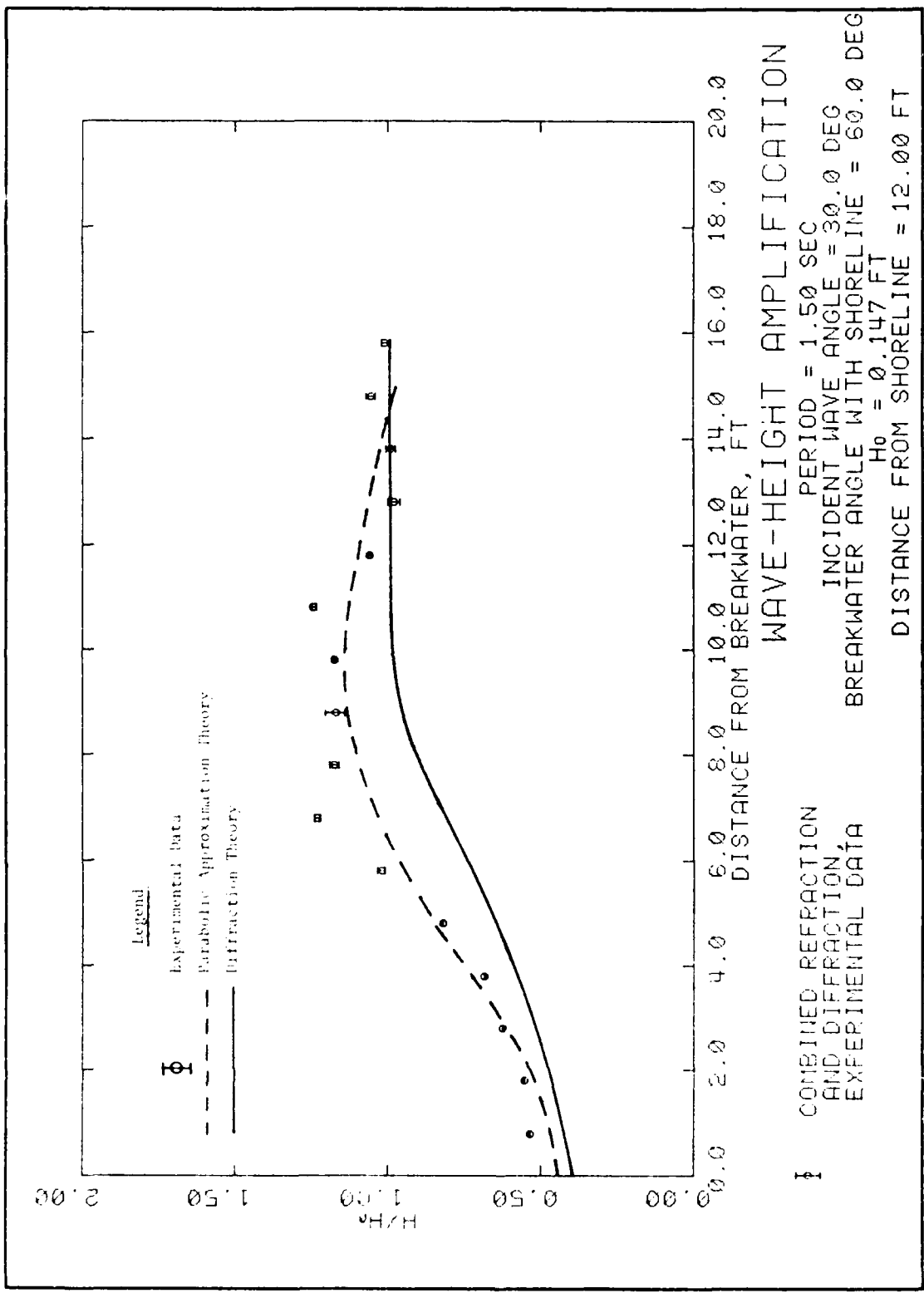
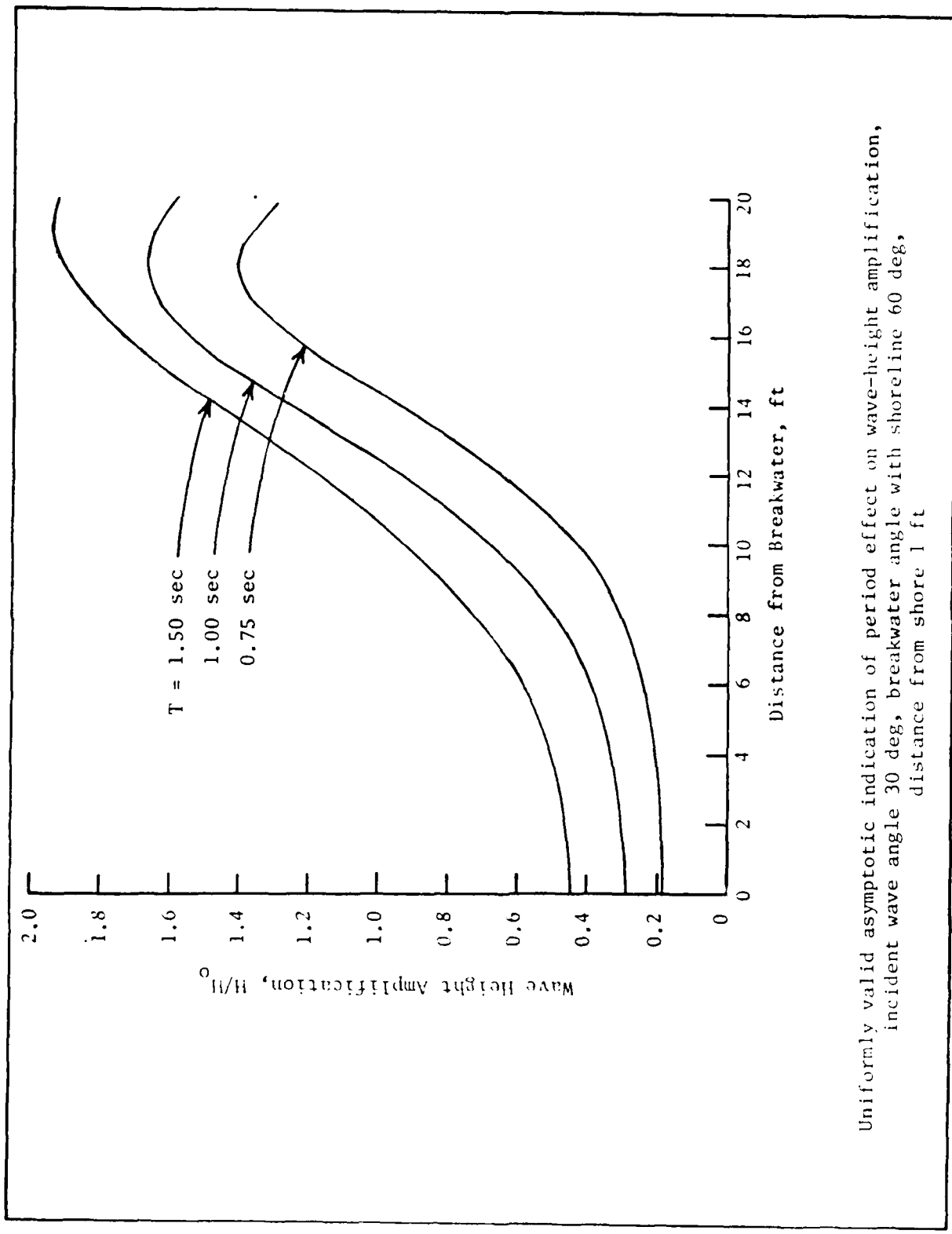
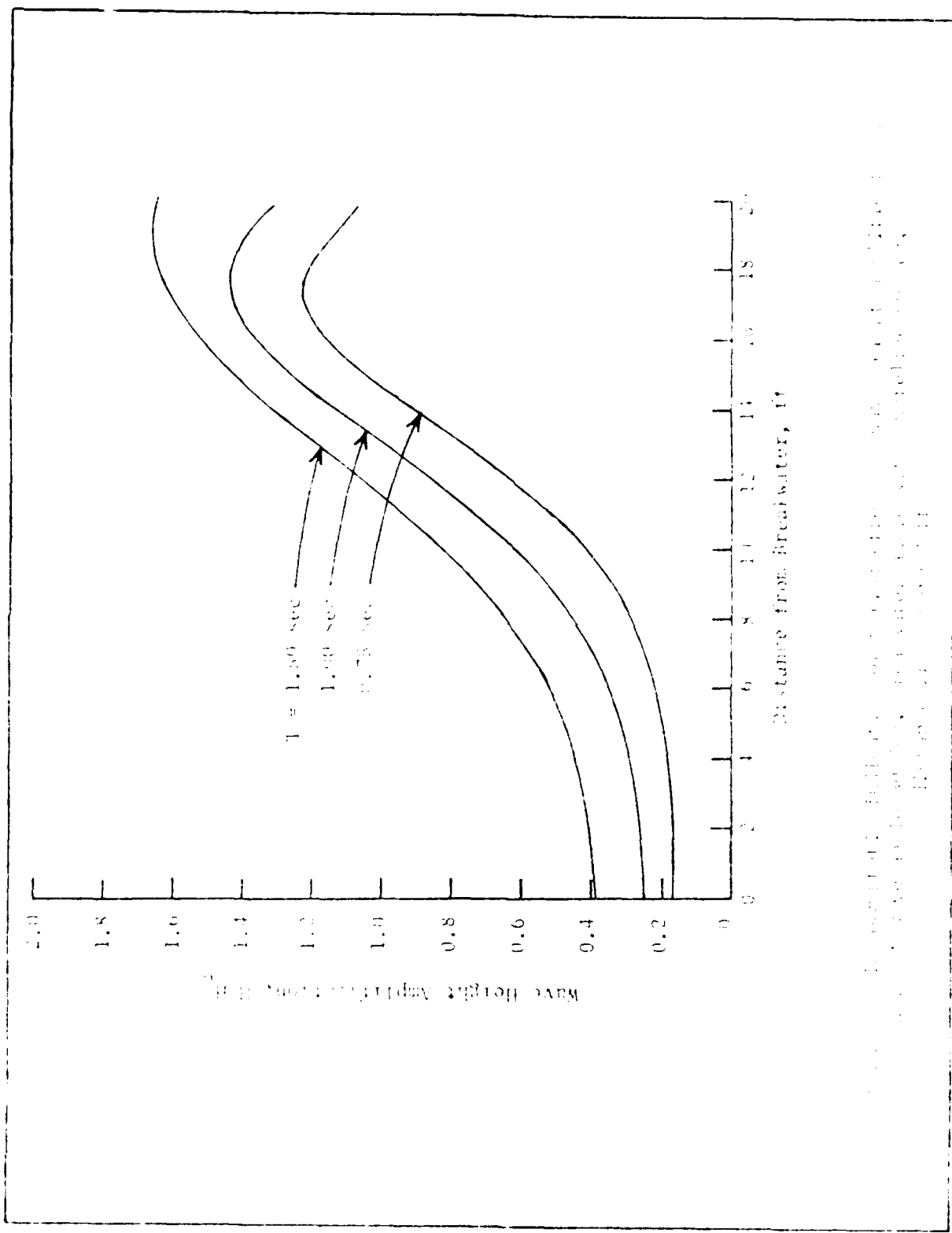


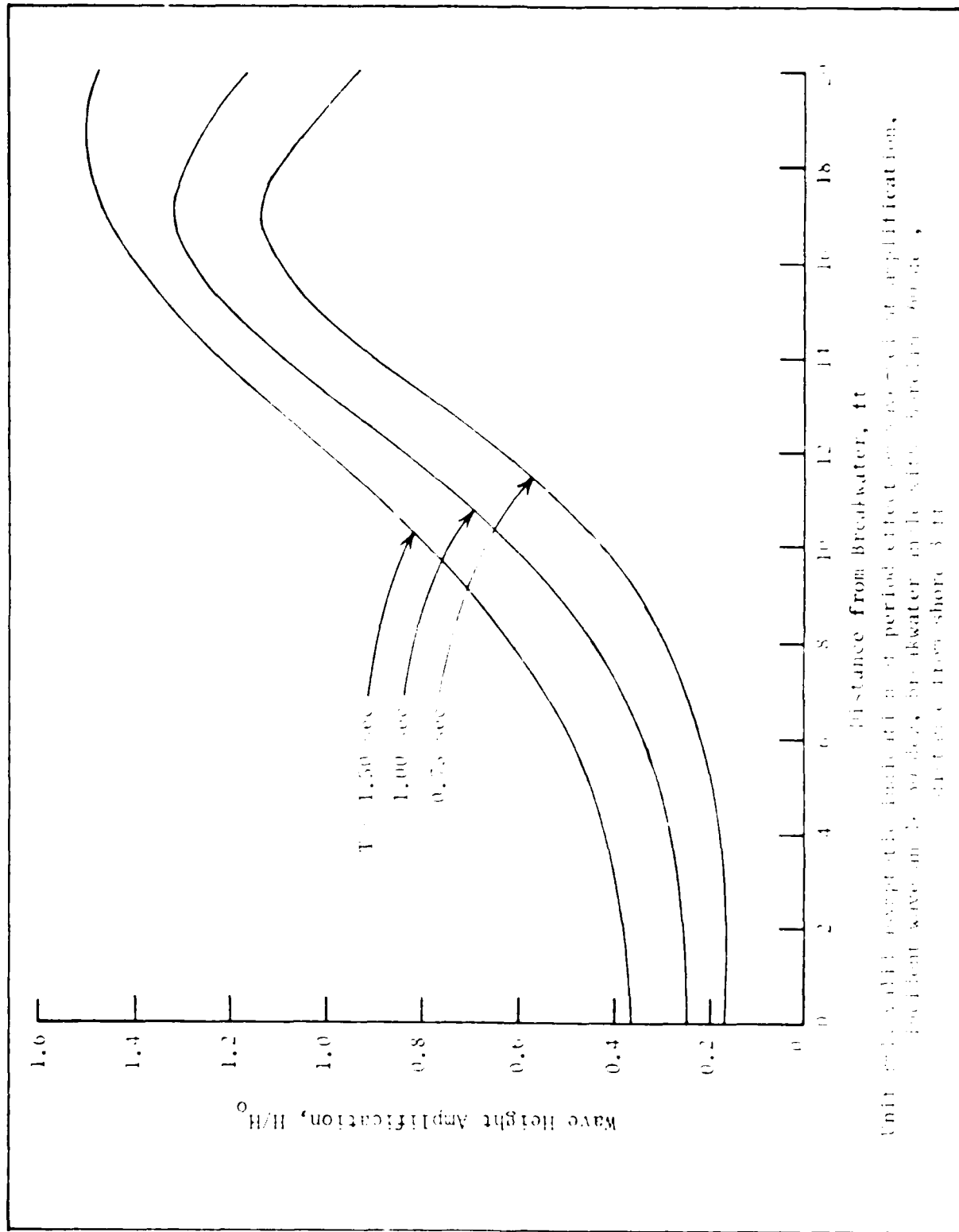
PLATE 36



Uniformly valid asymptotic indication of period effect on wave-height amplification,
incident wave angle 30 deg, breakwater angle with shoreline 60 deg,
distance from shore 1 ft

PLATE 37





Unit amplitude component of periodic effective waves at a point in the surf zone, H_0 , for a wave train, T , incident on a vertical, non-breaking, non-dissipating breakwater located 3 ft offshore from shore.

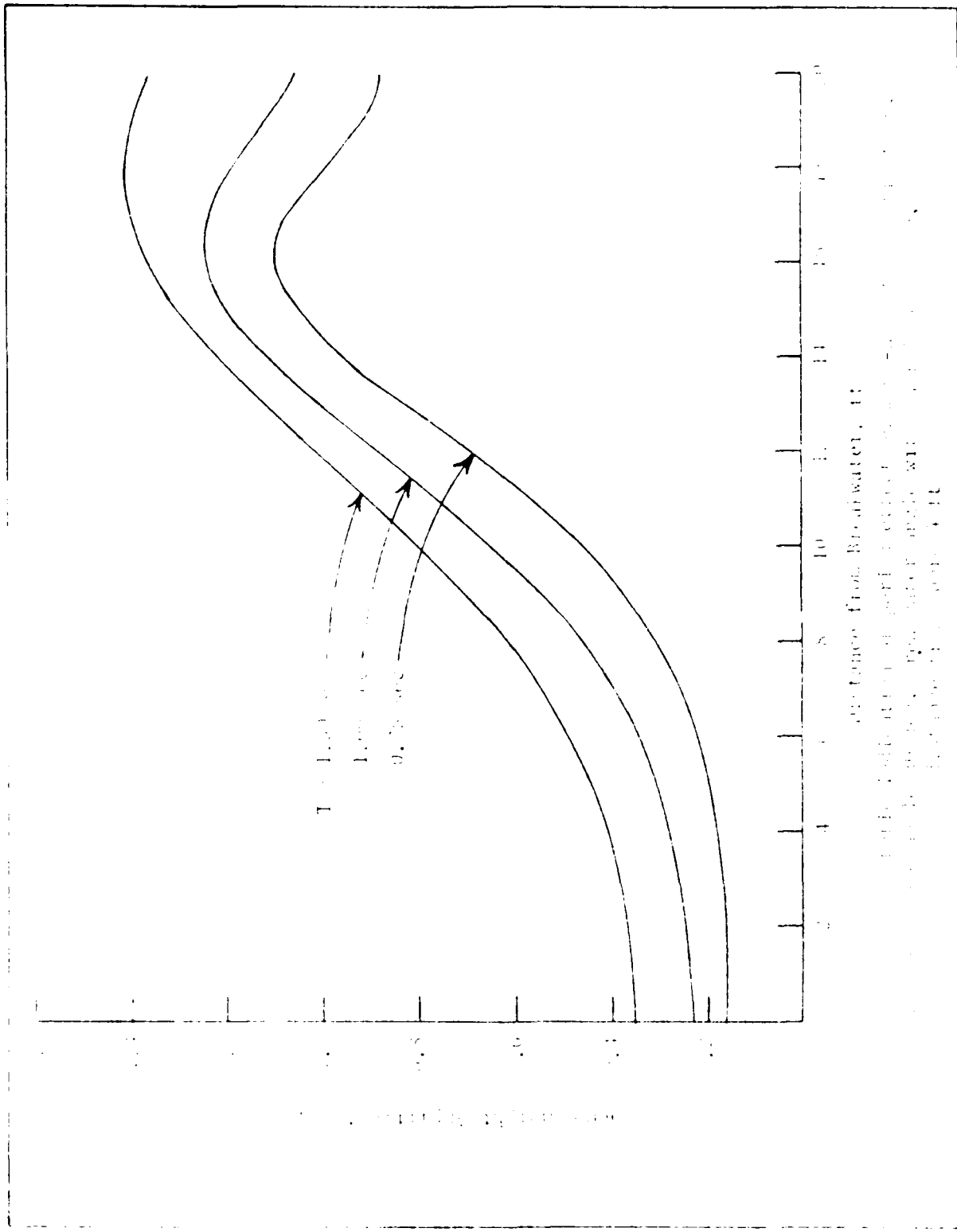
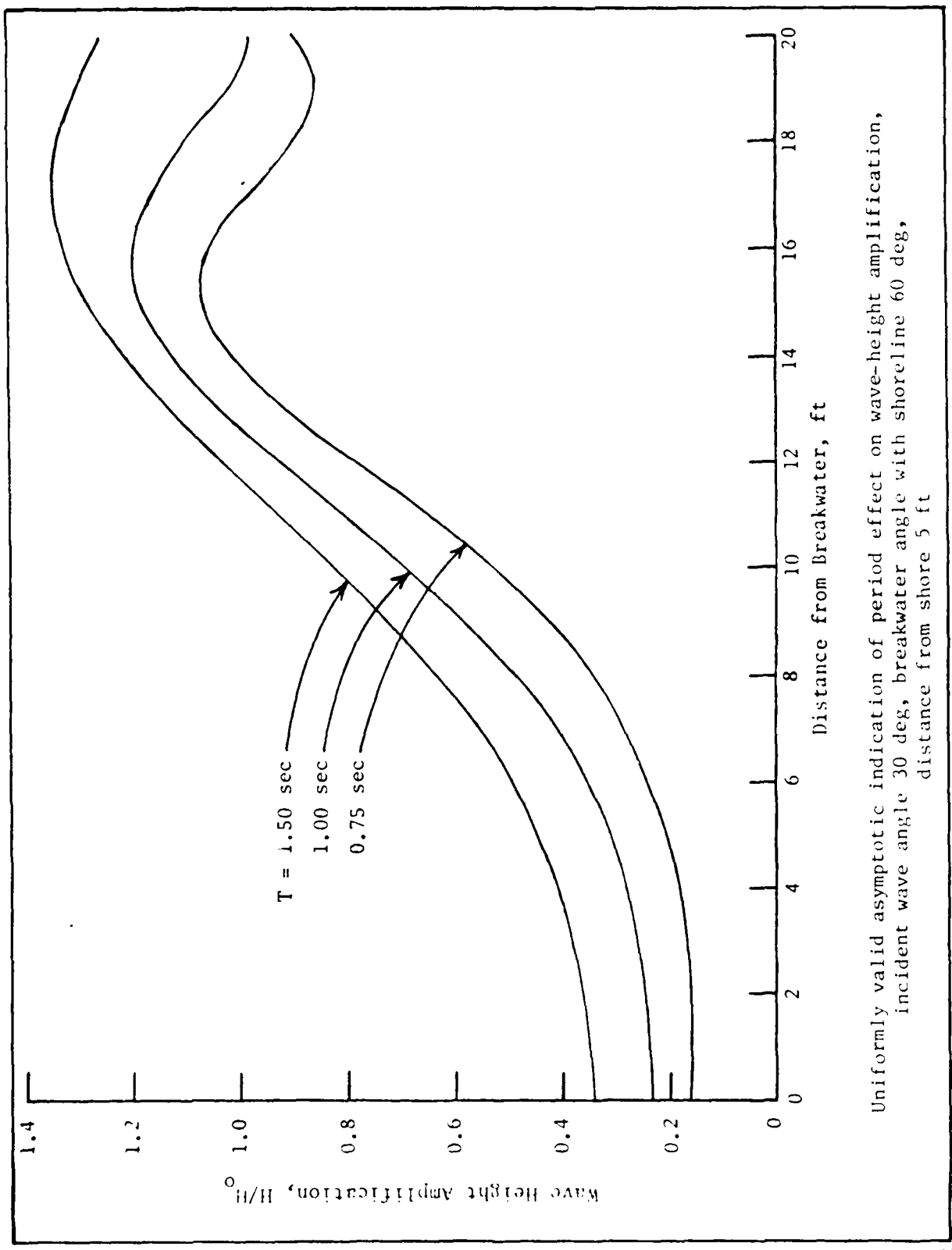


Fig. 1. Dependence of particle volume fraction on particle diameter. (1) $d = 10 \mu$; (2) $d = 20 \mu$; (3) $d = 30 \mu$; (4) $d = 40 \mu$.
Diameters of particles in water were determined by sedimentation analysis.



Uniformly valid asymptotic indication of period effect on wave-height amplification,
incident wave angle 30 deg, breakwater angle with shoreline 60 deg,
distance from shore 5 ft

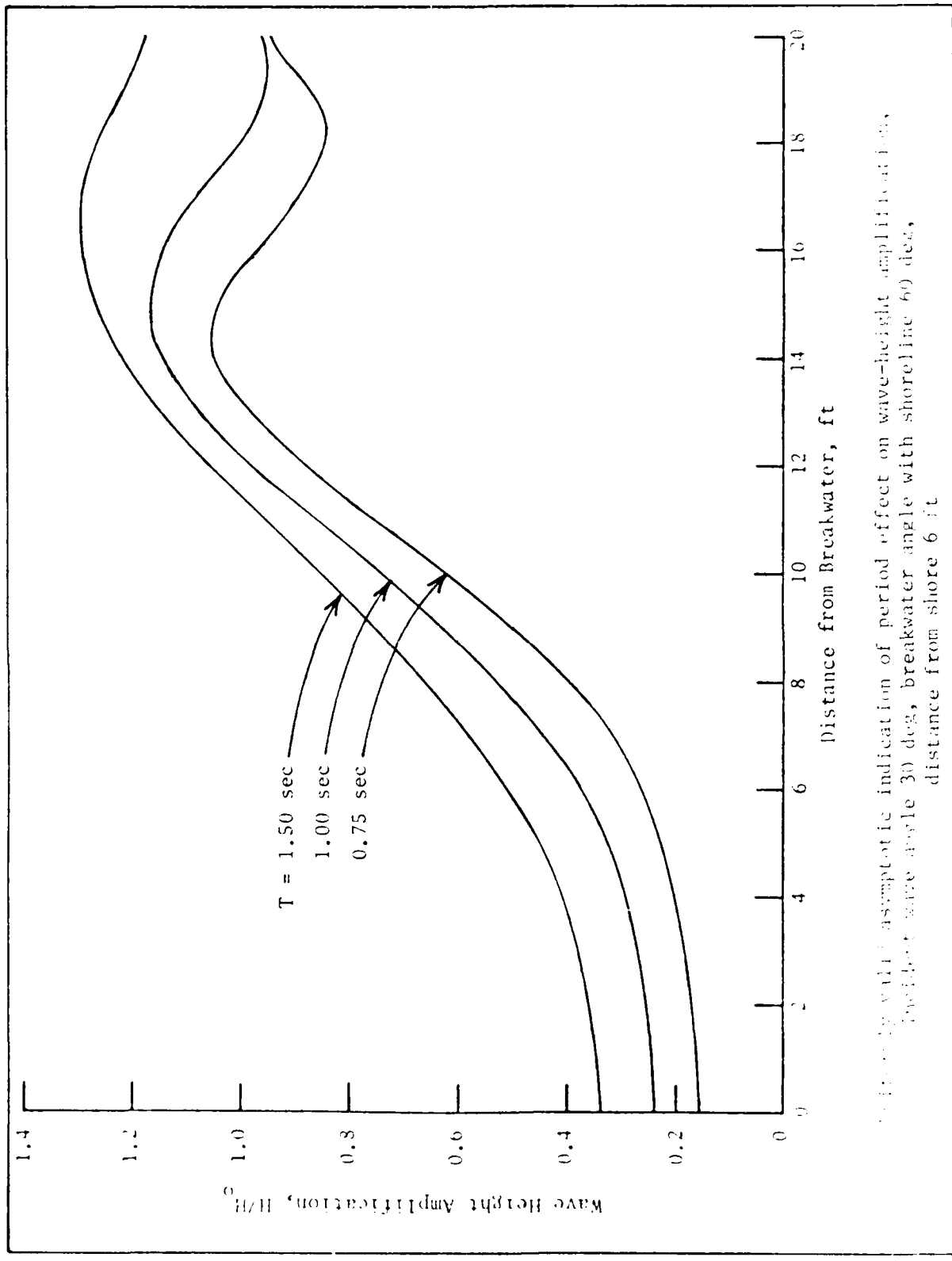
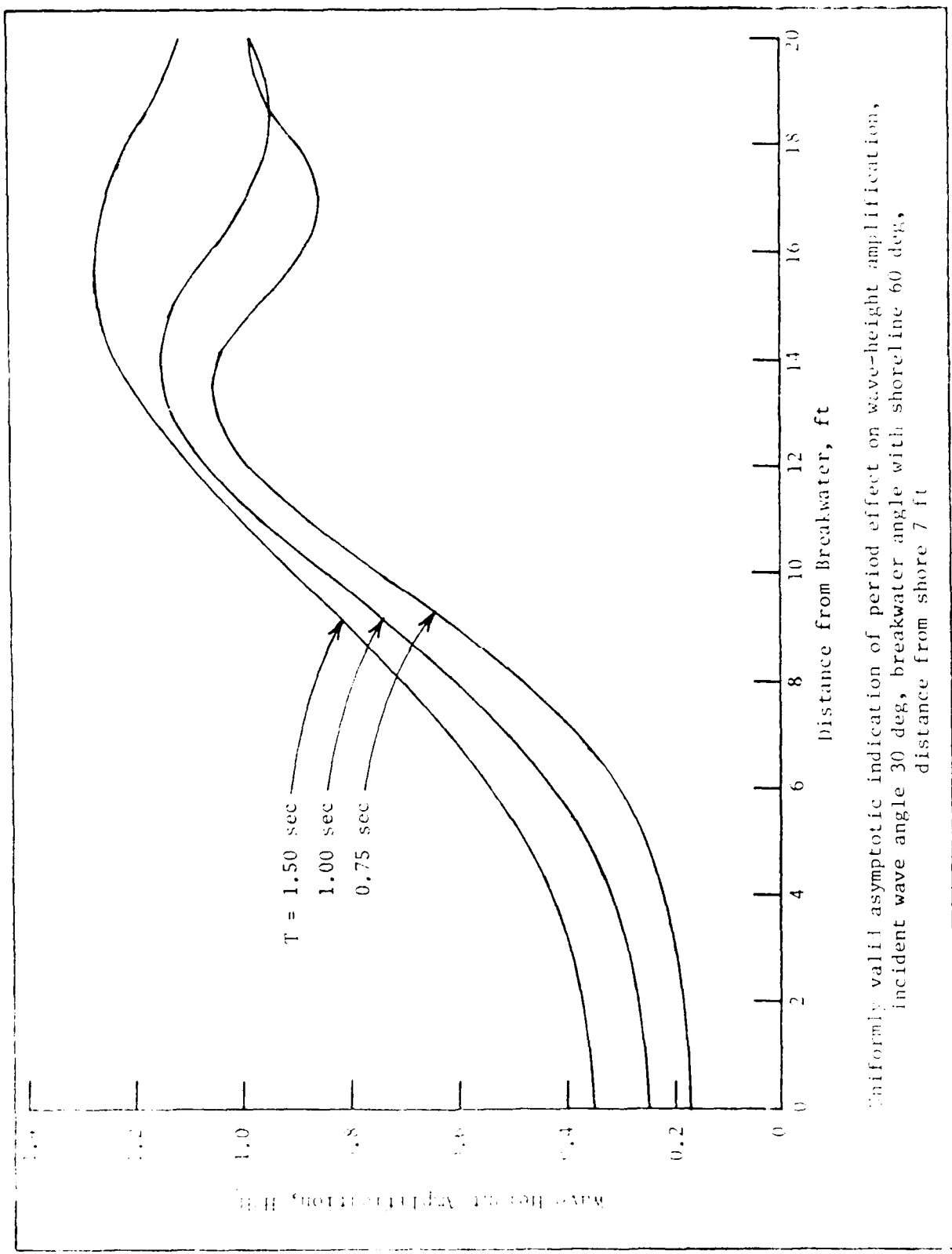


PLATE 42

Graph showing wave height amplification H/H_0 versus distance from a breakwater for three different wave periods $T = 0.75$ sec, 1.00 sec, and 1.50 sec. The graph shows that as the wave period increases, the distance over which the amplification occurs decreases.



Uniformly valid asymptotic indication of period effect on wave-height amplification,
incident wave angle 30 deg, breakwater angle with shoreline 60 deg,
distance from shore 7 ft

PLATE 13

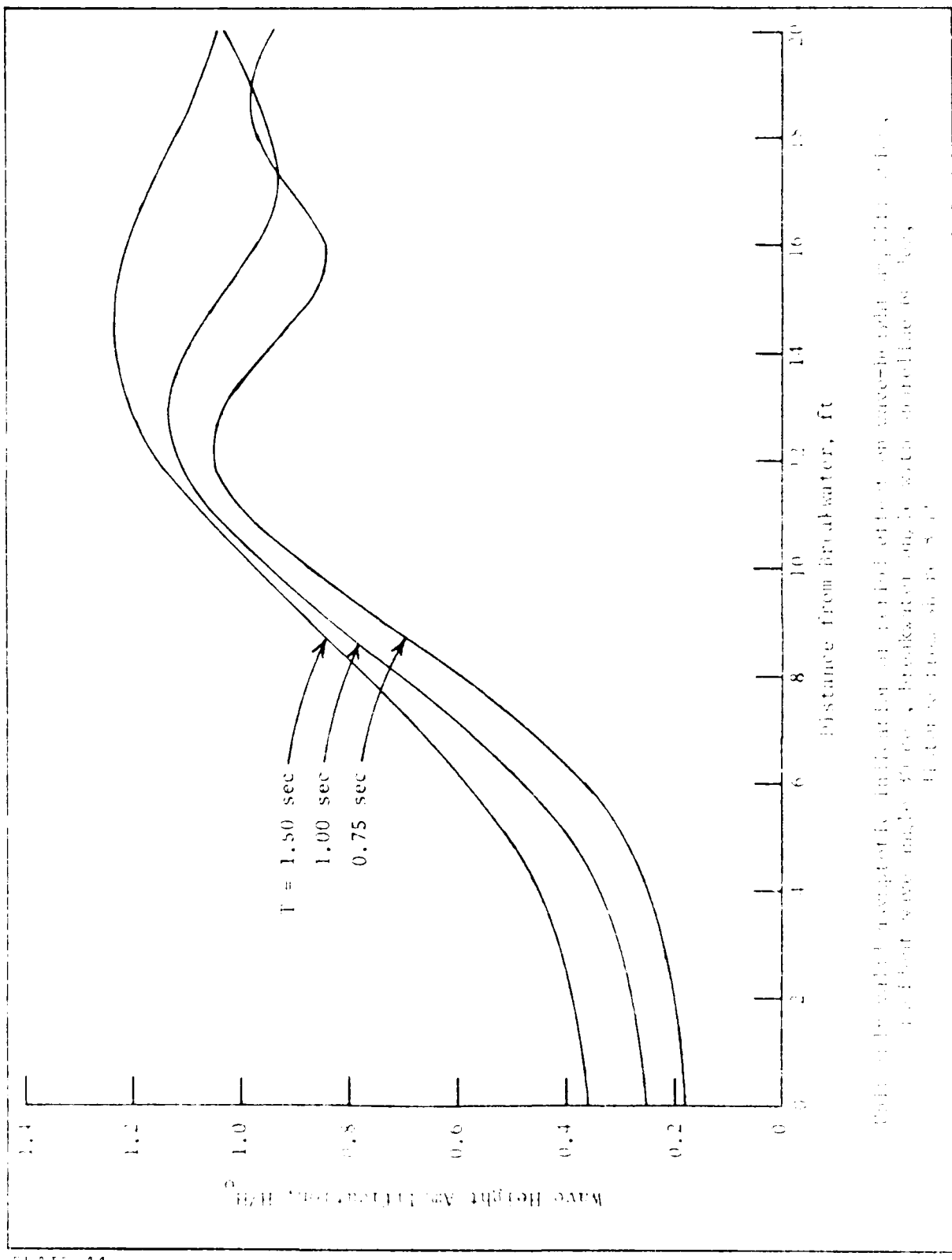
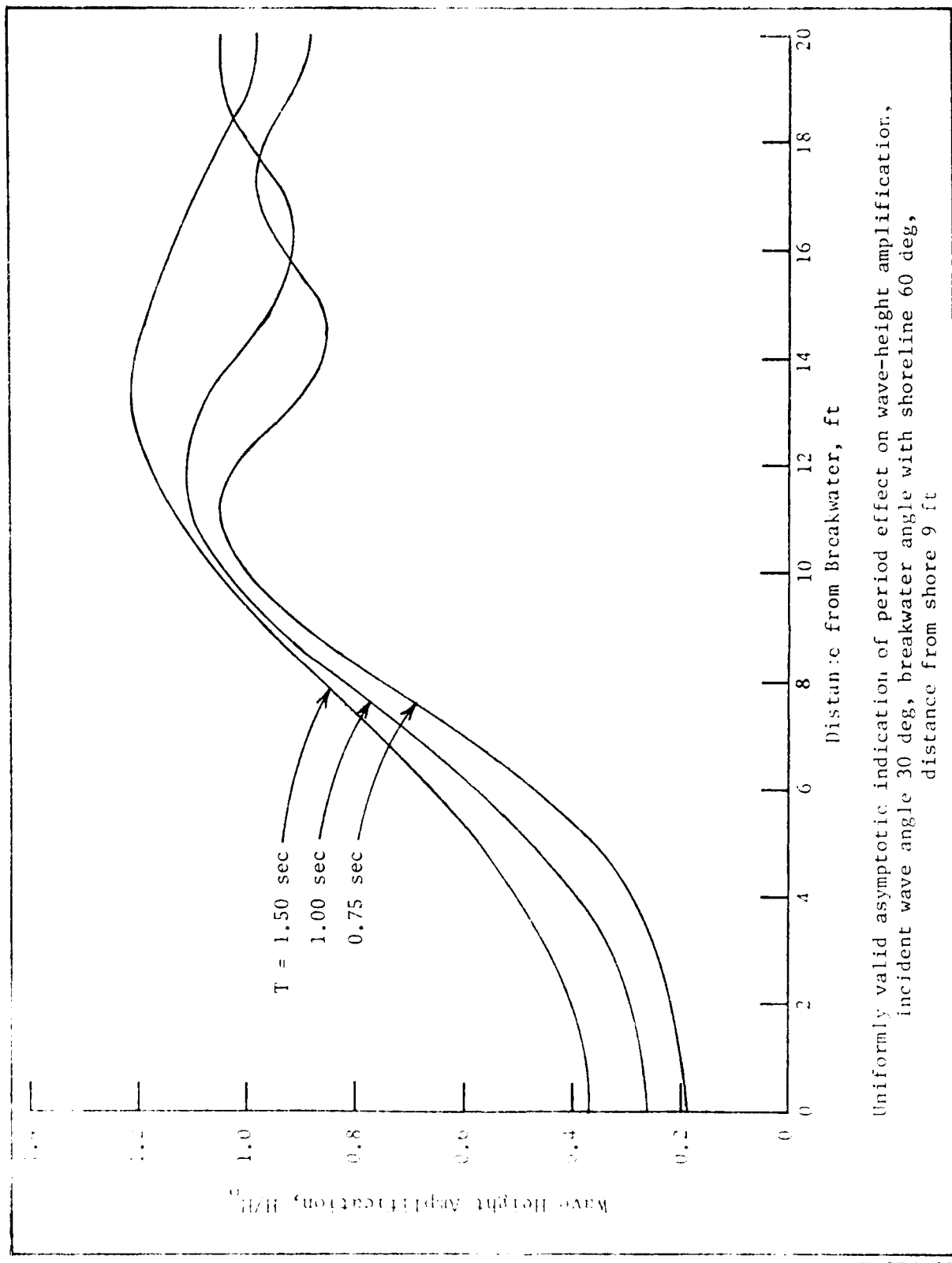
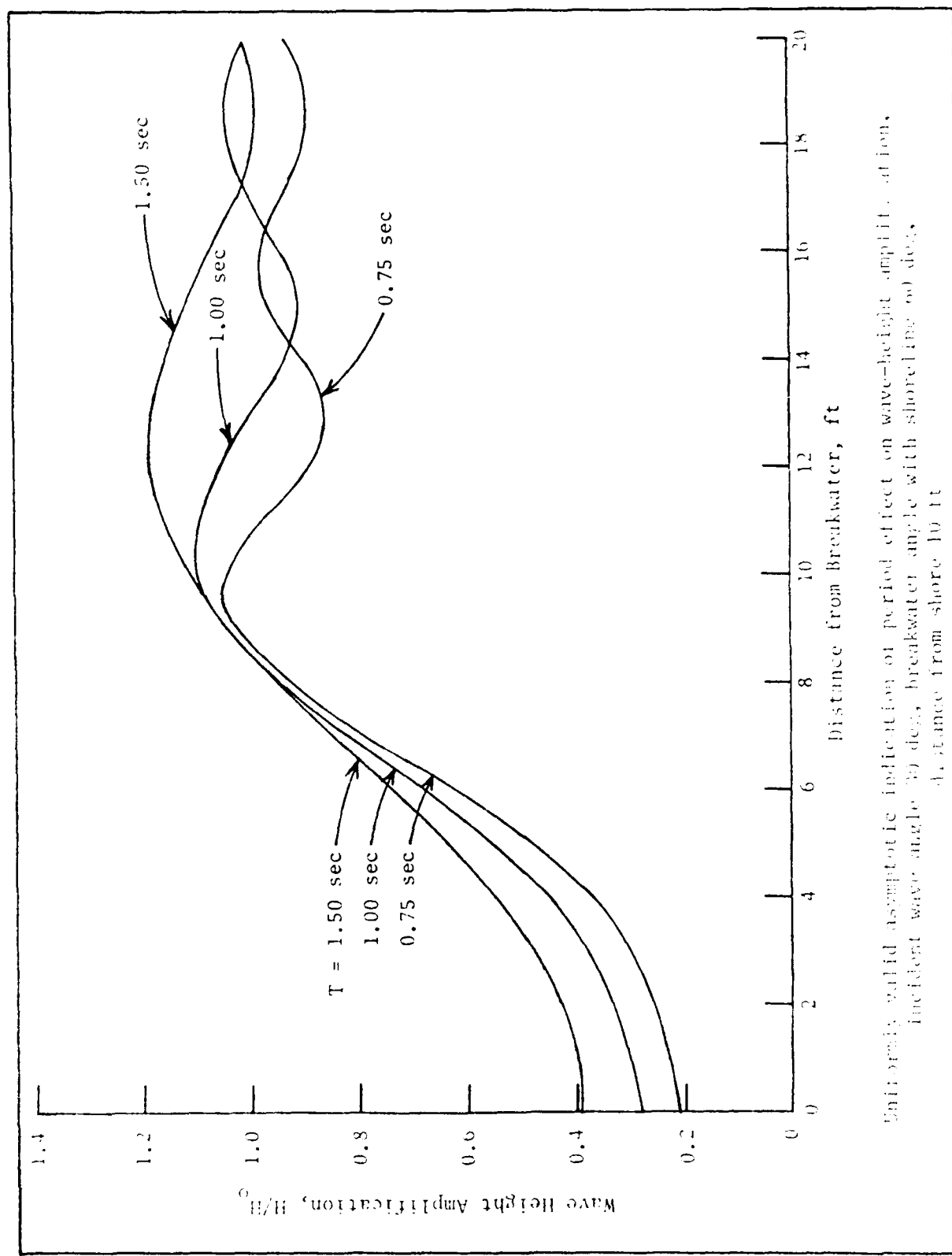


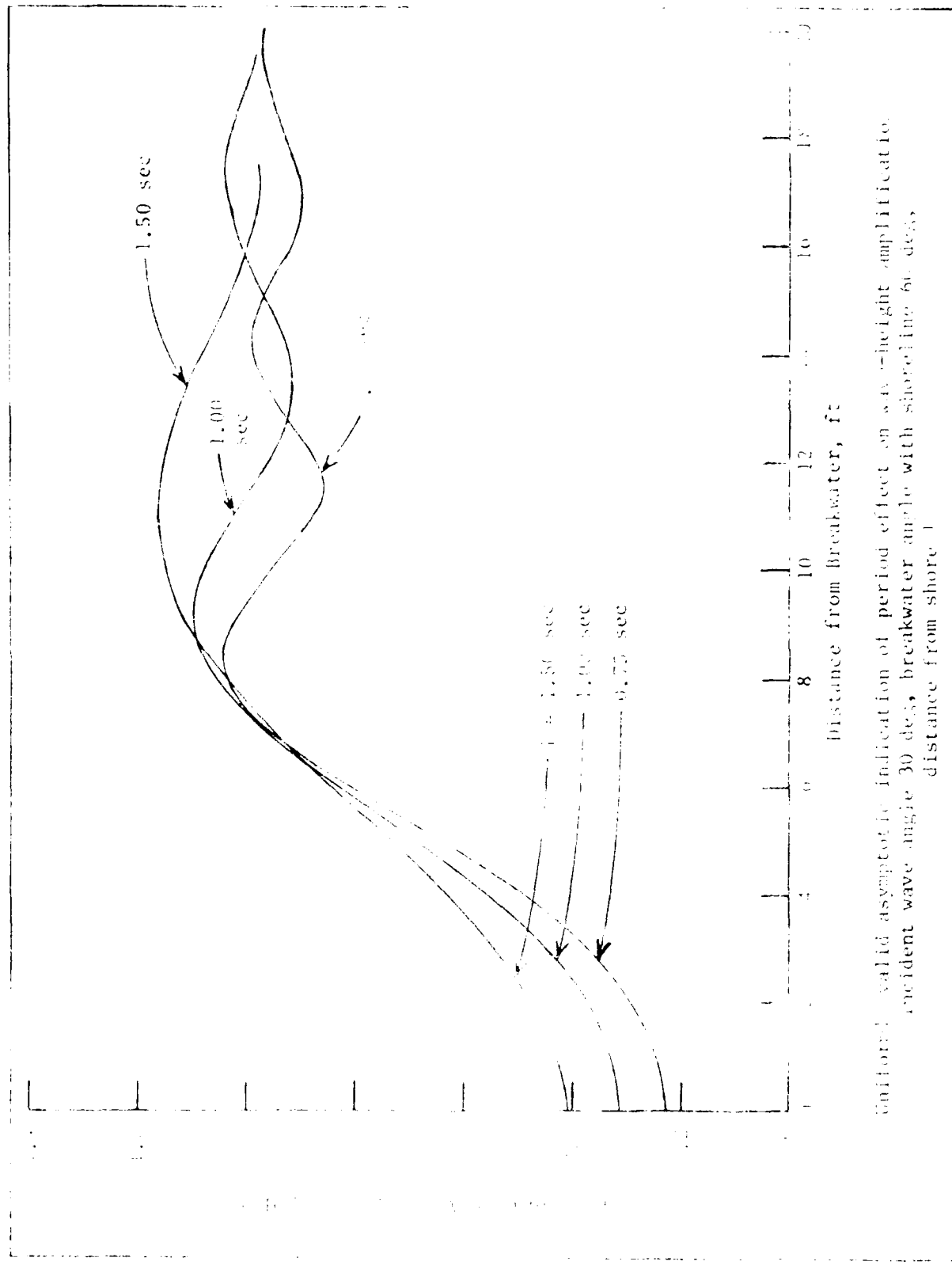
PLATE 44



Uniformly valid asymptotic indication of period effect on wave-height amplification,
incident wave angle 30 deg, breakwater angle with shoreline 60 deg,
distance from shore 9 ft



Unitarily valid asymptotic indication of period effect on wave-height amplification, incident wave angle 30 deg, breakwater angle with shoreline 60 deg,
distance from shore 10 ft



envelope) valid asymptotic indication of period effect on wave height amplification
incident wave angle 30 deg, breakwater angle with shoreline 60 deg,
distance from shore 1

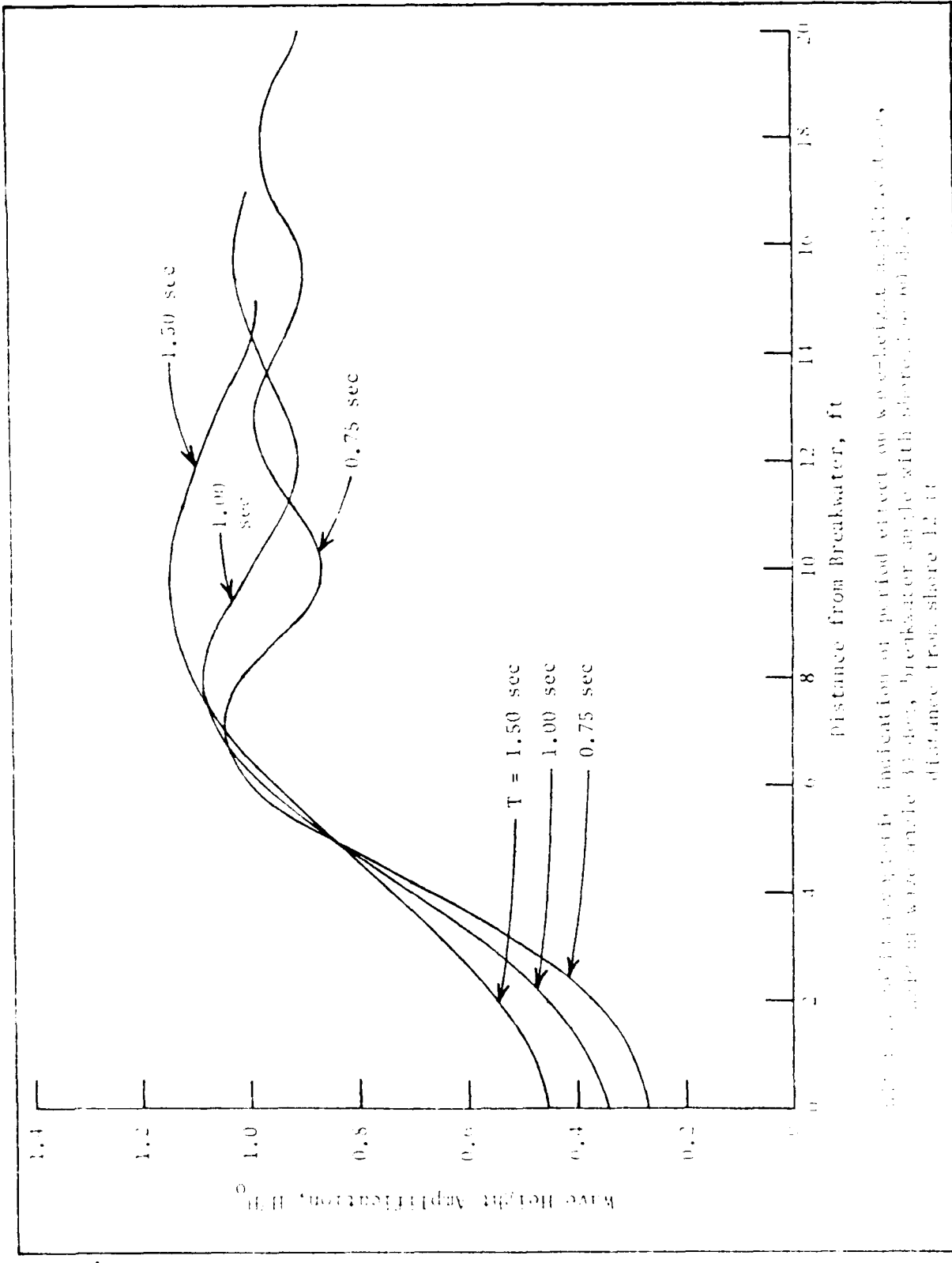
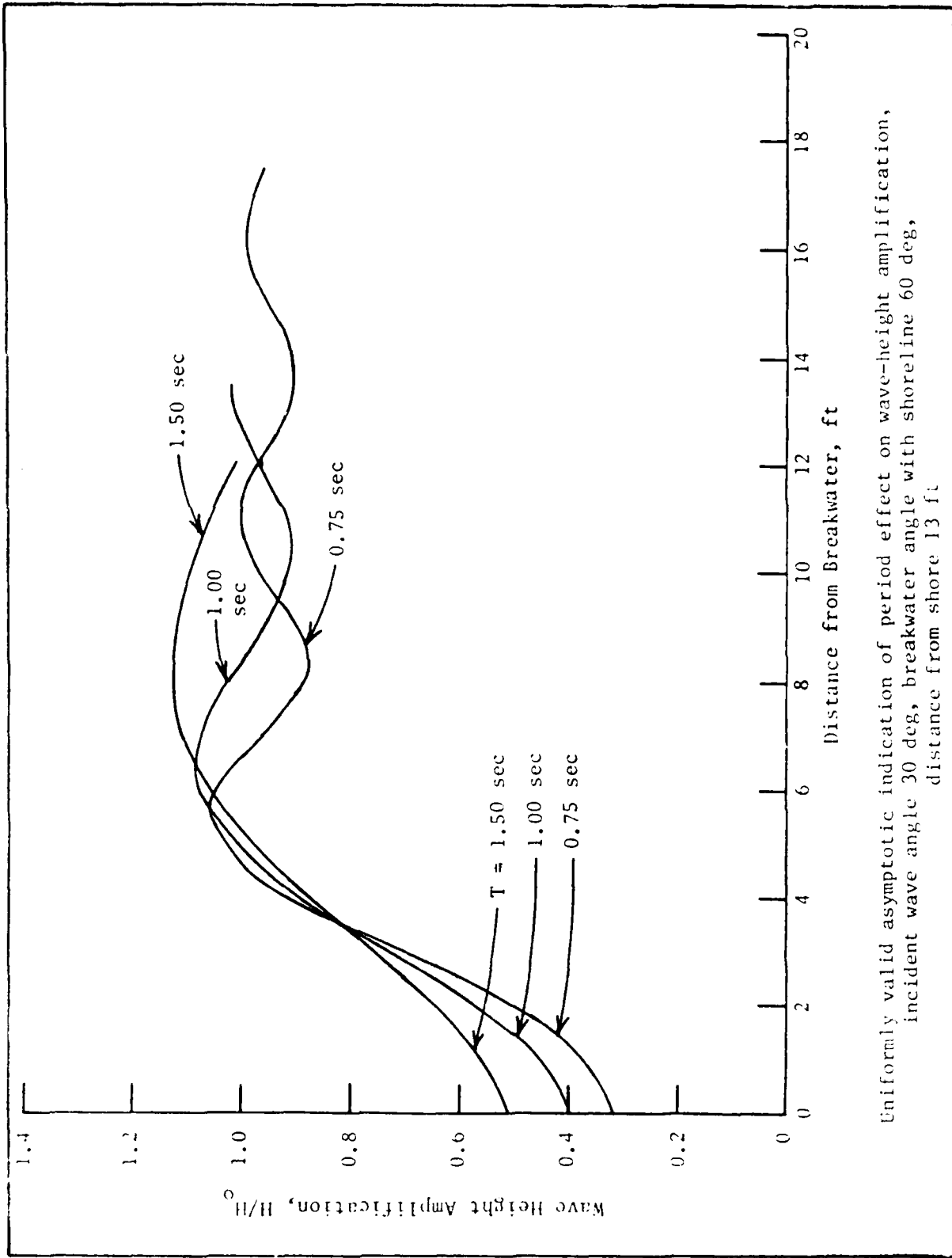


FIGURE 42

Fig. 42. Effect of wave period on the indication of periodic effect on wave height amplification near a breakwater in a wave tank, breakwater angle with shore 12°, distance from shore 12 ft.



Uniformly valid asymptotic indication of period effect on wave-height amplification,
incident wave angle 30 deg, breakwater angle with shoreline 60 deg,
distance from shore 13 ft

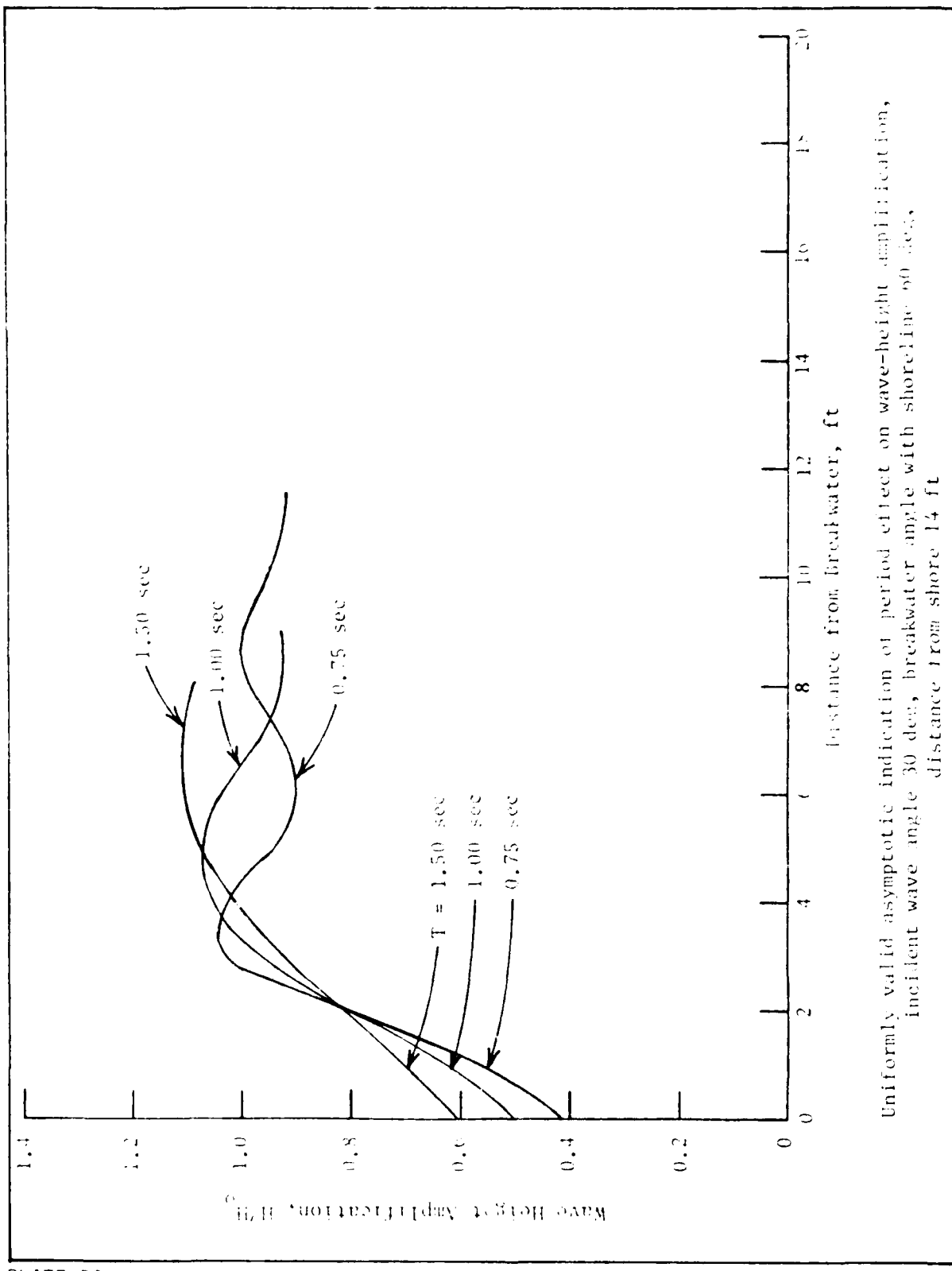


PLATE 50

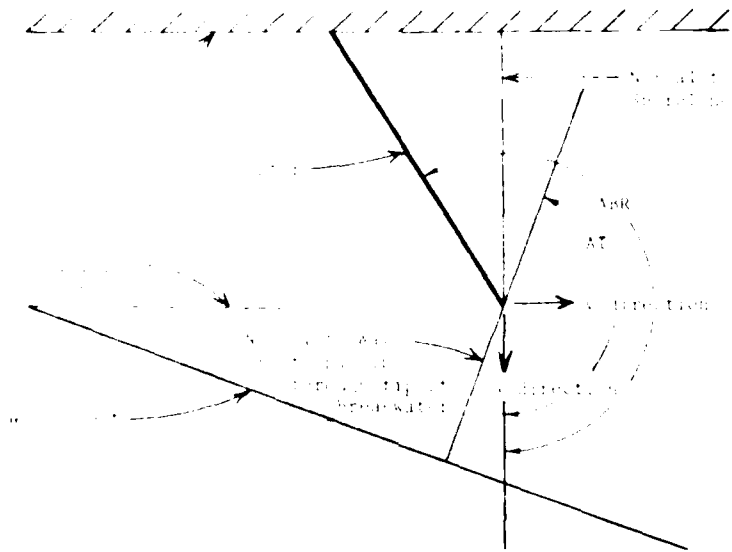
Uniformly valid asymptotic indication of period effect on wave-height amplification,
incident wave angle 30 deg, breaker angle with shoreline 60 deg,
distance from shore 14 ft

APPENDIX A: NOTATION

\tilde{K}_t	Arbitrary radiated wave parameter for straight breakwater, 1/ft
L	Wavelength at arbitrary location, ft
L_o	Incident wavelength, ft
L_r	Wavelength reflected from breakwater, ft
L_t	Wavelength radiated from breakwater tip, ft
n	Ratio of group velocity, c_g , to wave celerity, c , dimensionless
P	Rate of wave power transmission, lb/sec
r	Radial distance, ft
\bar{r}	Phase function parameter, ft
R	Phase function of waves radiated from curved breakwater tip, deg
R_s	Phase function of waves radiated from straight breakwater tip, deg
s	Bottom slope, dimensionless
S	Phase function of incident wave for curved breakwater, deg
S_s	Phase function of incident wave for straight breakwater, deg
$S_2(\rho_1^2)$	Fresnel sine integral, dimensionless
\bar{S}	Phase function of wave reflected from curved breakwater, deg
\bar{S}_s	Phase function of wave reflected from straight breakwater, deg
t	Time element, sec
T	Wave period, sec
u_1	Diffraction integration limits, dimensionless
u_2	Diffraction integration limits, dimensionless
\bar{u}	Two-dimensional horizontal velocity vector, ft/sec
x	Horizontal direction in Cartesian coordinate system, ft
y	Horizontal direction in Cartesian coordinate system, ft
z	Vertical direction in Cartesian coordinate system, ft
γ	Arbitrary parameter, dimensionless
δ	Battjes wave number correction factor $(a_{xx} + a_{yy})/k^2 a$, dimensionless
η	Local water-surface elevation and complex wave amplitude, ft
θ	Arbitrary wave angle, deg
θ_o	Incident wave angle, deg
θ_r	Reflected wave angle along breakwater, deg
θ_t	Radiated wave angle from oscillatory point source at breakwater tip, deg
π	3.141592654, dimensionless

ρ	Fluid density, kg/m ³
σ_p	Froude number, dimensionless
σ_t	Presumed interval parameter, dimensionless
τ	Presumed integral parameter, dimensionless
ϕ	Velocity potential, m ² /s
ω	Angular frequency, rad/s
Δb	Wave buoyancy force
Θ	Argument of mathematical function, dimensionless
$\tilde{\Theta}$	Argument of mathematical function, dimensionless
∇	Horizontal gradient operator, dimensionless
\leq	Inequality, dimensionless
\ll	Less than, dimensionless
\approx	Identical, dimensionless
∂	Partial derivative symbol, dimensionless
usm	universal, dimensionless

APPENDIX B: UNIFORM ASYMPTOTIC THEORY
LIU, LOZANO, AND PANTAZARAS (1979) FOR COMBINED REFRACTION AND
DIFFRACTION DOWNCOAST OF AN OBLIQUE BREAKWATER
(Program obtained by contract with Philip Liu, Cornell University)



Definitive Sketch


```

1   COSH(P+H)**2)
1F (ABS((P1-P)/P) .LT. 0.005) GO TO 772
P=P1
GO TO 772
SCD=P1*SIN(AREF(NN))
REFK(WN)=SCD
IF (WN .EQ. 1) S1=SCD
IF (WN .EQ. K2) S2=SCD
IF (K1 .EQ. NN) STPN=X1-X3
IF (K1 .NE. NN) STPN=ABS((X1-X3)/(K1-NN))
IF (WN .LE. K1) DC=1.
IF (WN .GT. K1) DC=-1.
RAYII=0.5*SCD/SQRT(P1**2-SCD**2)*(-1.)**C*STPN
PHAI=0.5*STPN*(-1.)*DC*SQRT(P1**2-SCD**2)
IF (WN .EQ. K1) K=1
IF (WN .NE. K1) K=(K1-NN)
IF (K .LT. 0) K=-K
IF (WN .EQ. K1) X=X1
IF (X .EQ. X3) GO TO 888
DO 882 L=1,K
IF (WN .NE. K1) X=STPN*L*DC+X3
IF (L .EQ. 1) GO TO 883
RAYII=RAYII-DC/SQRT(P1**2-SCD**2)*0.5*STPN*SCD
PHAI=PHAI-DC*SQRT(P1**2-SCD**2)*0.5*STPN
H=DEPTH(X)
882 P1=P-(G*P*TANH(P+H)-F2)/(G*TANH(P+H)+G*P+H/
1   COSH(P+H)**2)
IF (ABS((P1-P)/P) .LT. 0.005) GO TO 881
P=P1
GO TO 881
IF ((SCD/P1)**2 .GT. 1.) GO TO 887
RAYII=RAYII-DC/SQRT(P1**2-SCD**2)*0.5*STPN*SCD
PHAI=PHAI-DC*SQRT(P1**2-SCD**2)*0.5*STPN
889 CONTINUE
YRE(NN)=YBW>NN)+RAYII
SRE(NN)=SO>NN)+ABS(PHAI)*ABS(X3-X)/(X3-X)+SCD*(1
1   YRE>NN)-YBW>NN))
GO TO 779
888 YRE(NN)=YBW>NN)
SRE(NN)=SO>NN)
779 WRITE (10,200) NN,YRE>NN),SRE>NN)
777 CONTINUE
GO TO 83
887 DO 999 J=1,NN
M=NN-J+1
MM1=M+1
YRE(M)=YRE(MM1)+1.
SRE(M)=SRE(MM1)+SCD+1.
REFK(M)=SCD
WRITE (10,200) M,YRE(M),SRE(M)
999 CONTINUE
S1=SCD
C-----COMPUTE WAVE NUMBER AT THE CROSS SECTION-----
83 H=DEPTH(X1)
16 P1=P-(G*P*TANH(P+H)-F2)/(G*TANH(P+H)+G*P+H/COSH(P+H)
1   **2.)
IF (ABS((P1-P)/P) .LT. 0.005) GO TO 17
P=P1
GO TO 16
17 WNCS=P1
ACS=ARCSIN(SCI/WNCS)
C-----COMPUTE AMPLITUDE RATIO DUE TO REFRACTION-----
84 AMF=SQRT(ABS(WNCS*COS(AI*PI/180.)/WNI*COS(ARCSIN(SCI/WN
1   CS))/((1.+2.*WNCS*DEPTH(X1)/SINH(2.*WNCS*DEPTH(X1)))))*
AMF=AMF*SQRT(1.+2.*WNI/SINH(2.*WNI)))
WRITE (10,55)
65 FORMAT ('0','AMPLITUDE RATIO DUE TO REFRACTION ONLY')
WRITE (10,100) AMF
WRITE (10,64)
66 FORMAT ('0','ANGLE A OF INCIDENT RAY AT THE TIP')

```

```

      WRITE (10,100) AT
C-----COMPUTE WAVE NO'S AT GAUSS QUAD. X-POINT-----
      DO 5 K=1,8
      KK=]
      XG=(X1+X0)/2.+((X1-X0)/2.*GAUSS(1,K)
      7 H=DEPTH(XG)
      8 P1=P-((G*P*TANH(P*H)-F2)/(G*TANH(P*H)+G*P*H/(COSH(P*H)))
      1   *P))
      IF (ABS((P1-P)/P) .LT. 0.005) GO TO 9
      P=P1
      GO TO 3
      9 IF (KK-1) 10,11,6
      10 WN(2*K-1)=P1
      KK=KK+1
      XG=X1+X1-XG
      GO TO 7
      11 WN(2*K)=P1
      6 CONTINUE
C-----CALCULATE INCIDENT WAVE RAY PHASE INTEGRAL FROM
C-----TIP TO X-SECTION-----
      PHAI=0.
      DO 12 L=1,8
      PHAI=PHAI+(COTAN(ARSIN(SCI/WN(2*L-1)))+COTAN(ARSIN(
      1   SCI/WN(2*L))))*SCI*GAUSS(2*L)*(X1-X0)/2.
      12 CONTINUE
      WRITE (10,63)
      68 FORMAT ('10,7' ANGLE A (DEG) Y LOCATION AMP. RATIO DIR
      1   OF WAVES')
C-----PREPARE SCALLING LIMIT-----
      M1=A1/AS
      M2=A2/AS
C-----ENTER SCANNING LOOP-----
      DO 13 M=M1,M2
      A=AS*M
      IF (A .EQ. 90.) GO TO 13
      IF (A .EQ. 180.) GO TO 13
      IF (A .EQ. 270.) GO TO 13
      IF (A .EQ. 360.) GO TO 13
C-----INITIALIZE-----
      PHAID=0.
      RAYID=''.
      SCD=WN1*SIN(A*PI/180.)
      ADCS=ARSIN(SCD/WN1)
C-----COMPUTE DIFFRACTED RAY R AND Y INTEGRALS FROM
C-----TIP TO X-SECTION-----
      DO 15 N=1,8
      PHAID=PHAID+(COTAN(ARSIN(SCD/WN(2*N-1)))+COTAN(ARSIN(
      1   SCD/WN(2*N))))*SCD*GAUSS(2*N)*(X1-X0)/2.
      RAYID=RAYID+(TAN(ARSIN(SCD/WN(2*N-1)))+TAN(ARSIN(SCD/
      1   WN(2*N))))*GAUSS(2*N)*(X1-X0)/2.
      15 CONTINUE
      Y=-1.*RAYID
C-----COMPUTE R -----
      REARS(PHAID)+ARS(Y*SCD)
C-----COMPUTE S -----
      S=A*S(PHAID)*ABS(X0-X1)/(X0-X1)+Y*SCI
      FD1=1.
      FD2=-1.
C-----COMPUTE SH -----
      IF (APR .GT. 45.) GO TO 601
      IF (Y .GT. YRE(K2)) SR=SR+E(K2)+SK2*(Y-YRE(K2))
      IF (Y .GT. YRE(K2)) REK=SK2
      IF (Y .LT. YRE(1)) SB=SRF(1)+S1*(Y-YRE(1))
      IF (Y .LT. YRE(1)) REK=S1
      IF (Y .GE. YRE(1) .AND. Y .LE. YRE(K2)) GO TO 602
      GO TO 603
      602 DO 604 I=1,<2
      IF (Y .LE. YRE(I)) GO TO 605
      604 CONTINUE
      605 IF (Y .LE. YRE(I)) SR=SRF(I)

```

```

      IF (Y .EQ. YRE(I)) REK=REFK(I)
      IF (Y .LT. YRE(I)) SB=(Y-YRE(I))*(SRE(I-1)-SRE(I))
1   / (YRE(I-1)-YRE(I))+SRE(I)
      IF (Y .LT. YRE(I)) REK=(Y-YRE(I))*(REFK(I-1)-REFK(I))/
1   (REFK(I-1)-REFK(I))+REFK(I)
      GO TO 603
601  IF (Y .GT. YRE(I)) SB=SRE(I)+S1*(Y-YRE(I))
      IF (Y .GT. YRE(I)) REK=S1
      IF (Y .LT. YRE(K2)) SB=SRE(K2)+SK2*(Y-YRE(K2))
      IF (Y .LT. YRE(K2)) REK=SK2
      IF (Y .GE. YRE(K2) .AND. Y .LE. YRE(1)) GO TO 605
      GO TO 603
606  DO 607 I=1,<2
      IF (Y .GE. YRE(I)) GO TO 608
607  CONTINUE
608  IF (Y .EQ. YRE(I)) SB=SRE(I)
      IF (Y .EQ. YRE(I)) REK=REFK(I)
      IF (Y .GT. YRE(I)) SB=(Y-YRE(I))*(SRE(I-1)-SRE(I))
1   / (YRE(I-1)-YRE(I))+SRE(I)
      IF (Y .GT. YRE(I)) REK=(Y-YRE(I))*(REFK(I-1)-REFK(I))
1   / (YRE(I-1)-YRE(I))+REFK(I)
C-----ASSIGN SIGN OF THETA, THETAB FOR DIFFERENT REGIONS
C-----IN THE FIELD-----
603  IF (AT .GT. ABR) GO TO 633
      IF (A .GT. AT) FD1=-1.
      IF (A .GT. ABR) FD1=1.
      IF (A .GT. ABR) FD2=1.
      IF (A .GT. AREF(<0)*180./PI) FD2=-1.
      GO TO 33
633  IF (A .GT. AREF(K2)*180./PI .AND. A .LT. ABR) FD2=1.
      IF (A .GT. ABR .AND. A .LT. AT) FD1=-1.
C-----CALCULATE THETA, THETAB-----
33   THETA=SQRT(R-S)
      IF ((R-S)<0.) GO TO 13
      THETAB=SQRT(R-SB)
C-----COMPUTE SINES AND COSINES OF S, SB-----
      ESS=SIN(S)
      ESC=COS(S)
      ES9S=SIN(SB)
      ESBC=COS(SB)
      XX=THETA**2.
C-----COMPUTE FRESNEL INTEGRALS VIA SUBROUTINE CS-----
DO 35 NN=1,2
CALL CS(C,SS,XX)
FI(NN,1)=C
FI(NN,2)=SS
XX=THETA3**2.
35  CONTINUE
C-----COMPUTE AMPLITUDE RATIO-----
34   AMR=AMF*SQRT(((ESC+ES3C-ESS-ESBS)/2.+((ESC*FI(1,1)-ESS
1   *FI(1,2))*FD1+(ESBC*FI(2,1)-ESBS*FI(2,2))*FD2)**2+((ESC
2   +ESAC+ESS+ESBS)/2.+((ESS*FI(1,1)+ESC*FI(1,2))*FD1+
3   (ESBS*FI(2,1)+ESBC*FI(2,2))*FD2)**2)/2.)
AA1=0.5+FD1*FI(1,1)
AA2=0.5+FD1*FI(1,2)
B1=0.5+FD2*FI(2,1)
B2=0.5+FD2*FI(2,2)
C1=AA1*AA1+AA2*AA2
C2=B1*B2
D1=AA1*B1-AA2*B2
D2=B1*AA2-AA1*B2
CSS=ESC*ESBC+ESS*ESBS
SSS=ESS*ESBC-ESC*FSBS
DSINY=C1*SCI-C2*REK+(SCI-REFK)*(D1*CSS-D2*SSS)
IF (ABS(REK) .GT. ABS(WNCS)) GO TO 9876
DSINX=C1*SORT(WNCS*WNCS-SCI*SCI)+C2*SORT(WNCS*WNCS-REK*REK)
1   +(SQRT(WNCS*WNCS-SCI*SCI)-SQRT(WNCS*WNCS-REK*REK))*(D1*CSS-D2
2   *SSS)
GO TO 8765
9876  DSINX=SQRT(WNCS*WNCS-SCI*SCI)*(C1*D1*(CSS-D2*SSS))

```

Sample Python output

99.000	27.062	1.177	190.216
100.000	26.225	1.215	189.477
101.000	25.428	1.267	190.000
102.000	24.667	1.291	189.693
103.000	23.940	1.275	188.969
104.000	23.245	1.230	188.713
105.000	22.578	1.183	188.959
106.000	21.938	1.160	189.326
107.000	21.323	1.171	189.507
108.000	20.731	1.210	189.524
109.000	20.161	1.257	189.575
110.000	19.612	1.295	189.741
111.000	19.082	1.314	189.802
112.000	18.569	1.310	189.359
113.000	18.073	1.285	188.533
114.000	17.594	1.245	188.436
115.000	17.129	1.230	189.547
116.000	16.678	1.159	189.947
117.000	16.240	1.131	189.135
118.000	15.815	1.119	190.225
119.000	15.402	1.127	190.862
120.000	15.000	1.150	189.415
121.000	14.608	1.186	190.823
122.000	14.227	1.228	189.951
123.000	13.855	1.271	189.695
124.000	13.492	1.311	190.316
125.000	13.138	1.345	188.971
126.000	12.792	1.372	190.147
127.000	12.454	1.391	188.600
128.000	12.124	1.400	189.817
129.000	11.800	1.401	188.351
130.000	11.483	1.395	189.532
131.000	11.173	1.380	188.207
132.000	10.869	1.360	189.276
133.000	10.571	1.334	188.285
134.000	10.278	1.303	188.920
135.000	9.990	1.269	188.700
136.000	9.708	1.231	188.419
137.000	9.431	1.192	189.291
138.000	9.158	1.151	188.141
139.000	8.889	1.109	189.427
140.000	8.625	1.056	188.742
141.000	8.365	1.024	188.708
142.000	8.109	0.982	189.854
143.000	7.856	0.941	188.394
144.000	7.607	0.901	189.568
145.000	7.362	0.851	189.911
146.000	7.119	0.824	188.303
147.000	6.880	0.787	190.308
148.000	6.644	0.752	189.963
149.000	6.410	0.719	188.117
150.000	6.180	0.687	190.849

151.000	5.951	0.657	190.272
152.000	5.725	0.628	187.550
153.000	5.502	0.601	190.958
154.000	5.281	0.575	191.175
155.000	5.061	0.551	186.741
156.000	4.844	0.528	189.970
157.000	4.629	0.506	192.775
158.000	4.416	0.486	186.959
159.000	4.204	0.466	187.290
160.000	3.994	0.448	193.874
161.000	3.785	0.432	190.259
162.000	3.578	0.416	184.885
163.000	3.372	0.401	192.041
164.000	3.167	0.387	195.523
165.000	2.964	0.374	188.374
166.000	2.761	0.361	188.658
167.000	2.560	0.350	197.111
168.000	2.359	0.339	196.803
169.000	2.160	0.329	192.096
170.000	1.961	0.319	195.426
171.000	1.763	0.310	199.444
172.000	1.565	0.302	198.447
173.000	1.359	0.294	198.702
174.000	1.172	0.286	198.672
175.000	0.976	0.279	194.461
176.000	0.780	0.273	195.521
177.000	0.585	0.266	201.190
178.000	0.390	0.261	195.506
179.000	0.195	0.255	182.298
181.000	-0.195	0.245	201.580
182.000	-0.390	0.241	197.383
183.000	-0.585	0.236	186.856
184.000	-0.780	0.232	195.187
185.000	-0.976	0.228	205.808
186.000	-1.172	0.225	205.254
187.000	-1.369	0.222	205.018
188.000	-1.565	0.218	205.284
189.000	-1.763	0.215	196.671
190.000	-1.961	0.213	188.365
191.000	-2.160	0.210	200.896
192.000	-2.359	0.207	206.106
193.000	-2.560	0.205	191.716
194.000	-2.761	0.203	188.340
195.000	-2.964	0.201	205.698
196.000	-3.167	0.199	210.720
197.000	-3.372	0.197	208.668
198.000	-3.578	0.196	212.182
199.000	-3.785	0.194	204.668
200.000	-3.994	0.193	180.818
201.000	-4.204	0.192	189.190
202.000	-4.416	0.191	211.458
203.000	-4.629	0.190	212.071

204.000	-4.844	0.189	210.642
205.000	-5.061	0.188	213.792
206.000	-5.281	0.188	198.754
207.000	-5.502	0.187	186.079
208.000	-5.725	0.187	208.237
209.000	-5.951	0.187	214.457

Definition of Program Parameters

Name	Description
A	Scanning angle
ABR	Angle of tip of breakwater with normal to shoreline
ABW(110)	Local angle of breakwater
ACS	Angle of incidence at arbitrary cross section
ADCS	Angle of radiated ray at arbitrary cross section
AI	Angle of incidence at infinity (deep water)
AMF	Amplitude ratio due to shoaling effect
AMR	Amplitude ratio due to combined refraction and diffraction
APA	Local angle of wave propagation
AREF(110)	Angle of reflected wave along the breakwater
AS	Scanning angle step
AT	Angle of incidence at the tip of the breakwater
A1	Lower limit of the scanning angle (>90 deg)
A2	Upper limit of the scanning angle (<270 deg)
CS	Fresnel integral subroutine
DEPTH(X)	Water depth
ESBC	Cos(SB) (Cosine of phase function of reflected wave ray)
ESBS	Sin(SB) (Sine of phase function of reflected wave ray)
ESC	Cos(S) (Cosine of phase function of incident wave ray)
ESS	Sin(S) (Sine of phase function of incident wave ray)
FI(2,2)	Output for subroutine CS
G	Gravitational acceleration constant, 32.15184 ft/sec ²
GAUSS(2,8)	Location and weight factor for 16-point Gauss Quadrature
H	Water depth
PHAID	Integral part of phase function of radiated wave ray
PHAI	Integral part of phase function of incident wave ray
PI	3.14159265359

Name	Description
R	Phase function of radiated wave ray
RAYID	Integral part of the location of a radiated wave ray
RAYII	Integral part of the location of a reflected wave ray
S	Phase function of incident wave ray
SB	Phase function of reflected wave ray
SCD	Snell's constant for radiated wave ray from breakwater tip
SCI	Snell's constant for incident wave ray
SO(110)	Phase functions of incident waves along the breakwater
SRE(110)	Phase function of reflected wave along X1 cross section
STP	Step size of numerical integration along a ray by the trapezoidal rule
T	Wave period in seconds
THETA	Square root of (R - S)
THETAB	Square root of (R - SB)
WN(16)	Wave number at Gauss Quadrature points
WNCS	Wave number at arbitrary cross section
WNI	Wave number at infinity (deep water)
WNT	Wave number at tip of breakwater
X0	X-coordinate of tip of breakwater
X1	X-coordinate of arbitrary cross section
X2	X-coordinate of end of tracing region ($X2 > X0$)
XG	X-coordinate of Gauss Quadrature points
YBW(110)	Y-coordinates of the breakwater
YRE(110)	Y-coordinates of reflected wave rays along X1 arbitrary cross section

END

FILMED

2-85

DTIC

